

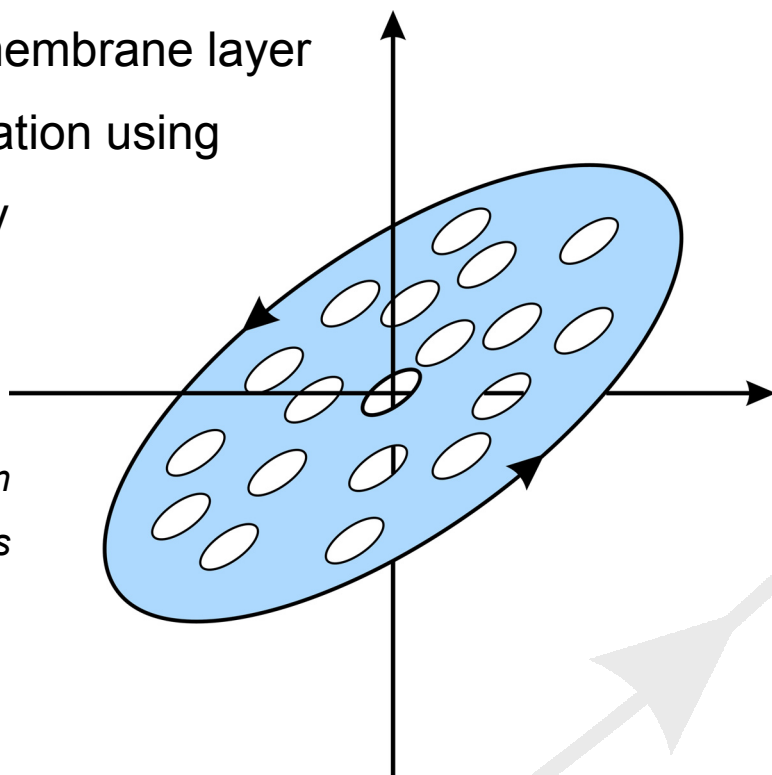


University of Twente
Faculty of Science and Technology
MESA+ Research Institute
Inorganic Materials Science Group



Inorganic membrane layer
characterization using
ellipsometry

*Water sorption study on
hydrogen-selective silica membranes*



Sjoerd Kuipers

Master Thesis
April 2004

Inorganic membrane layer characterization using ellipsometry

Water sorption study on hydrogen selective silica membranes

Sjoerd Kuipers

Master Thesis

Graduation committee:

- Prof. dr. ing. Dave Blank (Chairman)
- Drs. Tijana Zivkovic (Supervisor)
- Dr. ir. Nieck Benes
- Dr. ir. Arian Nijmeijer
- Dr. Holger Schönherr

April 16, 2004



Summary

This report describes the study of water sorption characterization on state-of-the-art hydrogen-selective porous silica membranes. Adsorption and desorption processes have been recorded using the technique of ellipsometry, which is based on the change in polarization of a light beam upon reflection from the sample surface. Change in optical properties due to adsorption and desorption, enables ellipsometry to record the processes.

The recording of adsorption and desorption was carried out at a single wavelength, whereas spectroscopic ellipsometry measurements were used to compare the blank samples before and after an adsorption/desorption cycle. From the blank comparisons, it was concluded that no structural change occurred due to the adsorption or desorption of water vapor.

The ellipsometric parameters that are obtained from ellipsometry measurements were taken to be proportional to the surface coverage of water. Consequently, the Langmuir model has been used to obtain isotherms at 31°C and 55°C using a first order estimation. As a consequence, a value for the isosteric heat of adsorption of 17 kJ/mol was obtained. Adsorption and desorption kinetics could be analyzed as well and a first order fit was in good agreement with the measured data. The first-order kinetics as well as the relatively low isosteric heat of adsorption give an indication of simple physisorption of water on the microporous silica membranes at the given temperature range.

Due to the assumption that surface coverage is proportional to the ellipsometry data, only few calculations could be carried out based on the results. Further relevant data such as pore size distribution and porosity can be obtained using a model such as the Bruggeman effective medium approximation. Such a model usually distinguishes the optical properties of the pores from those of the solid matrix to estimate the properties of the effective medium. Consequently, ellipsometry data is correlated to the effective medium approach.

In order to obtain the above results, a set-up had to be designed which enabled the delivery of water vapor to the ellipsometry sample cell. The set-up is based on a bubbler from where a carrier flow of helium delivers water vapor to the sample cell. In the cell, a continuous flow was present in order to optimize the mixing conditions inside. Water vapor was prevented from condensation in the system using a heating rope between bubbler and sample cell. The set-up could be used sufficiently to obtain results on sorption characteristics of water on microporous silica. A major advantage of the set-up is the flexibility of combining it with the existing ellipsometer. However, the major limitation is the temperature control of the sample cell. The temperature could only be set indirectly by an oil recycle via the double wall and the temperature measurement of the cell (i.e. of the sample) was not accurate enough. Also, measurements were restricted to cell temperatures up to ~100°C because of an unknown limit of the thermostatic bath for the sample cell oil recycle.

Despite the limitations of the set-up, the measurements show that sorption measurements using ellipsometry are very promising. The high sensitivity of the ellipsometer should be used as much as possible and hence, it would be advantageous to increase the accuracy of the gas-delivery set-up. A first step for the improvement of the set-up has been made with the design of a new sample cell. It is expected that all problems that have been experienced with the current cell will be solved with the new one.

Foreword

This is the report of the final assignment of the study Chemical Engineering at the University of Twente. The research was part of the PhD project of my supervisor Tijana Zivkovic in the Inorganic Materials Science group. Thanks go to Tijana for the full support, especially in the past few months when Marko joined her family.

Also, I would like to thank the rest of the graduation committee, especially Arian Nijmeijer as external member and Nieck Benes who left Enschede but still provided useful feedback in the last couple of weeks.

Further, the technical support of Attila Csáki and Gerrit Mollenhorst has been outstanding. Attila built the whole gas delivery set-up in a relatively short amount of time and Gerrit gave special effort in the design of a new sample cell.

Special thanks go to Herbert Wormeester and the Solid State Physics group where measurements were carried out using the ellipsometer set-up. The hospitality of all group members was highly appreciated and it has been a pleasure working there.

It was great working in the Inorganic Materials Science group. I have spent a wonderful time. Thank you all.

Sjoerd Kuipers
Enschede, April 2004

Table of contents

Summary	1
Foreword	3
1 Introduction	9
1.1 Microporous silica membranes	9
1.2 Topic description	11
1.3 Contents of this report	12
Theory	13
2 Sorption characteristics.....	15
2.1 Introduction	15
2.2 The adsorption isotherm	15
2.3 Micropore adsorption.....	17
2.3.1 Adsorption on microporous silica.....	17
2.3.2 Micropore filling and surface area.....	18
2.3.3 Estimation of microporosity	19
2.3.4 Estimation of mesoporosity	19
2.3.5 Langmuir isotherm.....	20
2.4 Adsorption kinetics.....	21
2.4.1 Adsorption paths.....	21
2.4.2 Sticking coefficient.....	21
2.4.3 Adsorption rate	22
2.4.4 Coverage dependence	22
2.4.5 Temperature dependence	23
2.5 Desorption kinetics	24
2.5.1 Desorption rate.....	24
2.5.2 Order of desorption.....	25
2.6 Dynamic equilibrium.....	25
3 Ellipsometry	27
3.1 Introduction	27
3.2 Reflection	28
3.3 Layer properties with ellipsometry	29
4 Sorption measurements with ellipsometry – a review	31
4.1 Introduction	31
4.2 Adsorption & ellipsometry	32
4.3 Further calculations	33
4.4 Other examples.....	34
Experimental	35
5 Measurements & data processing.....	37
5.1 Introduction	37
5.2 Experimental set-up.....	37

5.2.1	Ellipsometer.....	37
5.2.2	Gas delivery set-up	39
5.3	Procedure.....	44
5.3.1	Measurements.....	44
5.3.2	Sample preparation	44
5.3.3	Ellipsometry.....	46
5.3.4	Water vapor delivery	48
5.4	The Langmuir isotherm	48
5.4.1	Normalizing $\tan \Psi$	48
5.4.2	Estimating the Langmuir sorption constant	49
5.4.3	Isosteric heat of adsorption	49
5.5	Langmuir kinetics	49
5.5.1	Adsorption kinetics.....	49
5.5.2	Desorption kinetics	50
5.6	Samples.....	53
5.6.1	Sample names	53
5.6.2	Data files.....	53
5.7	Measurement statistics.....	54
6	Results & discussion.....	57
6.1	Introduction	57
6.2	Set-up operation and debugging	57
6.3	Long-term measurements	57
6.4	Blank measurements.....	58
6.5	Energy scans.....	58
6.6	Time scans	60
6.7	Langmuir isotherms.....	61
6.7.1	Coverage from $\tan(\Psi) : \theta_{\Psi}$	62
6.7.2	Fitting the Langmuir isotherms.....	64
6.7.3	Isosteric heat of adsorption	65
6.8	Adsorption kinetics.....	66
6.9	Desorption kinetics	68
6.9.1	Adsorptive pressure dependence.....	68
6.9.2	Temperature dependence	69
7	Conclusions	71
8	Recommendations	73
8.1	Adsorption and desorption characteristics of γ -alumina and silica separately.....	73
8.2	Fine-tuning gas-delivery.....	73
8.3	New ellipsometry sample cell.....	74
8.4	Further calculations	74
8.5	Use of the current cell.....	75
	References.....	76
	List of symbols.....	78
	Appendices	81

List of Tables

Table 1.1. Layer properties of a microporous silica membrane	10
Table 2.1. Main characteristics of the different sorption isotherms (Sing <i>et al.</i> , 1985).....	17
Table 2.2. Classification of non-specific (n) and specific (s) sorption for different types of adsorbate and adsorbent (Grillet and Llewellyn, 1998)	17
Table 2.3. Description of general cases of kinetic order of desorption	25
Table 4.1. Comparative characteristics of techniques used for the non-destructive characterization of porous low-k dielectric films (Baklanov and Mogilnikov, 2002 – Table 2).....	31
Table 6.1. Adsorption conditions for the given silica samples at $T_{\text{cell}} = 31 \pm 2$ °C. The time scan at $p_r = 0.94$ failed, although equilibrium was reached	61
Table 6.2. Adsorption conditions for the given silica samples at $T_{\text{cell}} = 52 - 56$ °C. The time scan at $T_{\text{water}}=50$ °C was not recorded due to an ellipsometer error, but equilibrium was reached.	61
Table 6.3. Desorption conditions for the given silica samples in dry helium (no water vapor pressure present)	61
Table 6.4. Results for adsorption isotherm at 31 °C sample temperature.....	63
Table 6.5. Results for adsorption isotherm at 55 °C sample temperature.....	63
Table 6.6. Results of the Langmuir constant estimation; cf = correction factor to determine $(\tan \Psi)_{\text{sat}}$	65
Table 6.7a. Adsorption constants determined at 31°C and different relative water vapor pressures. A first order fit has been used; R^2 indicates the accuracy of the regression and # indicates the number of measurements used for the fit. $\Delta\theta$ is the absolute coverage difference of the step. The last column gives the total time for the adsorption step.....	66
Table 6.8. Overview of desorption constants determined at constant temperature and in dry helium. A first order fit has been used; R^2 indicates the accuracy of the regression and # indicates the number of measurements used for the fit. The last column gives the total time for the adsorption step.	69
Table 7.1. Overview of main advantages and limitations of the used experimental set-up	71

List of Figures

Figure 1.1. Microporous silica membrane layer system.....	9
Figure 1.2. Cross section SEM micrograph of silica membrane. The silica membrane layer (SiO_2) is not visible in the graph since it is too thin.....	10
Figure 2.1. Six types of sorption isotherms according to Sing <i>et al.</i> (1985).....	16
Figure 2.2. Different possible adsorption paths.....	21
Figure 2.3. Lennard-Jones potential curves for simple physisorption and chemisorption (based on Oura <i>et al.</i> , 2003, p.303)	23
Figure 2.4. Lennard-Jones potential curves for (a) activated and (b) non-activated chemisorption (based on Oura <i>et al.</i> , 2003, p. 304)	24
Figure 3.1. Reflection of a light beam. E_s is directed out of plane, E_p is directed in plane. φ is the angle of incidence.	27
Figure 3.2. Example of change of polarization state due to a phase shift (Δ) a) linearly polarized; b) elliptically polarized.....	28
Figure 3.3. Reflection and refraction of light for supported thin layer.....	29
Figure 3.4. Examples of ellipsometric spectra of a silica/ γ -alumina sample and γ -alumina layer only, both applied onto an α -alumina substrate. The silica/ γ -alumina spectrum shows four peaks, whereas the thinner γ -alumina layer has three.....	29
Figure 5.1. Ellipsometry set-up	37
Figure 5.2. Photos of the ellipsometry set-up. Above: First part to sample cell (in circle). Below: Second part from sample cell to detector (outside picture). The gas-delivery set-up is located in the background.	38
Figure 5.3. Ellipsometry sample cell. Top: side view. Bottom: top view.....	39

Figure 5.4. Photos of the ellipsometry sample cell. Upper left: complete cell. Upper right: glass cell; the black tubes are connected to the oil bath. Below: side views of the roof.	40
Figure 5.5. Gas delivery set-up	41
Figure 5.6. Photos of the gas-delivery set-up	42
Figure 5.7. Bubbler schematically	43
Figure 5.8. Adjusting cell alignment. A: Lateral movement; B: Cell rotation; C: Cell tilting; D: Sample holder rotation.	46
Figure 5.9. Example of change in ellipsometry spectra upon water adsorption onto a silica sample. The arrow indicates the order of the measurements and hence, the progress of adsorption. Both “blank1” and “blank2” are measurements of the dry sample and are at the top of the series. For example, there is an obvious change in $\tan \Psi$ at 2.5 eV (≈ 496 nm) and hardly any change at 2.3 eV (≈ 539 nm). Sample: one silica layer and one γ -alumina intermediate layer on top of an α -alumina substrate.	47
Figure 5.10. Overview of valves for setting dry or wet flow.....	48
Figure 5.11. Plots of desorption rate vs. temperature for zero-, first- and second-order kinetics and several initial coverages θ_0 (Oura <i>et al.</i> , 2003).	52
Figure 6.1. Example of comparing blanks before and after an adsorption/desorption cycle. Sample is silica/ γ -alumina. $T_{\text{cell}} \approx 54^\circ\text{C}$	58
Figure 6.2. Adsorption sequence of energy scans. The arrow indicates the progress of adsorption. Sample is γ -alumina.....	58
Figure 6.3. Adsorption sequence of energy scans. The arrow indicates the progress of adsorption. Blank1 (\blacklozenge) and blank2 ($-$) are at the same position. Sample is silica/ γ -alumina.	59
Figure 6.4. Desorption from silica/ γ -alumina. No desorption occurred and all series of the sequence are at the same place: lower graph. The higher graph is blank2.....	59
Figure 6.5. A ‘correct’ series of energy scans. Each scan has been made at equilibrium, the moment of equilibrium being determined by a preceding time scan. The arrow indicates the progress of the adsorption.....	60
Figure 6.6. Example of a time scan. The start of a steady wet flow is marked on the left at ~ 280 s. The plateau is determined in the plot at sight.	60
Figure 6.7. Isotherms obtained for two different temperatures.	63
Figure 6.8. Adsorption on silica/ γ -alumina for $T_{\text{water}}=10^\circ\text{C}$. Due to a problem with the oil bath, T_{cell} dropped to 19°C	64
Figure 6.9. Adsorption plots at different relative pressures; in the left column, adsorption at 31°C and in the right column, adsorption at $52\text{--}56^\circ\text{C}$. The first and the third plot in the right column show a gap in the measurement series. That was because of a recording failure by the ellipsometer control software. Since the process of adsorption continued anyway, the recording was continued in a subsequent measurement taking into account the time elapsed during the error.	67
Figure 6.10. Desorption from silica/ γ -alumina at constant temperature in dry helium.....	68
Figure 6.11. Desorption steps in one run. The sample is silica/ γ -alumina and helium flow is ~ 46 ml/min.....	69
Figure 6.12. Desorption plots at different relative pressures and temperatures.....	70
Figure 8.1. Two water bubblers in a sequence in order to assure the carrier gas of being saturated with water vapor at the required temperature (T_{req}).	73
Figure 8.2. Design of new ellipsometry sample cell.	74

1 Introduction

In the current study, microporous silica membranes have been used to measure sorption characteristics using ellipsometry. In the following, a brief introduction is given on this type of membranes. Subsequently, the topic description is presented and finally, the content of the rest of the report is given.

1.1 Microporous silica membranes

Porous membranes separation processes can be divided into five different types according to their pore diameter:

- filtration ($d_p > 10^4$ nm)
- microfiltration ($10^2 < d_p < 10^4$ nm)
- ultrafiltration ($1 < d_p < 10^2$ nm)
- molecular sieving ($d_p < 1$ nm)
- reverse osmosis ($d_p < 1$ nm)

The processes are pressure driven and both porosity and pore size distribution are the most important characteristics that determine the separating behavior of the membrane. State-of-the-art microporous silica membranes are well suited for gas separation, i.e. molecular sieving, and are highly selective to hydrogen.

Microporous ceramic membranes are usually made of a stack of layers. The actual membrane layer, or so-called separating layer, is thereby supported by underlying layers. State-of-the-art microporous silica membranes are supported by a macroporous α -alumina layer and a mesoporous γ -alumina intermediate layer. The two supporting layers provide mechanical strength of the layer system. By definition (IUPAC), microporous materials have pore diameters of less than 2 nm, mesoporous materials 2–50 nm and macroporous materials have pore diameters of more than 50 nm. Figure 1.1 shows the layer system schematically.

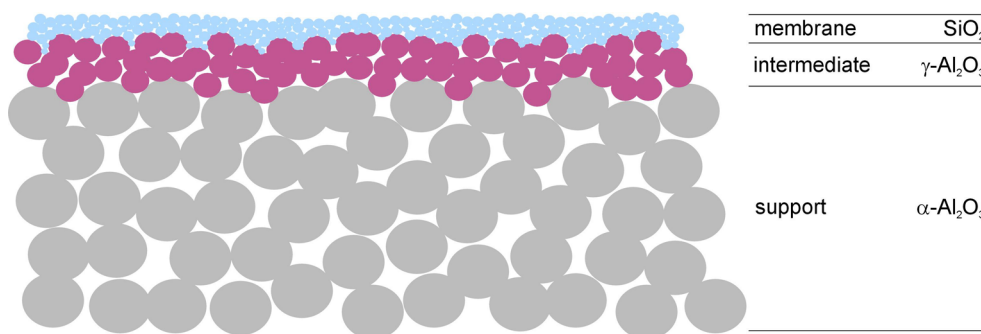


Figure 1.1. Microporous silica membrane layer system

The α -alumina supports are made by colloidal filtration after which they are sintered. Porosity is approximately 35%. The subsequent layers are applied by slip casting of a sol. The precursor sol for the γ -alumina layer is the acid-stabilized boehmite. Due to capillary forces of the underlying pore structure, the solvent goes into the pores and precipitation of sol particles occurs. After slip

casting, drying takes place at constant temperature (40°C) and constant relative humidity (60%). Subsequently, the layer is calcined during sintering occurs of the sol particles. A more detailed description on synthesis is given by Benes *et al.* (2000).

Table 1.1. Layer properties of a microporous silica membrane

Layer	Material	Thickness	Pore diameter (nm)
Top (membrane)	amorphous silica	~ 50 nm	0.3 – 0.5
Intermediate	γ -alumina	~ 3 μm	~ 4
Support	α -alumina	~ 2 mm	~ 160

Because of the microporosity, gas transport resistance is highly dependent on the thickness of the layer. Therefore, the thickness of the membrane layer is in the order of 50 nm and may not exceed 100 nm. The mesoporous and macroporous supporting layers show relatively negligible resistance to gas transport. As illustrated in Figure 1.1, the intermediate and top layer have penetrated their corresponding underlying layer to a certain extent. In that overlapping region, the porosity is relatively low and hence, gas transport resistance is relatively high.

Since a dip-coated layer penetrates the underlying layer, the surface is relatively rough. Surface coverage may not be sufficient and defects are likely to be present after drying and/or calcination. Therefore, both γ -alumina and silica layer are normally applied by dip coating twice. After the first dip, the membrane is dried and calcined. A second layer is applied subsequently. In this report, “one layer” of silica or γ -alumina indicates that the sample has been prepared by dip coating once and emphasizes the difference from the above mentioned standard procedure.

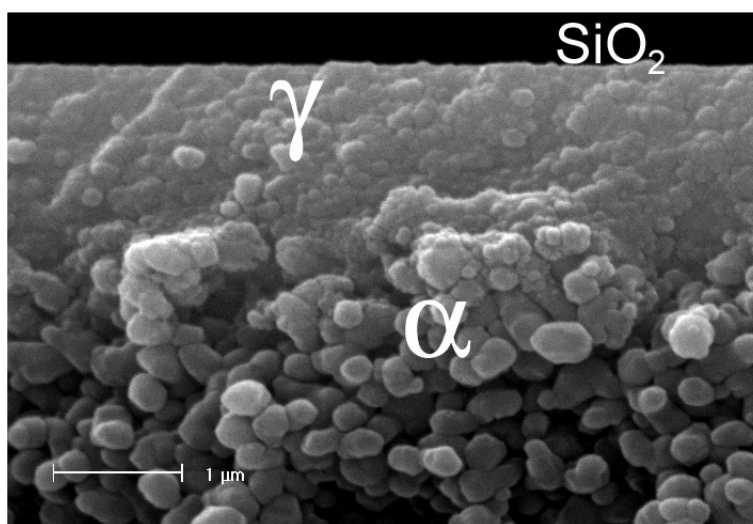


Figure 1.2. Cross section SEM micrograph of silica membrane. The silica membrane layer (SiO_2) is not visible in the graph since it is too thin.

1.2 Topic description

Porosity, surface area and pore size distribution (PSD) are important characteristics of porous thin layers for understanding chemical, thermal and mechanical properties (Muranova and Perveev, 1993). If pores are open, PSD and related characteristics can be obtained from adsorption porosimetry. A common method to apply adsorption porosimetry is nitrogen physisorption at the boiling point of nitrogen (77K). This technique uses bulk material of the layer of interest and hence, the measurements are not done on the actual layer itself. Moreover, layer properties are different from bulk. For example, pore diameter tends to decrease near the underlying layer (Benes *et al.*, 2001).

Ellipsometry is a non-destructive technique that can be used *in situ* and properties of the layer itself can be obtained. The technique is based on a change in polarization of light upon reflection. Ellipsometry can be used for adsorption of gases or vapors. The high sensitivity of the technique enables the recording of the small changes in optical response due to sorption.

The aim of the current research was to explore the possibilities of measuring sorption processes *in situ* on thin membrane layers with (spectroscopic) ellipsometry, specifically water vapor sorption. This involves:

- Design of the experimental set-up and measurement procedures, especially with respect to the supply of water vapor to the sample chamber.
- Obtaining useful adsorption and desorption characteristics from ellipsometry data.

The initial reason of using water vapor for sorption measurements in combination with ellipsometry was based on the known high-temperature (>300°C) effect of water. At low temperatures (< 300°C), water vapor is thought to adsorb physically onto the membrane layer (see more on physisorption in Chapter 2), whereas at high temperatures, water also reacts with the solid surface causing changes in microstructure. Not only does water change the microstructural properties of the silica top layer, it also causes the γ -alumina intermediate layer to become unstable. Therefore, the structure of the membrane as a whole changes as well.

Also, sorption data obtained from measurements with adsorbates of different molecular radii provide useful information on pore size distribution and porosity (Fardad *et al.*, 1995). Water is one of the smallest molecules (kinetic diameter) and the idea was to use a range of molecules of different sizes, for example NH_3 (2.6Å) \rightarrow H_2O (2.65Å) \rightarrow CO_2 (3.3Å) \rightarrow CH_4 (3.8Å) \rightarrow C_3H_8 (4.3Å).

However, one limitation of the set-up was the maximum temperature of around ~100 °C. Therefore, structural changes were not expected to be observed in the measurements. Nevertheless, the set-up involved the possibility of water vapor delivery and that is why water vapor was kept as an adsorbate in the current study.

1.3 Contents of this report

The report consists of mainly three parts: Theory, Experimental and a final part in which conclusions and recommendations are given.

In the theoretical part, sorption characteristics are discussed in Chapter 2. Special attention has been paid to microporosity since the samples in this research are microporous. Chapter 3 explains the basic principles of ellipsometry. The combination of sorption measurements and ellipsometry is reviewed in Chapter 4 involving a brief literature review.

The experimental part contains two chapters. Chapter 5 elaborates on the measurements done and gives explanation about the experimental set-up. Furthermore, the processing of obtained measurement data is explained. Chapter 6 presents and discusses the results.

The final part gives the conclusions in Chapter 7 and recommendations for further research in Chapter 8. Further information is provided with a list of references, a list of symbols and appendices. A separate overview of the different appendices is given.

Theory

2 Sorption characteristics

2.1 Introduction

Measurement of adsorption and desorption characteristics give valuable information on surface properties, such as porosity, pore size distribution and specific surface area.

When a gas or vapor (*adsorptive*) comes in contact with a solid (*adsorbent*), it will be adsorbed onto the solid surface (where it is named *adsorbate*). The reverse process is called *desorption* and in general, the processes of both adsorption and desorption are referred to as *sorption*.

During adsorption, enhancement occurs of the adsorbate-adsorbent interactions of the same order as those that exist between the molecules of a liquid (Grillet and Llewellyn, 1998). The type of interaction between adsorbent and adsorbate depends on the interfacial forces. Physical adsorption (*physisorption*) takes place due to Van der Waals forces and heats of adsorption are in the range of -20 kJ/mol (Atkins, 1994). Because of the relatively weak forces, the process does not lead to bond breaking and a physisorbed molecule retains its identity. In the case of a chemical bond, chemical adsorption occurs (*chemisorption*) and heats of adsorption are in the order of -200 kJ/mol (Atkins, 1994).

Distinguishing between physisorption and chemisorption is hard and a first estimation is based on the measured enthalpy change upon adsorption. In general, physisorption has enthalpy values less negative than -25 kJ/mol, whereas chemisorption is linked to values more negative than -40 kJ/mol (Atkins, 1994).

2.2 The adsorption isotherm

The extent to which adsorption has taken place is indicated by the *coverage* θ of the adsorbate on the adsorbent surface:

$$\theta = n_a / n_{\text{sat}} \quad (2.1)$$

where: n_a amount of adsorption sites occupied
 n_{sat} total amount of adsorption sites, or monolayer capacity

The amount of adsorbate depends on the partial vapor pressure of the adsorptive at a certain temperature. Coverage vs. relative pressure will give the adsorption isotherm and represents the adsorptive-adsorbate dynamic equilibrium at a constant temperature. The relative pressure is defined as follows:

$$p_r = p / p_{\text{sat}} \quad (2.2)$$

where: p partial vapor pressure of the adsorptive
 p_{sat} adsorptive vapor pressure at which the adsorbent is saturated

Theoretically, p_{sat} is the saturated vapor pressure of the adsorptive (for known temperature and ambient pressure) at which the adsorptive starts to condensate instead of adsorb onto the solid surface.

Three phenomena may be involved in physisorption:

- Monomolecular adsorption (*monolayer*);
- Multimolecular adsorption (*multilayer*);
- Condensation in pores or capillaries.

These phenomena are mainly dependent on the type of adsorbent. Six types of isotherms have been classified according to the type of adsorbent. Sing *et al.* (1985) described six different isotherms and the first five of them are applicable to silica (Ranke, 2002).

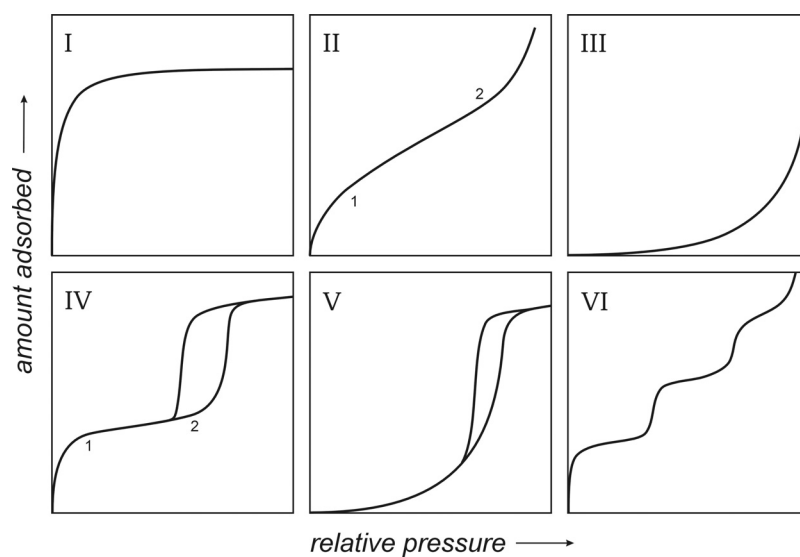


Figure 2.1. Six types of sorption isotherms according to Sing *et al.* (1985)

The sorption behavior is not specific for the type of adsorbent itself but for the adsorbate-adsorbent interactions as a whole. Therefore, a combination of the mentioned adsorption behaviors is possible resulting in a more complex isotherm.

The isotherms are shown schematically in Figure 2.1. Usually, point 1 marks the end of monolayer formation and the start of multilayer adsorption in the quasi-linear middle region 1-2. In Table 2.1, the types are discussed briefly with the main characteristics.

Table 2.1. Main characteristics of the different sorption isotherms (Sing *et al.*, 1985)

Type I (Langmuir isotherm)	Type II	Type III
<ul style="list-style-type: none"> ▪ Microporous adsorbents and also chemisorption onto solid surfaces ▪ Restriction of adsorbate multilayer formation due to steric constraints ▪ n_a approaches n_{sat} as $p_r \rightarrow 1$ 	<ul style="list-style-type: none"> ▪ Macroporous or non-porous adsorbent ▪ Multilayer formation ▪ The adsorption energy for the first layer is higher than the condensation enthalpy of the adsorbate. 	<ul style="list-style-type: none"> ▪ Macroporous or non-porous adsorbent ▪ Multilayer formation ▪ The energy of first layer formation is of the same order as adsorbate condensation energy. As a result, point 1 cannot be determined.
Type IV & V		Type VI
<ul style="list-style-type: none"> ▪ Mesoporous adsorbent ▪ Capillary condensation after monolayer formation ▪ Hysteresis due to capillary condensation 		<ul style="list-style-type: none"> ▪ Non-porous adsorbent ▪ Stepwise, discrete multilayer formation

2.3 Micropore adsorption

The samples used in the current research are membranes that contain a top microporous selective layer (see also paragraph 1.1). Therefore, more information is provided on micropore adsorption.

2.3.1 Adsorption on microporous silica

According to Kiselev (reference of Grillet and Llewellyn, 1998) adsorbent/adsorbate interactions as well as adsorbate/adsorbate interactions can be classified with two terms: non-specific interactions and specific interactions. The first type of interactions only involves intermolecular attraction and repulsion forces. In the case of specific interactions, the electric moment is not zero and, e.g., dipole moments are present. Table 2.2 gives the complete classification.

Table 2.2. Classification of non-specific (n) and specific (s) sorption for different types of adsorbate and adsorbent (Grillet and Llewellyn, 1998)

	Adsorbate type			
	A	B	C	D
	spherical symmetry (e.g. Ar)	locally concentrated electronic density (e.g. N ₂)	locally concentrated positive charge (e.g. CO ₂)	functional groups with a locally concentrated positive charge + locally concentrated electronic density (e.g. H ₂ O)
Adsorbent type				
I Neutral surfaces (without active groups)	n	n	n	n
II Locally concentrated positive charges	n	n+s	n+s	n+s
III Locally concentrated negative charges	n	n+s	n+s	n+s

The microporous silica samples subject to the current study are hydroxylated and therefore, the samples are of type II. With regard to this classification, the generally used nitrogen as well as water vapor induces both non-specific and specific interactions. Regardless of the surface charge of silica, argon adsorption (at 77K) always involves only non-specific interactions and the isotherm can directly give information on the texture of silica.

Grillet and Llewellyn (Legrand, 1998) give an example of a nitrogen adsorption isotherm at 77K and a water adsorption isotherm at 300 K on ‘Rhone Poulenc’ microporous silica samples, type S. Water gives a better estimation of total surface area because of the smaller kinetic diameter (0.265 nm) which enables the water molecule to enter pores with openings of smaller than 0.4–0.5 nm. They observed activated desorption due to the smaller micropore openings.

2.3.2 Micropore filling and surface area

The classical explanation of the isotherm (type I) plateau at high relative pressures refers to the end of monolayer adsorption and hence, the value of the plateau at $p_r \rightarrow 1$ can be used for surface area calculation. Surface area A_s is defined as:

$$A_s = n_{\text{sat}} N_{\text{AV}} a_m \quad (2.3)$$

where: N_{AV} Avogadro number
 a_m effectively occupied area by an adsorbed molecule

The *specific* surface area is the surface area A_s per unit mass of adsorbent.

The term *micropore filling* has been introduced to distinct the primary process of pore space filling from the secondary process of capillary condensation in mesopores (Sing *et al.*, 1985; Legrand, 1998). Micropore filling can occur at lower relative pressures than capillary condensation.

Nowadays, another explanation is used for adsorbate layer formation. The steep first part of the isotherm (type I) is related to micropore filling whereas the subsequent part is due to multilayer adsorption onto the relatively small external surface (outside the micropores). It seems to be likely that there are two different mechanisms of pore filling: 1) at low p_r , individual adsorbate molecules enter very narrow pores and 2) at somewhat higher p_r , cooperative adsorption occurs involving adsorbate-adsorbate interaction. The latter mechanism is likely to be present in the case of water vapor (as the adsorbate) due to the relatively high intermolecular forces of hydrogen bonds. Cooperative adsorption may induce multilayer adsorption.

In case of micropore filling, the interpretation of the adsorption isotherm in terms of surface coverage may lose its physical significance. The limiting amount of adsorbate, n_{sat} , is determined by the accessible micropore volume, rather than by the internal surface area. Therefore, although the BET estimation is widely used to characterize the surface area, it fails to give the true value for microporous adsorbents. It may then be convenient to define a “monolayer equivalent area”. This equivalent area would be the specific area if the molecules required to fill the micropores, were spread in a close-packed monolayer of molecules.

2.3.3 Estimation of microporosity

Porosity is by definition (IUPAC) the volume ratio of open pores to the total volume of the body. Hence, closed pores that are not reachable by an adsorptive molecule, are not determined. Several different models have been developed to evaluate microporosity (Legrand 1998, and references herein). Dubinin and Radushkevich have based their model on the concept of a characteristic curve independent on temperature. Subsequently, micropore volume is determined assuming a liquid phase of the adsorbate present in the micropores. The volume of adsorbate inside the pores W is related to the total micropore volume W_0 at a certain relative pressure p_r by:

$$\ln W = \ln W_0 - \left(\frac{-RT \ln p_r}{\beta E_0} \right)^2 \quad (2.4)\text{-a}$$

with: $w_0 = K/E_0$ (2.4)\text{-b}

and: $E_{\text{ads}} = \beta E_0$ (2.4)\text{-c}

where: E_{ads} isosteric heat of adsorption
 β affinity coefficient
 E_0 characteristic heat of adsorption
 w_0 average pore width
 K coefficient slightly changing with E_0

De Boer's t -plots have been created by measuring different reference isotherms. The t method makes use of the BET equation for determination of the volume adsorbed by the sample. A similar method has been proposed by Sing.

The method of Horvath and Kawazoe (HK) is probably the most used in commercial high-resolution apparatus. The model is based on the shift of the Lennard-Jones type potential functions for isothermal data and determines the 'effective' micropore diameter. Although the HK method can give accurate results, it requires critical assessment by the user since artifacts can be introduced easily.

2.3.4 Estimation of mesoporosity

In contrast to the above methods, evaluation of mesoporosity is carried out by different methods (Legrand 1998, and references herein). Generally, the Gibbs-Thomson or better known as Kelvin equation is used. Since capillary condensation is an important process in mesoporous materials, the Kelvin equation not only relates the coverage to relative pressure, but also to the curvature of the meniscus, which is formed by the liquid adsorbate inside the pores and on the adsorbent surface. The curvature is determined by surface tension and the wetting angle (Shaw, 1992). In the case of microporous adsorbents, the concept of a meniscus fails because the pore diameter is of the same order as the size of the adsorbate molecules. That is why the Kelvin equation is not valid for micropores.

An important method that uses the Kelvin equation is the BJH method (Barret, Joiner and Halenda), which specifically analyses the desorption branch of the isotherm. The desorption branch should represent the capillary condensation region (Kelvin eq.) and pores are assumed to be cylindrical or flat. Furthermore, it is assumed that a multimolecular layer covers the pore walls.

2.3.5 Langmuir isotherm

The Langmuir adsorption model is applicable to physisorption onto solids with a very fine pore structure and also to chemisorption onto solid surfaces. In the adsorption model, the following assumptions have been made:

- The adsorbent surface is flat.
- Adsorption is restricted to monolayer formation.
- All adsorption sites are energetically equivalent.
- Each adsorption site can host one adsorbate particle (non-dissociated molecule or atom) (1-to-1 adsorption).
- Adsorbate particles do not interact with each other.

For the sake of simplicity, the process of micropore filling is referred to as surface coverage, although there is a difference in mechanism (see the previous paragraph 2.3.2).

Under isothermal conditions, the rate of adsorption and hence, the change in surface coverage, is proportional to the partial vapor pressure p of the adsorptive and of the amount of free adsorption sites $(1 - \theta)$. This leads to the following expression:

$$\frac{d\theta}{dt} = k_{\text{ads},n} p_r (1 - \theta)^n \quad (2.5)$$

where: n kinetic order of the process [-]
 $k_{\text{ads},n}$ adsorption rate constant for kinetic order n

The desorption rate is proportional to the amount of occupied adsorption sites θ :

$$\frac{d\theta}{dt} = k_{\text{des},n} \theta^n \quad (2.6)$$

where: $k_{\text{des},n}$ desorption rate constant for kinetic order n

At equilibrium, the net rate of sorption is zero. Then, using eq. (2.5) and (2.6), the Langmuir isotherm is obtained:

$$\theta = \frac{(K_L p_r)^{1/n}}{1 + (K_L p_r)^{1/n}} \quad (2.7)$$

with: $K_L = k_{\text{ads},n} / k_{\text{des},n}$ (2.8)

where: K_L Langmuir sorption equilibrium constant [-]

In the following paragraphs¹, both adsorption and desorption kinetics are discussed in more detail. The above Langmuir equation is deduced subsequently.

¹ The paragraphs 2.4, 2.5 and 2.6 are mainly based on Oura *et al.* (2003), unless indicated otherwise.

2.4 Adsorption kinetics

2.4.1 Adsorption paths

In general, the adsorption of a gas molecule depends on the probability of reaching an adsorption site. As a molecule nears the solid surface, it can proceed in the following possible directions:

- Instantaneous adsorption directly onto an adsorption site; or
- Transition to a precursor state:
 - o Extrinsic precursor state (EP): onto an occupied adsorption site.
 - o Intrinsic precursor state (IP): onto a free adsorption site

From the EP position, the molecule may either desorb or move into IP from where final adsorption may occur at the free adsorption site or desorption back to the gas phase. Figure 2.2 shows the different possibilities schematically.

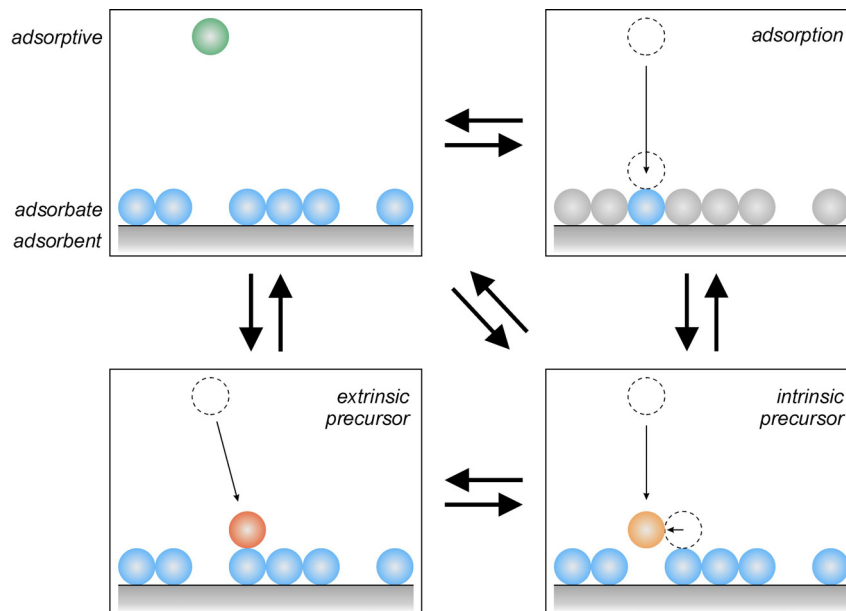


Figure 2.2. Different possible adsorption paths

2.4.2 Sticking coefficient

The probability that molecules will adsorb onto the solid surface is indicated by the *sticking probability* or *coefficient* s . This coefficient is the proportion of collisions with the surface that successfully lead to adsorption. The general expression for the sticking coefficient is:

$$s = \sigma f(\theta) \exp(-E_{\text{act}}/k_{\text{B}}T) \quad (2.9)$$

Here, three terms affecting the sticking coefficient are distinguished:

- σ condensation coefficient, includes steric effects and accommodation of adsorbate molecules (atoms) [-]
- $f(\theta)$ coverage dependent function which describes the probability of finding an adsorption site [-]

$\exp(\cdot)$ temperature-dependent Boltzmann term, which is associated with activated adsorption [-]

2.4.3 Adsorption rate

The flux I with which adsorptive molecules reach the solid surface is dependent on the type of molecule (or atom), the partial vapor pressure and temperature.

$$I = \frac{p}{\sqrt{2\pi m k_B T}} \quad (2.10)$$

where: I flux [$\text{m}^{-2} \cdot \text{s}^{-1}$]
 p partial pressure of adsorptive [Pa]
 m particle (molecule or atom) mass [kg]
 k_B Boltzmann constant [$\text{J} \cdot \text{K}^{-1}$]
 T temperature [K]

For a specific surface area A , the adsorption rate [s^{-1}] becomes:

$$r_{\text{ads}} = s I A \quad (2.11)$$

In the following, the coverage dependence and the temperature dependence of the sticking coefficient, i.e. the adsorption rate, are discussed in more detail.

2.4.4 Coverage dependence

The coverage dependent function $f(\theta)$ in eq. (2.9) is affected by the type of the adsorption reaction, statistics of site occupation and the mobility of adsorbate molecules in a precursor adsorption state. In this report, the focus lies on the type of adsorption: non-dissociative or dissociative¹.

Non-dissociative Langmuir adsorption

According to the Langmuir model for non-dissociative adsorption, every free adsorption site is readily available and independent of possible occupied neighboring sites:

$$f(\theta) = 1 - \theta \quad (2.12)$$

In this case, the adsorption rate is:

$$\frac{d\theta}{dt} = s_0 (1 - \theta) I A \quad (2.13)$$

with s_0 being the sticking coefficient at zero coverage.

¹ When an adsorptive molecule as a whole adsorbs onto the solid surface, the process is non-dissociative. Otherwise, it is dissociative. For example, a CO molecule could stay as it is (non-dissociative) or it can dissociate into a C and an O atom upon adsorption. According to the Langmuir model, both the C and the O atom will occupy separate adsorption sites subsequently.

Dissociative Langmuir adsorption

When the adsorptive molecule dissociates into n atoms (parts) upon adsorption, the coverage-dependent function becomes:

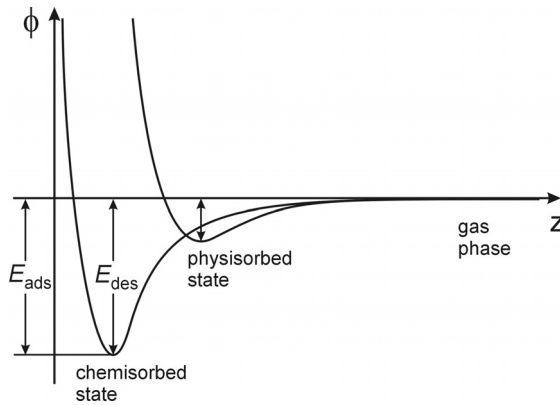
$$f(\theta) = (1 - \theta)^n \quad (2.14)$$

Consequently, each atom occupies an adsorption site. The order of the adsorption process is indicated by this number, n .

2.4.5 Temperature dependence

For most simple chemisorption processes (without precursor state), the sticking coefficient (eq. (2.9)) is practically temperature independent. This is because for most chemisorption processes,

the heat of adsorption is much larger than the value of $k_B T$, which means that possible desorption has little effect on the adsorption energetics.



The one-dimensional Lennard-Jones potential shows the general trend for gas/surface interaction (Figure 2.3). This graph shows simple adsorption (non-dissociative and without a precursor state). Compared to chemisorption, physisorption has a shallower well in which the adsorbate is present.

Figure 2.3. Lennard-Jones potential curves for simple physisorption and chemisorption (based on Oura *et al.*, 2003, p.303)

In the case of precursor-mediated chemisorption (Figure 2.4), a second well is present, representing the physisorption of the adsorptive into the precursor state. The next step for the molecule in the precursor state is a deeper well for the final chemisorption or it desorbs back into the gas phase.

The rates for adsorption and desorption from the precursor state are given by:

$$r_{\text{ads}}^{\text{p}} = \theta_{\text{p}} k_{\text{ads}}^{\text{p}} \exp(-\varepsilon_{\text{ads}}/k_B T) \quad (2.15)$$

$$r_{\text{des}}^{\text{p}} = \theta_{\text{p}} k_{\text{des}}^{\text{p}} \exp(-\varepsilon_{\text{des}}/k_B T) \quad (2.16)$$

where: θ_{p} precursor coverage [-]
 $\varepsilon_{\text{ads}}, \varepsilon_{\text{des}}$ precursor energy barriers for adsorption and desorption, respectively [J]

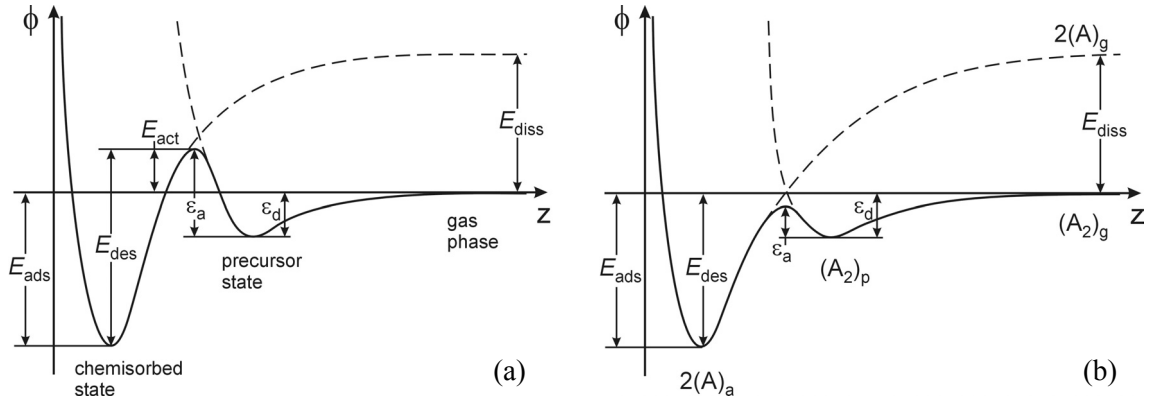


Figure 2.4. Lennard-Jones potential curves for (a) activated and (b) non-activated chemisorption (based on Oura *et al.*, 2003, p. 304)

Consequently, the initial sticking coefficient is given by:

$$s_0 = \frac{r_{\text{ads}}^{\text{p}}}{r_{\text{des}}^{\text{p}} + r_{\text{ads}}^{\text{p}}} = \left[1 + \frac{k_{\text{des}}^{\text{p}}}{k_{\text{ads}}^{\text{p}}} \exp\left(\frac{\varepsilon_{\text{ads}} - \varepsilon_{\text{des}}}{k_{\text{B}}T}\right) \right]^{-1} \quad (2.17)$$

Figure 2.4a shows activated dissociative chemisorption and Figure 2.4b non-activated dissociative adsorption. In the case of activated adsorption, $\varepsilon_{\text{des}} < \varepsilon_{\text{ads}}$ and eq. (2.17) gives an increasing s_0 with increasing temperature. Non-activated adsorption involves $\varepsilon_{\text{des}} > \varepsilon_{\text{ads}}$ and consequently, s_0 decreases with increasing temperature.

2.5 Desorption kinetics

2.5.1 Desorption rate

Basically, the process of desorption occurs when the energy of the adsorbate is high enough to surmount the energy barrier E_{des} . This process is called *thermal desorption*. In the case of activated chemisorption (see Figure 2.4a), E_{des} is equal to $(E_{\text{ads}} + E_{\text{act}})$ and in the case of non-activated chemisorption (see Figure 2.4b), E_{des} is equal to E_{ads} .

The Polanyi-Wigner equation describes the desorption rate [s^{-1}] with the same assumptions as Langmuir (equivalent adsorption sites and no interaction between adsorbed molecules):

$$r_{\text{des}} = -\frac{d\theta}{dt} = k_{\text{des},n} \theta^n \quad (2.18)\text{-a}$$

$$\text{with: } k_{\text{des},n} = k_{\text{des},n}^0 \exp(-E_{\text{des}}/k_{\text{B}}T) \quad (2.18)\text{-b}$$

where: $k_{\text{des},n}$ desorption rate constant [s^{-1}]
 E_{des} desorption activation energy [J]
 n kinetic order of desorption [-]

2.5.2 Order of desorption

The kinetic order of desorption is given by n in eq. (2.18). Table 2.3 gives the most general cases. More complex cases are possible, including fractional orders of desorption.

Table 2.3. Description of general cases of kinetic order of desorption

Kinetic order	Properties	Expression	
zero-order ($n = 0$)	<ul style="list-style-type: none"> - coverage-independent - normally in diluted systems - desorption from homogeneous multilayer film 	$\theta = \theta_0 \left(1 - \frac{k_{\text{des},0} t}{\theta_0} \right)$	(2.19)
first-order ($n = 1$)	<ul style="list-style-type: none"> - proportional to θ - simple desorption of an adsorbate, independent of neighboring sites - $k_{\text{des},1}^0$ is the <i>attempt frequency</i> 	$\theta = \theta_0 \exp(-k_{\text{des},1} t)$	(2.20)
second-order ($n = 2$)	<ul style="list-style-type: none"> - proportional to θ^2 - associative desorption 	$\theta = \frac{\theta_0}{1 + k_{\text{des},2} \theta_0 t}$	(2.21)

The attempt frequency (first-order) is normally expressed as the *mean stay time* or *mean surface lifetime*, τ [s]:

$$\tau = 1/k_{\text{des},1}^0 \quad (2.22)$$

2.6 Dynamic equilibrium

When there is a thermodynamic equilibrium between adsorptive and adsorbate, the net rate of sorption is zero, i.e. $r_{\text{ads}} = r_{\text{des}}$. For Langmuir adsorption, the general expression is a combination of eq. (2.13) and (2.14):

$$\frac{d\theta}{dt} = s_0 (1 - \theta)^n I A \quad (2.23)$$

There, the initial sticking coefficient s_0 and flux I are temperature-dependent. Furthermore, the flux is also pressure-dependent. In the case of constant temperature, the expression is reduced to eq. (2.5) with:

$$k_{\text{ads},n} = k_{\text{ads},n}^0 \exp(-E_{\text{act}}/k_{\text{B}}T) \quad (2.24)$$

in which the rate constant $k_{\text{ads},n}$ is related to the initial sticking coefficient s_0 and $k_{\text{ads},n}^0$ to the temperature-dependent term of the flux. Combination of eq. (2.5) and (2.18) gives the Langmuir equation (2.7). Since E_{des} is equal to $(E_{\text{ads}} + E_{\text{act}})$, the ratio of K_{L} can be given in an Arrhenius expression:

$$K_{\text{L}} = K_{\text{L}}^0 \exp(E_{\text{ads}}/k_{\text{B}}T) \quad (2.25)$$

where:

$$\begin{aligned} K_{\text{L}}^0 & \quad K_{\text{L}} \text{ at constant temperature for an ideal mono-atomic gas [-]} \\ E_{\text{ads}} & \quad \text{isosteric heat of adsorption [J]} \end{aligned}$$

3 Ellipsometry

3.1 Introduction

The principle of ellipsometry is based on the interaction between light and matter. Ellipsometry is the measurement of the change in polarization state of an incident light beam upon reflection on a surface. The name of ellipsometry stems from the fact that the most general state of fully polarized light is elliptic.

The most common use of this technique is the analysis of (stacks of) thin layers, ranging from several micrometers down to a few Ångstroms. In case of a supported thin film, the incident light beam is partly reflected from the film/ambient interface and partly from the film/support interface after penetration into the film. As a result, optical constants and thickness of the sample can be determined.

Electrons of the material get polarized due to the electric field of the incident light beam. The *polarizability* α of a solid is the ease with which an atom or ion can be polarized by an electric field (Shriver, 1994). For an ensemble of particles, the polarizability is given by the dielectric function (Born and Wolf, 1986):

$$\tilde{\epsilon} = \epsilon_1 + i\epsilon_2 \quad (3.1)$$

The complex refractive index \tilde{n} is related to the dielectric function and is a representation of the optical constants of a material:

$$\tilde{n} = n + ik \quad (3.2)$$

and: $\tilde{n}^2 = \tilde{\epsilon}$ (3.3)

where: n refractive index (real part)
 k extinction coefficient (imaginary part)

The refractive index is related to the speed of light in the material and the change of direction of the light beam, whereas the extinction coefficient represents to which extent the amplitude of the light wave decreases in the material.

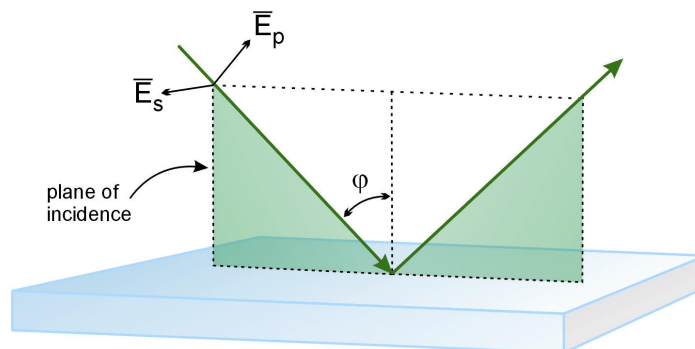


Figure 3.1. Reflection of a light beam. E_s is directed out of plane, E_p is directed in plane. ϕ is the angle of incidence.

3.2 Reflection

Reflection induces a change of the p and s waves in their phases and their amplitudes. The p direction is parallel to the plane of incidence and the s direction is perpendicular to the plane of incidence. Figure 3.1 shows the reflection schematically.

The incident light beam is linearly polarized, which means that there is no phase difference between the p and s waves. After reflection, the light is elliptically polarized due to a phase shift in the p and/or s direction.

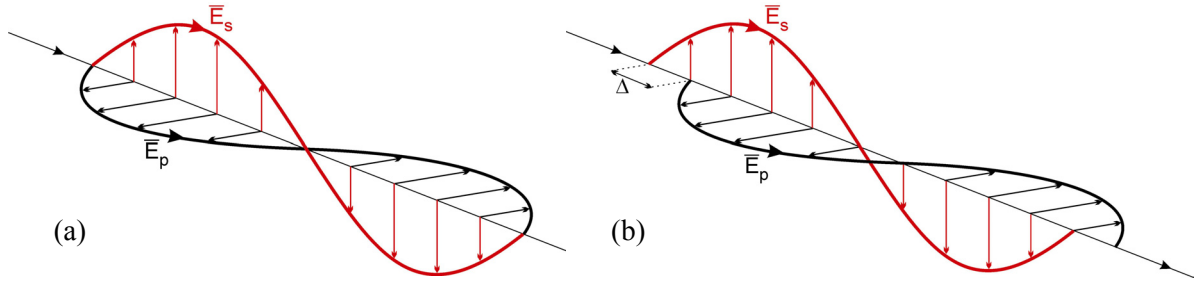


Figure 3.2. Example of change of polarization state due to a phase shift (Δ)
a) linearly polarized; b) elliptically polarized.

The change in phases is characterized by the angle Δ and the change in amplitudes by the angle Ψ . The phase shift is defined as:

$$\Delta = \delta^i - \delta^r \quad (3.4)$$

where δ^i and δ^r are the phase differences between the p and s waves before and after reflection, respectively. The angle Ψ is related to the ratio of amplitude ratios before and after reflection:

$$\tan \Psi = \frac{A_p^r / A_p^i}{A_s^r / A_s^i} \quad (3.5)$$

The total change is expressed with a complex quantity ρ :

$$\rho = \frac{R_p}{R_s} = \tan(\Psi) e^{i\Delta} \quad (3.6)$$

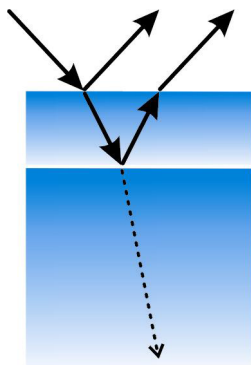
where R_p and R_s are the complex (total) Fresnel reflection coefficients (Azzam & Bashara, 1986).

The angles Δ and Ψ are a function of the

- wavelength of incident light λ
- angle of incidence φ
- refractive index of the ambient n_0
- refractive index of layer i n_i (in case of a (stack of) supported thin film(s))
- thickness of each layer i t_i (")
- refractive index of the support n_s (")

3.3 Layer properties with ellipsometry

As mentioned previously, the layer properties can be determined using the optical properties. As a light beam hits the surface of the transparent dielectric, it is partly reflected while the rest enters the layer. Then, the beam reflects onto the interface of the layer and the underlying layer.



Again, part of the beam refracts and continues in the underlying layer. Extinction occurs to a certain extent in subsequent and thicker layers. The resulting total reflected beam in the ambient is a combination of differently reflected/refracted beams and hence, interference effects are present.

For a stack of dielectric material, such as alumina and silica, the value of Δ remains close to 0° or 180° (Benes *et al.*, 2001) and hence, the signal of interest is $\tan \Psi$. A measurement of $\tan \Psi$ as a function of wavelength¹ shows an oscillating character which is due to the layer thickness: the thicker the layer the more oscillations.

Figure 3.3. Reflection and refraction of light for supported thin layer.

In Figure 3.4, examples are given for the typical ellipsometric spectra obtained. Silica and γ -alumina are relatively thin and a measurement of both layers applied onto an α -alumina substrate will result in a combined signal of both layers. Therefore, layer characteristics have to be obtained separately.

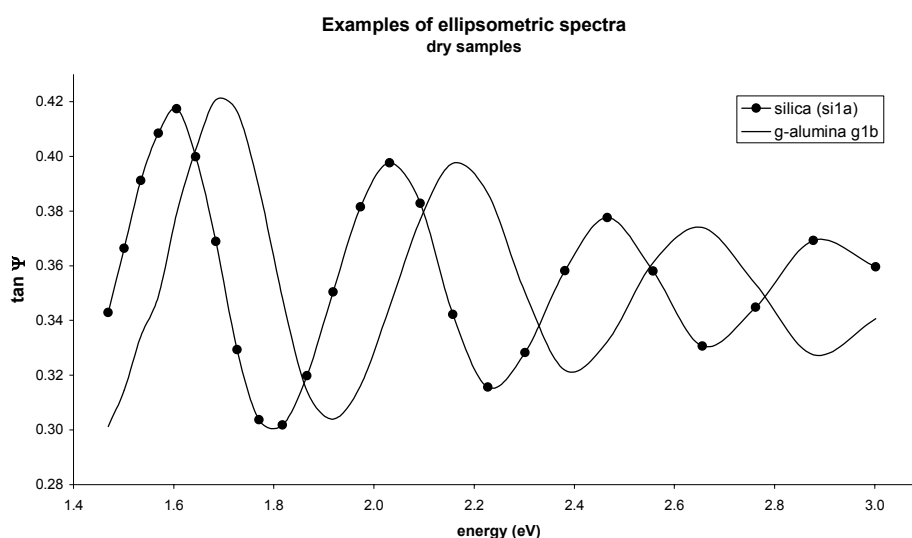


Figure 3.4. Examples of ellipsometric spectra of a silica/ γ -alumina sample and γ -alumina layer only, both applied onto an α -alumina substrate. The silica/ γ -alumina spectrum shows four peaks, whereas the thinner γ -alumina layer has three.

More about applications of (spectroscopic) ellipsometry related to adsorption studies is discussed in Chapter 1.

¹ Wavelength can be converted into energy of light using: $E = 1240/\lambda$ (E in [eV], λ in [nm]).

4 Sorption measurements with ellipsometry – a review

4.1 Introduction

It is widely acknowledged that ellipsometry is a promising technique for the characterization of porous thin films. The fact that it is non-destructive and *in situ* provides several advantages. Baklanov and Mogilnikov (2002, and references herein) provide an elaborate comparison between the advanced non-destructive techniques of today, with regard to the characterization of porous dielectrics:

- Spectroscopic ellipsometry (SE)
- Ellipsometric porosimetry (involves ellipsometric recording of adsorption) (EP)
- Small-angle neutron and X-ray scattering (SANS, SAXS)
- Specular X-ray reflectivity (XRR)
- Positron annihilation spectroscopy (PALS, PAS)
- Surface acoustic wave spectroscopy (SAWS)

An overview of their conclusions is given in Table 4.1 (terms used in the table are not explained further; please refer to the source: Baklanov and Mogilnikov, 2002 – Table 2).

Table 4.1. Comparative characteristics of techniques used for the non-destructive characterization of porous low-k dielectric films (Baklanov and Mogilnikov, 2002 – Table 2)

Problem	SE	EP	SANS	SAXS	XRR	PALS	PAS	SAWS
Open pore size		•	•	•		o	•	
Closed pore size			•	•		•	•	
Full porosity	o	o	o		o	o	o	o
Closed pore volume		o	o			o	o	
Open pore volume		•	o			o	•	
PSD		•				•	•	
Film density	o	o			•			•
Film thickness	•	•						
Refractive index	•	•						
Specific surface area		•	o					

• = proven option; o = option that has been realized but may have problems

4.2 Adsorption & ellipsometry

Table 4.1 shows that sorption studies using ellipsometry (EP) are promising since it is possible to determine many important characteristics. Tolmachev (1999) gives a short overview of the ‘current status’ of ellipsometric studies of physisorption and states that the investigation of thin layers is done best using optical methods. The refractive index is a typical characteristic of a film and can be obtained easily with ellipsometry. The process of water adsorption inside the pores corresponds to an increase of the (effective) refractive index and SE is sensitive to that change (so, $\tan \Psi$ changes). Therefore, it is possible to determine the pore size distribution using the isotherm of the change of refractive index vs. relative pressure.

Moreover, Alvarez-Herrero *et al.* (2001) indicate that the plot of $\tan \Psi$ vs. RH (relative humidity, the p_r of water vapor) has the same shape as the refractive index vs. RH. Subsequently, a linear relationship has been presented between $\tan \Psi$ and the refractive index and hence, the change in $\tan \Psi$ is proportional to the extent of surface coverage. They verify this relationship mathematically in the corresponding article.

They also point out that, in literature, it is assumed that water vapor is not the most suitable gas for PSD calculations. Water is polar with strong intermolecular forces (e.g., H-bonds), which may induce multilayer adsorption before the monolayer is finished. Dultsev and Baklanov (1999) agree that non-polar liquids without a permanent dipole moment are preferred. They searched for a liquid that could serve as adsorptive at room temperature and found that toluene was suitable, also because of the fact that it is often used for surface area determination. However, most publications reviewed here have reported water vapor as an adsorptive and PSD and porosity are determined consequently.

Tolmachev (*et al.*) developed a so-called adsorption-ellipsometric method (AE), first reported in 1991 (ref. 22 in the publication of 1999). The AE technique focuses mainly on the determination of pore size (diameter) and pore size distribution, whereas the adsorptive is mainly water vapor. Also, the refractive index of the porous sample has been determined by applying this adsorption-ellipsometric method. The samples have a porosity of $\sim 10\%$. Although that value is probably too small for effective operation of inorganic gas-separating membranes ($\sim 20\%$), the principle of the AE method is very well applicable. The publication of Benes *et al.* (2001) is one of the first instances of ellipsometric sorption studies on thin layers of microporous *membranes*. They used the same ellipsometer, the same sample cell and samples prepared in an identical manner as in the current research. Sorption isotherms were obtained with CO_2 and they obtained values for thickness and heat of adsorption of the silica top-layer as well as the γ -alumina intermediate layer.

Alvarez-Herrero *et al.* (2001, 2002) have performed ellipsometric characterizations on mesoporous samples (porous Vycor glass and evaporated TiO_2 , respectively). They have used a combination of SE and side-polished fiber (SPF) optics. For SPF, the sample film is directly deposited onto the fiber. SE data gives global information on PSD, refractive index and roughness, whereas SPF provides local info on PSD near the film/fiber interface. Hence, SPF could determine anisotropy, which was verified by SE.

Denoyel (2002) acknowledges the fact that ellipsometry can be used well for determining adsorption isotherms but he adds the restrictions that ellipsometry would require well-defined reflecting flat surfaces. The use of silicon wafers as a substrate for a thin layer is emphasized.

Microporous amorphous silica is reflecting to a certain extent but definitely not flat. The roughness of the silica layers is even increased by applying this layer on top of a rough γ -alumina layer instead of, for example, a flat silicon wafer. In practice, the roughness of a silica or γ -alumina is obvious since the light spot of the ellipsometer light beam is clearly visible due to the scattering of the light. This is in contrast with flat silicon samples, for example, from which the light beam is reflected relatively well in the same direction.

Also, Denoyel indicates that a great advantage of ellipsometry is the fact that not only the adsorption isotherm can be obtained but also the *process* (kinetics) of adsorption can be monitored. In the last decade, ellipsometry has been successfully used for monitoring surfactant adsorption processes. Information on the very early stages of adsorption is obtained which is practically impossible for classical adsorption porosimetry techniques, such as nitrogen physisorption.

Another application of adsorption-ellipsometry is the effect of water during the synthesis of a silica sol, which has been carried out by Fardad *et al.* (1995). Water vapor adsorption has been reported for a few samples made with different amounts of water and calcined at different temperatures. The results were Langmuir-type isotherms (the temperature at which the measurements were done is not mentioned, though). Unfortunately, the articles focuses on the difference in characteristics of the samples more than on the technique of ellipsometry in combination with the sorption measurements.

Further, they report results on the technique of *molecular probe ellipsometry* (as they call it). The technique is based on using different (sizes of) adsorbate species in order to probe pore sizes. The smaller the adsorbate, the more (smaller) pores can be filled. PSD's are indicated by graphs of volume fraction of porosity vs. adsorbate size. The graphs indicate a broad distribution, which can also be seen in the Langmuir isotherms due to the relatively small slope at low pressures. The different dimensions of the various adsorbates that Fardad *et al.* used, were estimated using bond length and Van der Waals atomic radii. The estimation of the water molecule was 3.28 Å and was significantly different from the value reported by Alvarez-Herrero *et al.* (2002). The latter use a water molecular diameter of ~1.3 Å, 'depending on the orientation'. Chaplin (2004), presents a mean Van der Waals diameter of ~3.2 Å and adds that the molecule is clearly not spherical, resulting in a variation of $\pm 5\%$.

Imai *et al.* (1997) reported studies on the structural change due to water vapor exposure of sol-gel derived dried silica gels. They were compared to amorphous porous silica films heated in dry atmosphere at temperatures above 500°C. The latter are of more interest in the current study but unfortunately, the focus lay on the silica gels and no useful results are provided.

4.3 Further calculations

The determination of characteristics as layer thickness, PSD and porosity requires knowledge of the absolute value of the amount of adsorbate. Calculations from ellipsometric sorption data are based on the estimation of effective refractive index (or dielectric function) using various equations. It is an effective value since it represents a combination of two or more fractions of material. As different material, normally the pores and the solid matrix are distinguished.

The relation between total polarizability and dielectric behavior is described by equations such as *Lorentz-Lorenz*, *Newton-Laplace* and *Bragg-Pippard* (Muranova and Perveev, 1993). The

equations give similar results but the Lorentz-Lorenz equation is more widely used. Some researches do not elaborate on the model that they used and only mention the use of the Lorentz-Lorenz equation (Baklanov *et al.*, 2000).

Tolmachev *et al.* (1993) use both Maxwell-Garnett and Lorentz-Lorenz and the results show that values for refractive index obtained by the Lorentz-Lorenz estimation are 13–15% lower. Benes *et al.*, Tolmachev and Alvarez-Herrero *et al.* explain the use of the Bruggeman effective medium approximation (EMA). The Bruggeman EMA gives the effective dielectric function:

$$f \frac{\epsilon_{\text{pore}} - \langle \epsilon \rangle}{\epsilon_{\text{pore}} + 2\langle \epsilon \rangle} + (1-f) \frac{\epsilon_{\text{solid}} - \langle \epsilon \rangle}{\epsilon_{\text{solid}} + 2\langle \epsilon \rangle} = 0 \quad (4.1)$$

where: f volume fraction of pores [-]
 ϵ_{pore} dielectric function of the pores (or adsorbate in the pores)
 ϵ_{solid} dielectric function of the solid matrix

4.4 Other examples

The following publications may be interesting, too:

Vedam K., ‘Spectroscopic ellipsometry: a historical overview’, *Thin Solid Films* 313–314 (1998) 1-9.

Wongmanerod C., Zangoie S. and Arwin H., ‘Determination of pore size distribution and surface area of thin porous silicon layers by spectroscopic ellipsometry’, *Appl. Surf. Sci.* 172 (2001) 117–125.

Liu Y., Chen H., Zhang L. and Yao X., ‘Preparation and characteristics of porous silica films by a modified base-catalyzed sol-gel process containing PVA: II. Film preparation’, *J. Sol-Gel Sci. Technol.* 25 (2002) 103–111.

Sano N., Shibata T., Kanki T. and Asano T., ‘Characterization of adsorption properties of H₂O on Si(001) and Si(111) by Ellipsometry and *ab initio* molecular orbital calculations’, *J. Chem. Eng. Jap.* 34(5) (2001) 684–691.

Tan G.-L., Lemon M.F. and French R.H., ‘Optical properties and London dispersion forces of amorphous silica determined by vacuum ultraviolet spectroscopy and spectroscopic ellipsometry’, *J. Am. Ceram. Soc.* 86(11) (2003) 1885–1892.

Experimental

5 Measurements & data processing

5.1 Introduction

The basic principles of the performed ellipsometry measurements in combination with the sorption of water vapor are discussed in the following. The first paragraph describes the experimental set-up. Then, background information is provided for the data processing. Since the investigated silica membranes are microporous, the Langmuir model is used. It is shown how the Langmuir isotherm (θ vs. p_r) can be determined as well as kinetic parameters of the adsorption and desorption processes.

5.2 Experimental set-up

There are two main parts of the experimental set-up, which are discussed in the following paragraphs:

1. The spectroscopic ellipsometer;
2. The gas delivery set-up connected to the ellipsometry sample cell.

5.2.1 Ellipsometer

The spectroscopic ellipsometer that was used is a home-built¹ rotating polarizer-analyzer equipped with a Xe lamp and a scanning monochromator behind the analyzer. The set-up is shown schematically in Figure 5.1.

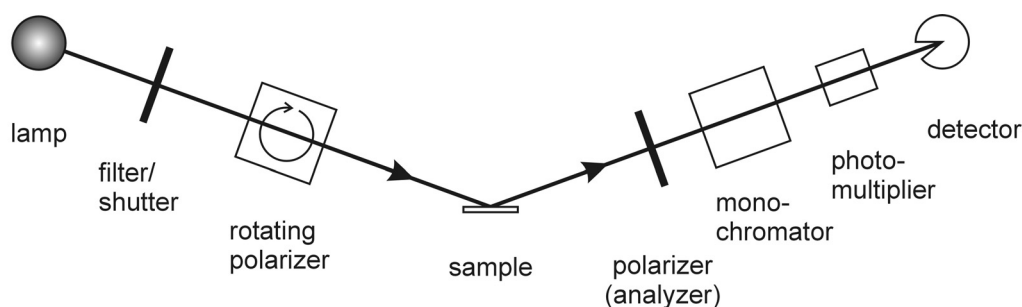


Figure 5.1. Ellipsometry set-up

¹ Owner: Solid State Physics group, Mesa+ Research Institute, University of Twente, Enschede, The Netherlands.

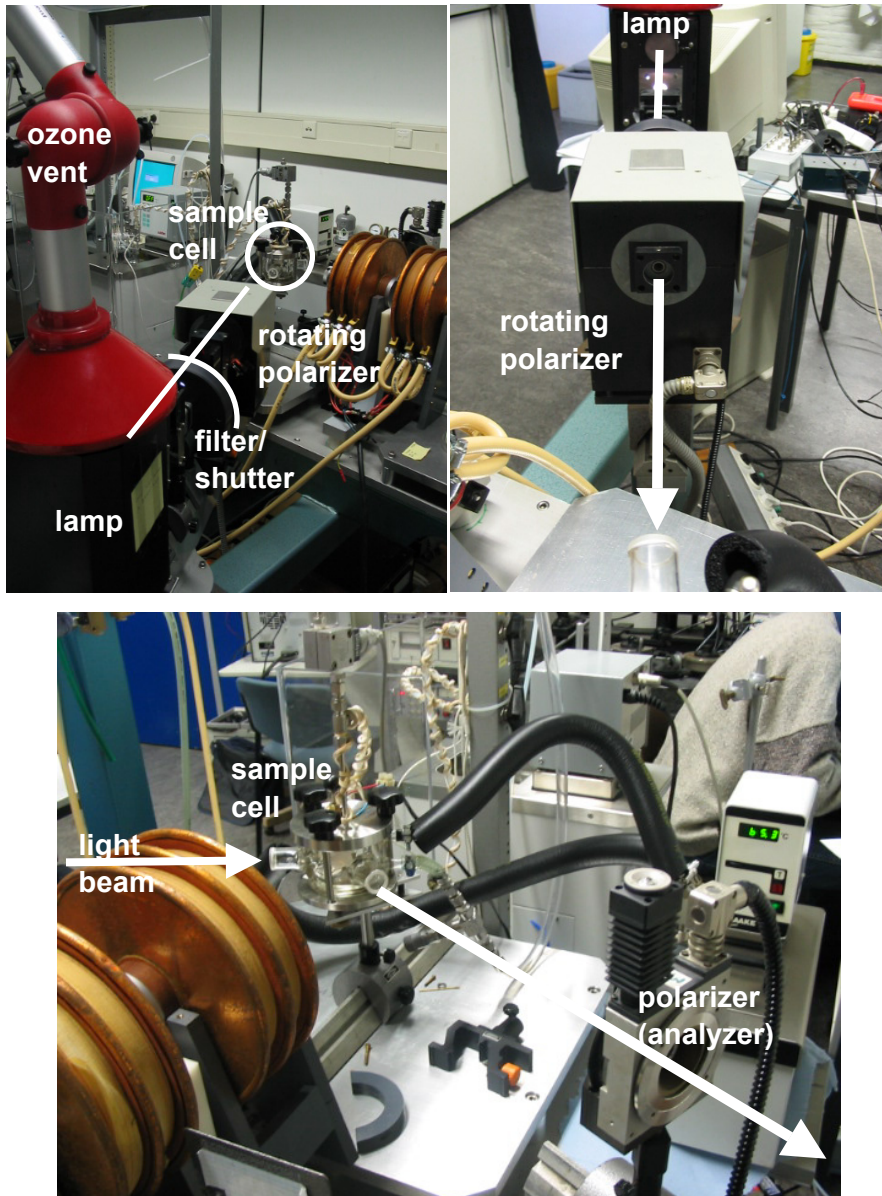


Figure 5.2. Photos of the ellipsometry set-up. Above: First part to sample cell (in circle). Below: Second part from sample cell to detector (outside picture). The gas-delivery set-up is located in the background.

5.2.2 Gas delivery set-up

The aim of the set-up was to deliver gas or vapor to the ellipsometry sample cell in a controlled way. In order to connect the set-up, the original design¹ of the cell had to be changed. In the following, the design of the cell is discussed after which the rest of the set-up is explained.

Sample cell

The ellipsometry sample cell is drawn schematically in Figure 5.3. The top drawing is a side view and the bottom drawing is a top view. The cell consists of two main parts: the roof (black) and the glass cell. The cell has a double wall in order to control the temperature inside. In the current study, a silicon oil cycle has been applied using an external thermostatic bath.

Through the double wall, glass tubes are located providing the windows for the light beam of the ellipsometer. The angle relative to the normal of the sample surface is $\sim 67.5^\circ$. Quartz windows are placed vertically at the end of the tubes using a Torr Seal (Varian) sealing. These tubes are necessary to compensate safely for temperature differences since the expansion of the glass is different from that of the window sealings. Anti-fogging liquid has been applied successfully onto the inner side of the windows to prevent water vapor condensation, which would interfere with the ellipsometer light beam.

In order to prevent possible blocking of the gas outlet, the gas inlet goes through the roof and the gas leaves at the bottom of the cell. If the gas would flow through the cell in the opposite direction, possible liquid water formation might fill up the tube and might also flow back into the cell. Blocking the outlet prevents the user from controlling the cell pressure. Also, the gas outlet passes the heated double wall, which helps preventing water from condensing before the gas stream has left the cell. Finally, in the current design, the flexible tube connected to the gas outlet is directed downwards.

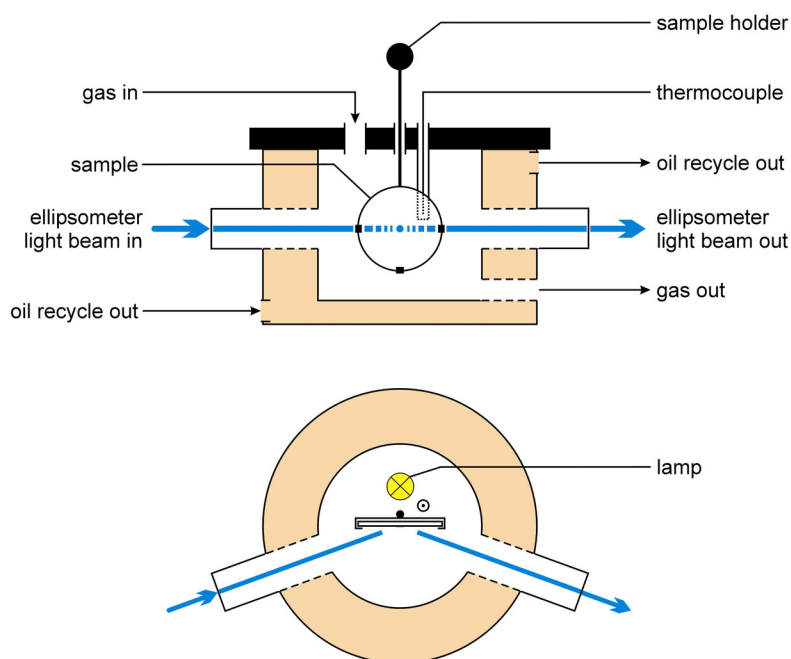


Figure 5.3. Ellipsometry sample cell. Top: side view. Bottom: top view.

¹ The original cell has been designed by Benes *et al.* (2001).

Next to the gas inlet, the sample holder is placed (more or less in the center of the roof). The sample holder enters the cell via a bolt below which an O-ring is placed in order to make the hole gas-tight. The sample holder can be used to rotate the sample inside the cell. Behind the sample, there are a 'pit' for the thermocouple and a 50W halogen lamp for direct heating of the sample.

Actually, the roof is wider than presented in Figure 5.3. The roof is placed onto the glass cell by connecting it to a (stainless) steel base. In Figure 5.4, the principle of this construction is pointed out. The whole assembly is located on top of a triangular shaped plate. The plate height can be adjusted at the three corners causing the cell to tilt, which is necessary for an optimal alignment of the ellipsometer light beam (see paragraph 5.3.3).

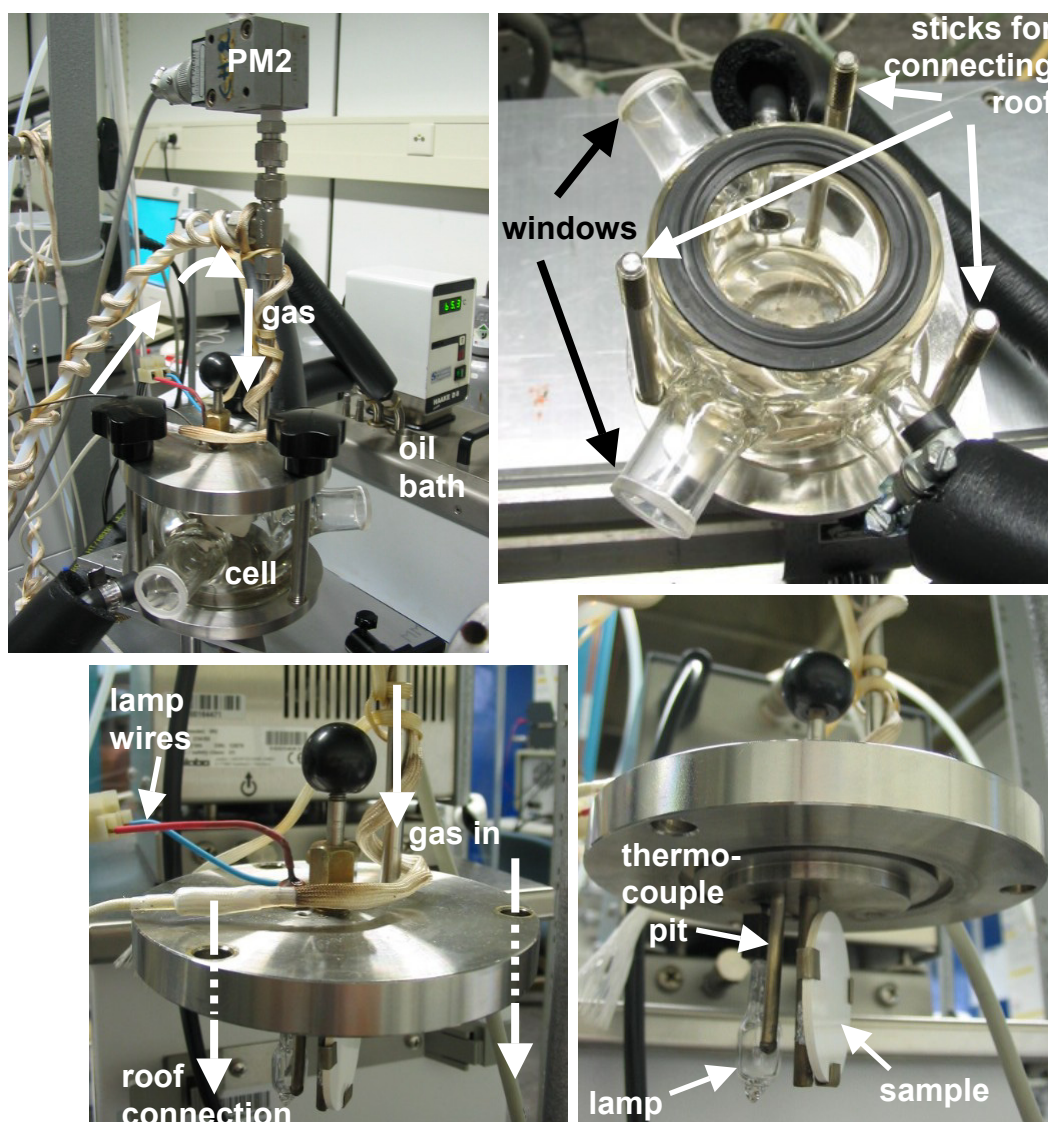


Figure 5.4. Photos of the ellipsometry sample cell. Upper left: complete cell. Upper right: glass cell; the black tubes are connected to the oil bath. Below: side views of the roof.

Set-up

The set-up has been designed to meet the following criteria:

- Gas or vapor transport to the sample cell, both temperature and pressure controlled;
- Possibility of mixing gases in a certain ratio;
- Controlled delivery of water vapor (*gas* phase) since the source is a liquid.

In Figure 5.5, the set-up is drawn schematically. The set-up contains the following parts:

- Two mass flow meters (MFM);
- Two pressure controllers (PC);
- Control unit to which both MFM's and PC's are connected;
- Two pressure meters (PM1 and PM2) providing the values p_1 and p_2 ;
- Water vessel (bubbler) containing a sieve, placed in a thermostatic bath;
- Oil bath for the ellipsometry cell;
- Heating rope applied to the gas streams after the water vessel (#6, #7, #8);
- Two- and three-way valves (V1 – V6)

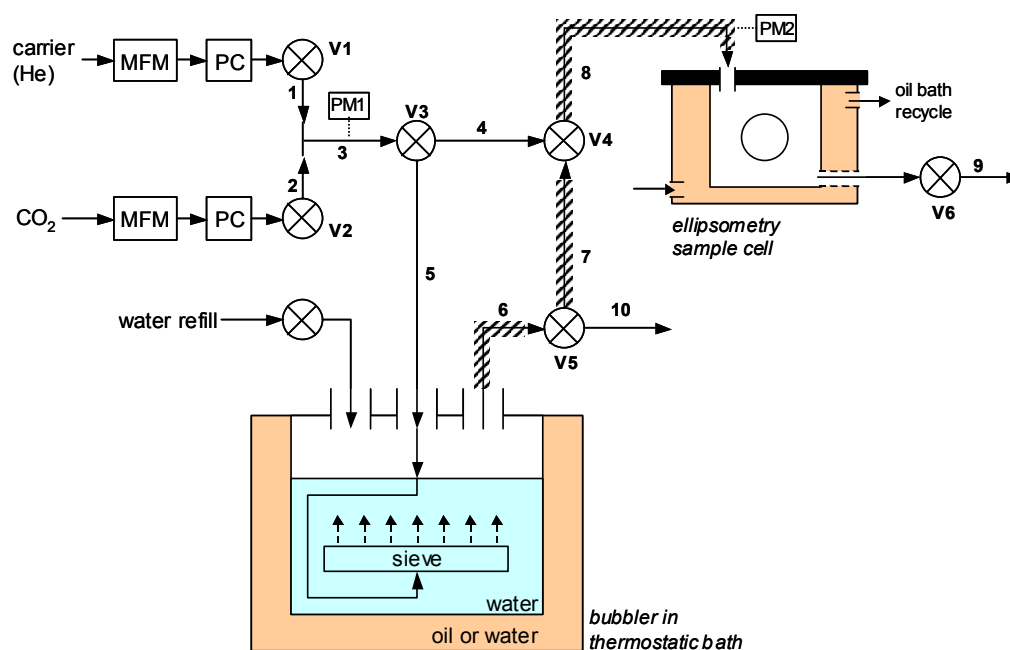


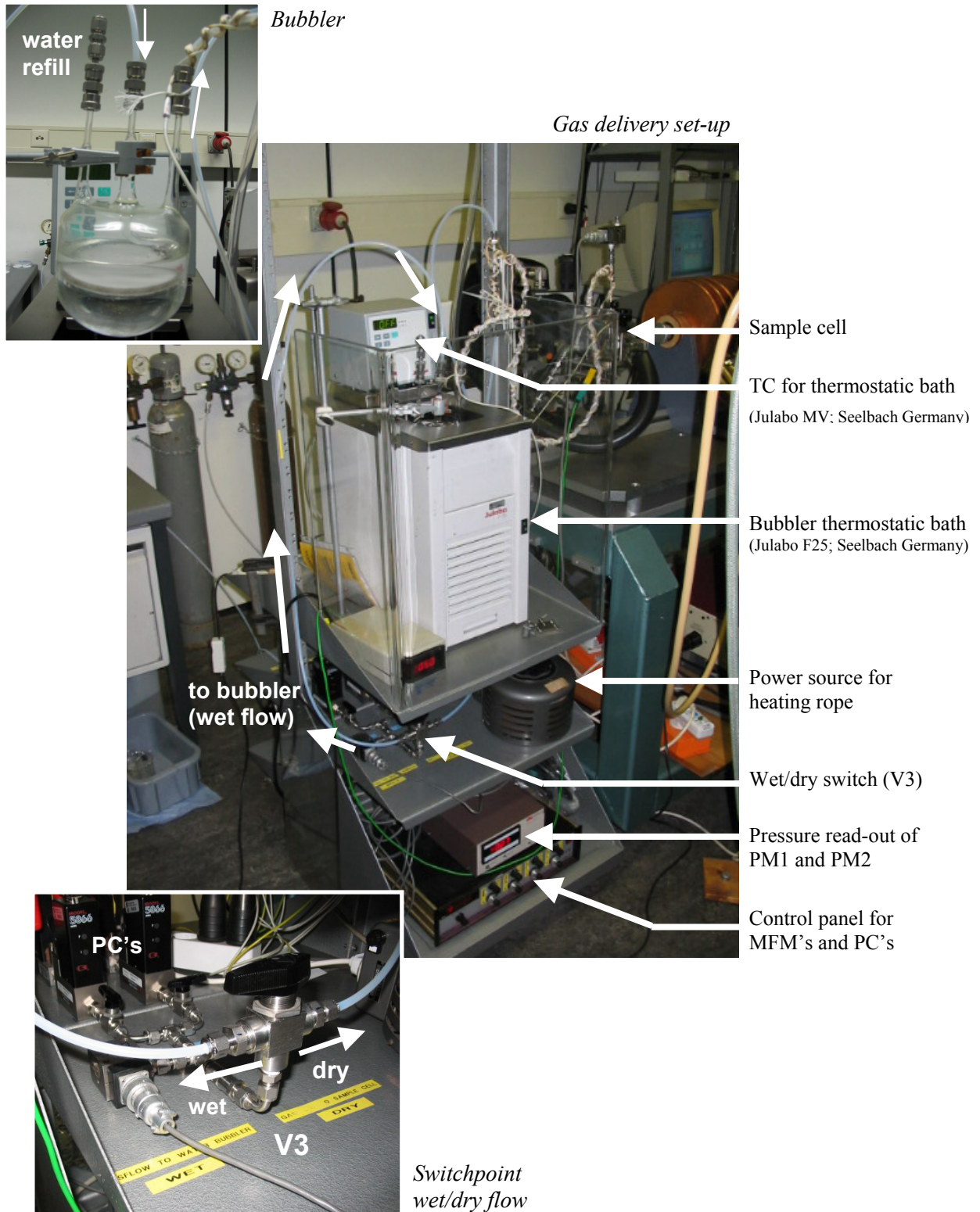
Figure 5.5. Gas delivery set-up

The first pressure meter (PM1) has been used during the initial testing of the set-up. For measurements, PM2 has been used, since it gives the pressure inside the sample cell. PM1 is also suitable of mixing two gases. After setting the pressure for one gas, the additional pressure is given by the other gas.

The sieve inside the water vessel is used to maximize the contact surface of the carrier gas with water and water vapor.

The heating rope is controlled by a tunable power source and the resulting temperature of the rope is proportional to the applied voltage. A calibration plot is given in Appendix 3.

Figure 5.6. Photos of the gas-delivery set-up



Bubbler

The following describes the operation of the bubbler, since it has to be known how much water vapor the carrier gas (helium) delivers to the ellipsometry sample cell.

In general, water vapor should be delivered to a cell that is at higher pressure than de equilibrium water vapor pressure. Otherwise, the bubbler does not work well because vapor will flow into the cell without the carrier.

The water in the water vessel has a water vapor pressure above the liquid. This vapor pressure will be carried by the helium flow to the sample cell (Dobkin, 2003). For that, the following assumptions have been made:

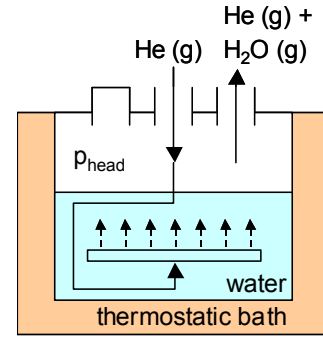


Figure 5.7. Bubbler schematically

- There is a steady state.
- Ideal gases are used.
- Only vapor leaves the system (no splashing).
- The head pressure in the bubbler, p_{head} , is equal to the pressure in the sample cell, i.e. $p_{\text{head}} = p_2 + 1$ [bar].
- The water vapor pressure above the liquid is the equilibrium vapor pressure at the current head pressure and temperature.
- The temperature of the water is equal to the temperature of the surrounding bath.

Using above assumptions, the vapor delivery can be expressed as follows:

$$\frac{x_v \text{ (vapor)}}{x_c \text{ (carrier)}} = \frac{p_v}{p_c} = \frac{p_v}{p_{\text{head}} - p_v} \quad (5.1)$$

where:

- x_i mole fraction of component i
- p_v (equilibrium) water vapor pressure
- p_c (partial) carrier gas pressure
- p_{head} total atmospheric pressure above the liquid

Consequently, the water vapor flow leaving the bubbler is given by:

$$F_{v,\text{out}} = F_{c,\text{in}} \frac{p_v}{p_{\text{head}} - p_v} \quad (5.2)$$

where:

- $F_{v,\text{out}}$ water vapor mole flow leaving bubbler
- $F_{c,\text{in}}$ carrier mole flow entering bubbler

And hence, the total mole flow reads:

$$F_{\text{out}} = F_{c,\text{in}} \frac{p_{\text{head}}}{p_{\text{head}} - p_v} \quad (5.3)$$

Change in water vapor flow will be proportional to the change in carrier flow. So, the flow conditions do not necessarily have to be the same for different measurements in order to combine or compare them.

Since the Langmuir model requires relative water vapor pressures (see eq. (2.2)), the partial water vapor pressure is of interest. Values of water vapor pressure above a liquid can be found in tables (Lide, 2002). However, the values are given at standard pressure, whereas the current head pressure might be different. Therefore a correction should be made according to the following equation (Atkins, 1994, p.193):

$$p_v = p_v^* \exp(V_m \Delta P / RT) \quad (5.4)$$

where:

p_v^*	water vapor pressure at standard conditions
V_m	molar volume of water
ΔP	pressure difference

This also counts for the saturated water vapor pressure, which means that the resulting relative vapor pressure (see eq. (2.2)) based on the corrected values, is equal to the relative vapor pressure at standard conditions.

The assumption of steady state requires a constant water level inside the bubbler. It has been determined empirically that the level is constant and hence, the amount of water used in experiments is negligible related to the volume of the water vessel.

5.3 Procedure

5.3.1 Measurements

Two types of measurements have been carried out. In the beginning, the effect of water on the sample was unknown with regard to the ellipsometry parameters obtained. Long-term measurements (>24 h) were done on γ -alumina layers in order to determine if it was possible to detect a change in optical properties in a water vapor environment. If a possible change could be determined, it could give more insight in the process of this change. This includes the moment at which it occurs, the kinetics of the change and the extent to which it occurs. The measurement did not provide quantitative information, only the fact that change had been observed.

Since the silica top layer showed more significant change upon water adsorption, the focus stayed on this sample. Different scans have been carried out with the ellipsometer, i.e. so-called *time scans* and *energy scans*. Both techniques are explained in paragraph 5.3.3. The control of water vapor delivery is explained in the subsequent paragraph (5.3.4).

5.3.2 Sample preparation

In principle, all samples have only one layer of γ -alumina and silica. In further research, the results of spectroscopic ellipsometry scans may be used in fitting the data to a model. A similar model is used in the research of Benes *et al.* (2001). Fitting the model to data of two layers of the same material would be too complex. Moreover, if an adsorbate penetrates into the layers, it cannot be determined to which extent the adsorbate has penetrated in one layer and the other, because optical properties of both layers are too similar.

Placing the sample

A sample was placed onto the sample holder and fixed by a piece of aluminum foil (as a wedge) at the back of the sample. Subsequently, the roof was connected as described in paragraph 5.2.2. Before each measurement, the cell was tested for being gas-tight. For that, the gas outlet was closed and a dry helium flow was provided. A leak was easily detected when the flow meter did not reach zero. Possible leaking points were tube connections, the lamp wire passage through the roof, the sample holder passage through the roof and the fixation of the roof onto the glass cell. Especially the lamp wire passage took a lot of time to make it gas tight.

Outgassing

It is essential for each measurement to have a reference (*blank*) measurement of the dry sample before and after the adsorption-desorption cycle. This blank measurement has to be controlled in order to obtain reproducible isotherms.

Especially with microporous materials, a so-called *low-pressure hysteresis* may occur (Sing *et al.*, 1985). Therefore, all of the residual physisorbed molecules have to be removed before each measurement of an adsorption isotherm. Usually, this step involves outgassing by applying a high vacuum at elevated temperature. Also, sufficient outgassing may be obtained by flushing the adsorbent with an inert gas at elevated temperature.

Instead of applying a (high) vacuum, the sample cell is flushed with helium, which is also the carrier of water vapor in the sorption measurements. This method has two advantages:

- During the measurement of the dry sample, the helium flow can be maintained without influencing the measurement. So subsequently, the switch to the wet flow (helium is passed through the bubbler) can be done while the only change in cell environment is the addition of water vapor.
- The outgassing is done at elevated temperature, which is ~200 °C. This temperature is set using the halogen lamp at the backside of the sample. Since the lamp is not in contact with the sample, improved heat transfer is provided by the (turbulent) helium flow through the sample cell.

A blank is measured with a so-called *energy scan*, in which a spectroscopic ellipsometry measurement is performed. Details about this type of scan are given in the next paragraph (5.3.3).

5.3.3 Ellipsometry

Alignment

The first step of an ellipsometry measurement is the alignment of the light beam. Beam positioning is done by changing the sample holder position: lateral movement (back and forth) and rotation. A plate with a plus-sign marking the middle is placed at two checkpoints:

- one in front of the exit window of the sample holder: lateral movement;
- one in front of the slit of the detector: rotation.

The sample holder can be rotated but this is very sensitive. Therefore, it is recommended to rotate the whole sample cell or to use the screws at the underside with which the sample cell is tilted, too. The beam should be positioned in the middle of the entrance and exit windows of the sample holder as much as possible to prevent hitting the edges upon fine-tuning the alignment.

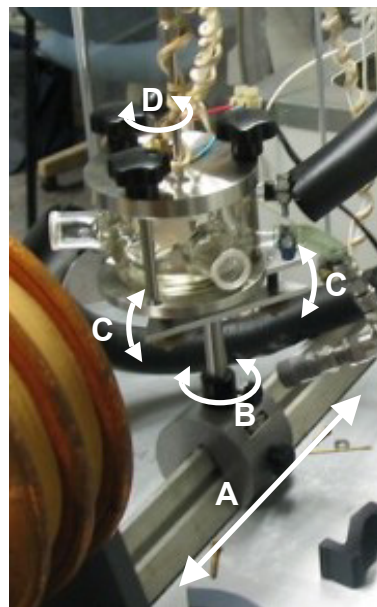


Figure 5.8. Adjusting cell alignment.
A: Lateral movement; B: Cell rotation;
C: Cell tilting; D: Sample holder rotation.

When the light beam enters the monochromator correctly, fine-tuning has to be done subsequently. During the measurement, the polarizer (analyzer) angles will be approximately 130° and 170° (the exact values are based on the calibration which is explained later) and therefore, fine-tuning of the alignment takes place at these polarization angles as well. Also, the alignment is done at single wavelength (energy). Since the spectroscopic range of the measurements is 1.5–3.0 eV (826.6–413.3 nm), the alignment (and calibration) is done at 2.25 eV. The shutter loops are set to 50/20 (open/closed). The amount of loops can be changed depending on the quality of the signal. The shutter blocks the signal periodically to determine the null level. When closed, the system measures the background noise and hence, it can be eliminated in the actual signal (when shutter is open).

The quality of the signal is represented by three output values that represent different errors in the measured signal. The signals should be as low as possible and can be reduced by changing the position of the sample (rotation or lateral movement). As a rule of thumb, it is sufficient to have each error signal below -30 dB, whereas errors below -40 dB result in a ‘good’ alignment and even lower values result in the indication of ‘best’.

Calibration

After the alignment, the measured signal is calibrated and measurement offset values are obtained: the polarization angle at which the amplitude is zero, ‘ p_{cal} ’ and offset values for the rotating polarizer (between lamp and sample). The shutter loops are normally set to 50/20 and at 2.25 eV (i.e. 551.1 nm).

The value for p_{cal} is around 150° and therefore, calibration is carried out from 145° to 155° using the so-called phase-calibration ($0 + 90^\circ$). A linear relation between signal amplitude and

polarization angle of the analyzer is obtained and p_{cal} is calculated from the x -axis intersect. Dielectrics give a straight line near the p_{cal} value, whereas non-dielectrics (metals) have a parabolic one for which residual calibration is carried out.

Scans

Energy scans are carried out over a range of energy values from 1.5 to 3.0 eV. The energy scans are the basis of obtaining layer properties. For every measurement, the monochromator is set to a certain wavelength and a scan is made at a certain polarization angle of the analyzer.

The polarization angle is set to the *zone angles* $+20^\circ$ and/or -20° relative to the calibrated polarization angle p_{cal} . Measurements from both zone angles should give the same value, but due to the errors in the signal (reduced during the alignment), the corresponding values are different. The better the alignment, the more equal the values of the two zones will be. In order to minimize the signal error, a *two zone measurement* is recommended. The resulting $\tan \Psi$ value is the mean value of both zones.

Time scans are used to measure the process of adsorption and desorption in time. Also, a plateau region can be determined from these scans, which indicates equilibrium at a certain relative pressure during adsorption.

The scan is done at a single wavelength. The value of $\tan \Psi$ changes with wavelength (see also Chapter 1) and hence, a wavelength has to be determined at which the change in $\tan \Psi$ upon sorption is significant. In Figure 5.9, an example is shown of ellipsometry spectra upon water adsorption on a microporous silica layer. The progress of adsorption is indicated by the arrow and it is shown that, for example, the change at 2.5 eV is obvious, whereas there is hardly any change at 2.3 eV. Subsequently, $\tan \Psi$ is preferably measured for a longer period of time in order to determine and decrease the error in the signal.

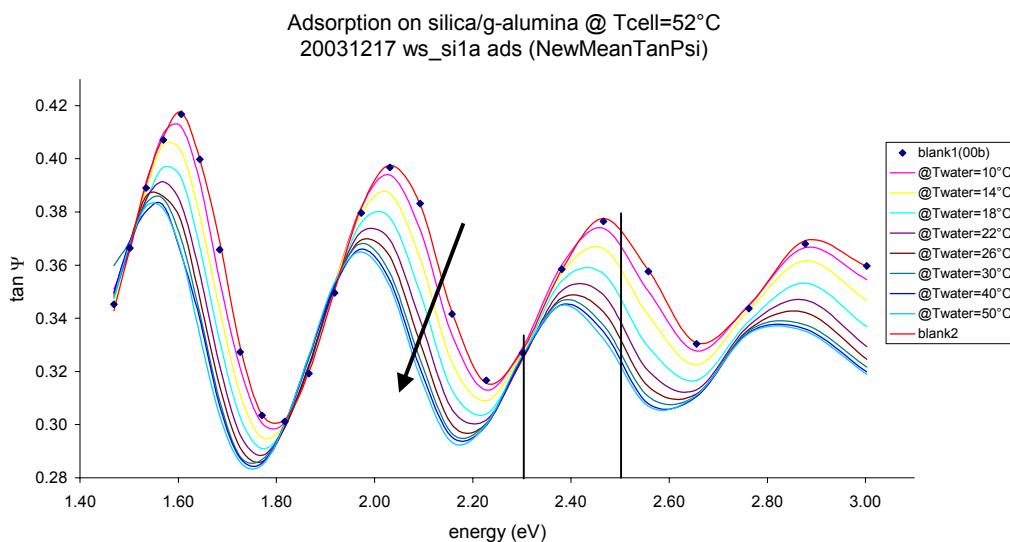


Figure 5.9. Example of change in ellipsometry spectra upon water adsorption onto a silica sample. The arrow indicates the order of the measurements and hence, the progress of adsorption. Both “blank1” and “blank2” are measurements of the dry sample and are at the top of the series. For example, there is an obvious change in $\tan \Psi$ at 2.5 eV (≈ 496 nm) and hardly any change at 2.3 eV (≈ 539 nm). Sample: one silica layer and one γ -alumina intermediate layer on top of an α -alumina substrate.

5.3.4 Water vapor delivery

The water vapor pressure delivered to the sample cell is dependent on the water temperature of the bubbler. Therefore, different water vapor pressures can be obtained by setting the thermostatic bath of the bubbler to a certain temperature. The bubbler temperature is controlled by the accompanying temperature control unit of the water bath. Temperature can be set with steps of 0.1 °C and is kept constant with an error of less than 0.1 °C.

Based on the explorative measurements, the helium pressure was set to approximately 0.70 bar pressure difference from standard (ambient) pressure (p_2), since this value gave sufficient results in the sorption data. The pressure controller has been calibrated at 2 bar, so the gas supply was set to this value. The accuracy of the PM2 read-out was determined to be ± 0.1 bar. Finally, the flow of carrier gas was controlled by valve V6 in the outlet stream of the sample cell (see Figure 5.10).

The switch to wet flow occurred by switch valves V3, V4 and V5 in the following order. First, V5 has to be in the position where it directs the incoming gas to #10. Then, V3 is switched from #4 to #5: The helium is directed through the bubbler and leaves the system via #10. This gives the possibility of switching V4 subsequently from #4 to #7. Finally, V5 is switched and the helium/water vapor mixture is directed to the sample cell.

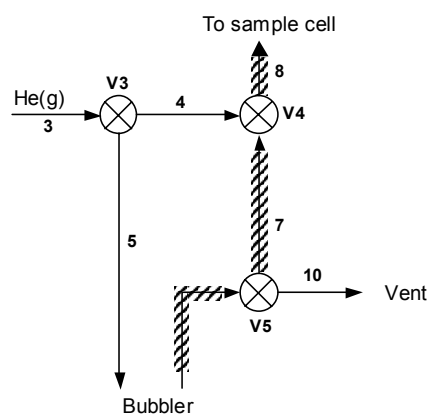


Figure 5.10. Overview of valves for setting dry or wet flow

5.4 The Langmuir isotherm

Under equilibrium conditions, the Langmuir isotherm can be obtained. Therefore, values for $\tan \Psi$ have to be determined as a function of relative pressure, p_r . The $\tan \Psi$ values are obtained from the plateau region in the adsorption time scans at different relative pressures.

5.4.1 Normalizing $\tan \Psi$

A major assumption for the processing of data is that $\tan \Psi$ is linearly proportional to the adsorbate coverage θ (Alvarez-Herrero *et al.*, 2001). However, it cannot simply replace θ . Since the value of θ lies between zero and one, the same must count for the $\tan \Psi$ related value. Therefore, $\tan \Psi$ has to be normalized as follows:

$$\theta_{\Psi} = \frac{|(\tan \Psi)_0 - (\tan \Psi)|}{|(\tan \Psi)_0 - (\tan \Psi)_{\text{sat}}|} \quad (5.5)$$

where: θ_{Ψ} coverage expressed in terms of Ψ
 $(\tan \Psi)_0$ value of $\tan \Psi$ at zero coverage (blank)
 $(\tan \Psi)_{\text{sat}}$ value of $\tan \Psi$ at maximum coverage

If the $(\tan \Psi)$ value is equal to $(\tan \Psi)_0$, there is no coverage and eq. (5.5) returns a value of 0. If $(\tan \Psi)$ is equal to $(\tan \Psi)_{\text{sat}}$, the coverage is maximum and eq. (5.5) becomes 1.

5.4.2 Estimating the Langmuir sorption constant

The Langmuir sorption constant, K_L , can be estimated using the adsorption data at different relative pressures. Another way of expressing the Langmuir equation (2.7) is as follows:

$$K_L = \frac{\theta^n}{(1-\theta)^n p_r} \quad (5.6)$$

Under the assumption that the kinetics are first order, a linear plot can be made of $\theta^n/(1-\theta)^n$ vs. p_r from which K_L is equal to the slope.

5.4.3 Isosteric heat of adsorption

Based on the Langmuir equation (2.7), an Arrhenius plot can be made in order to obtain an estimation for the isosteric heat of adsorption.

Also, K_L (eq. (5.6)) is expressed as an Arrhenius relation (eq. (2.25)) and taking the natural logarithm results in the following linear expression:

$$\ln K_L = \ln K_L^0 + E_{\text{ads}} \frac{1}{k_B T} \quad (5.7)$$

So, in a plot of $\ln(\theta^n/(1-\theta)^n p_r)$ vs. $1/k_B T$ the slope gives a reasonable estimation of the heat of adsorption E_{ads} . Since K_L can be estimated according to the previous paragraph (5.4.2), the estimates can be used to make a plot of $\ln K_L$ vs. $1/k_B T$.

Note that this Arrhenius plot can only be made if Langmuir adsorption isotherms at different temperatures are known. Theoretically, there should be at least two isotherms since eq. (5.7) is linear. Due to the fact that θ_Ψ is used for the value of the coverage, the value for the y-axis intercept ($\ln K_L^0$) is not necessarily correct and should therefore be neglected.

5.5 Langmuir kinetics

The previous paragraph explained the processing of measurement data at equilibrium conditions between adsorbate and adsorptive. Since the processes of adsorption and desorption have been measured as well, kinetic parameters can be obtained from those measurements consequently.

5.5.1 Adsorption kinetics

The adsorption process is always accompanied by desorption, since sorption is an equilibrium process. Hence, as long as adsorption is the net result, the adsorption rate is actually higher than the desorption rate. By the end of the adsorption process desorption is of the same order as adsorption. Eventually, equilibrium is reached and both adsorption and desorption rates are

equal. So, in general, the increase in surface coverage is determined by the adsorption rate (eq. (2.5)) as well as the desorption rate (eq. (2.18)) (assuming first order):

$$\frac{d\theta}{dt} = k_{\text{ads}} p_r (1 - \theta) - k_{\text{des}} \theta \quad (5.8)$$

At equilibrium, the constant, K_L is given in eq. (5.6). The change in surface coverage can be expressed in terms of K_L in the following relations:

$$\frac{1}{k_{\text{ads}} p_r} \frac{d\theta}{dt} = 1 - \left(\frac{1 + K_L p_r}{K_L p_r} \right) \theta \quad (5.9)$$

The coverage at equilibrium, θ_e , can be used to simplify the above equation since that coverage is expressed in terms of K_L and p_r with the Langmuir equation. This leads to the following expression:

$$-\theta_e \ln \left(1 - \frac{\theta}{\theta_e} \right) = k_{\text{ads}} p_r t + C_0 \quad (5.10)\text{-a}$$

$$\text{with: } C_0 = \theta_e \ln \left(1 - \frac{\theta_0}{\theta_e} \right) \quad (5.10)\text{-b}$$

C_0 is a constants related to the coverage at t_0 . As only k_{ads} is of interest, C_0 is disregarded.

Subsequently, a plot can be made of $\ln(1 - \theta/\theta_e)$ vs. t , which gives a straight line and k_{ads} can be obtained from the slope. If the k_{ads} is known for different temperatures, an estimate can be made of the E_{act} using the Arrhenius-dependent equation of k_{ads} (eq. (2.24)). Then, the slope of a plot of k_{ads} vs. $1/k_B T$ gives the E_{act} .

5.5.2 Desorption kinetics

There are two methods of determining the kinetics of desorption (Oura *et al.*, 2003), an isothermal method and a temperature-programmed method. In the methods, the desorption rate or coverage is determined as a function of time.

The isothermal desorption has been performed in this study. In the set-up, the sample cell temperature could only be controlled indirectly and therefore, the temperature-programmed method could not be used. Since a new sample cell will be used in further research in which the sample temperature can be controlled directly, the temperature-programmed method might be applicable as well.

Isothermal method

In the isothermal method, the temperature is increased rapidly after which the temperature is held constant. Hence, desorption occurs under isothermal conditions. Analogously to adsorption, the desorption process is described by:

$$(\theta_c - 1) \ln \left(\frac{\theta - \theta_c}{1 - \theta_c} \right) = k_{\text{des}} t + C'_0 \quad (5.11)\text{-a}$$

$$\text{with: } C'_0 = (\theta_c - 1) \ln \left(\frac{\theta_0 - \theta_c}{1 - \theta_c} \right) \quad (5.11)\text{-b}$$

A plot of $\ln \left(\frac{\theta - \theta_c}{1 - \theta_c} \right)$ vs. t gives a straight line and k_{des} can be obtained from the slope.

Furthermore, if several k_{des} are known at different temperatures, E_{des} can be determined from a graph of $\ln k_{\text{des}}$ vs. $1/k_B T$ (using eq. (2.18)-a).

Temperature-programmed method

In the temperature-programmed method, the temperature is increased gradually at a certain ramp (K per unit time). Oura *et al.* (2003) describe a measurement in which the increase in partial vapor pressure of the adsorptive due to desorption is measured during the temperature increase. In a UHV system, the pumping equation describes this process:

$$-\frac{d\theta}{dt} = \frac{V}{k_B T} \left(\frac{dp}{dt} + \frac{S}{V} p \right) \quad (5.12)$$

where: V volume of UHV chamber [m^3]
 p partial pressure of adsorptive [Pa]
 S pumping speed [$\text{m} \cdot \text{s}^{-1}$]

The most commonly used technique is at a high pumping speed at which the partial pressure is proportional to the change in surface coverage ($p \propto -d\theta/dt$). The temperature is increased with a linear ramp, i.e.:

$$T(t) = T_0 + \beta t \quad (5.13)$$

where: T_0 temperature at $t = 0$
 β heating rate [$\text{K} \cdot \text{s}^{-1}$]

The following expression can be derived from (2.18) and (5.13):

$$-\frac{d\theta}{dt} = \frac{k_{\text{des},n}^0 \theta^n}{\beta} \exp(-E_{\text{des}}/k_B T) \quad (5.14)$$

At sufficiently high temperatures, the rate of desorption increases according to the Boltzmann term. Desorption slows down due to the decrease in coverage and the desorption rate will be zero eventually. Therefore, the r - T plot has a maximum at a certain characteristic temperature T_m . A series of r - T plots for different initial coverages, θ_0 , provides information on the kinetic order n . In Figure 5.11, plots for zero- first- and second-order behavior are shown and they have the following characteristics:

- Zero-order: The curves at different θ_0 have the same leading edge and a rapid drop at T_m . The value of T_m increases with higher θ_0 .

- First-order: The curves at different θ_0 have the same T_m .
- Second-order: The T_m shifts to higher values with decreasing θ_0 .

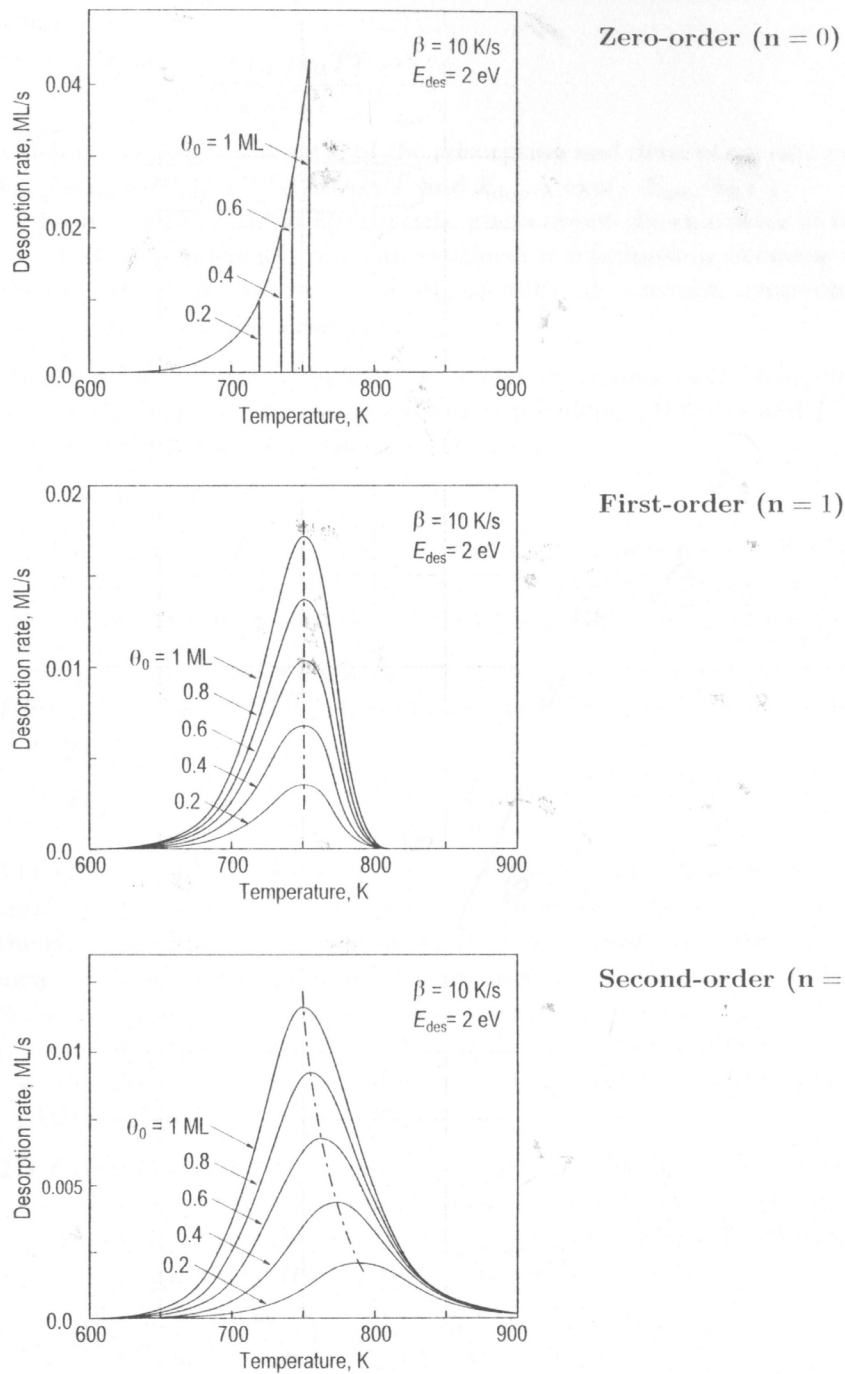


Figure 5.11. Plots of desorption rate vs. temperature for zero-, first- and second-order kinetics and several initial coverages θ_0 (Oura *et al.*, 2003).

5.6 Samples

5.6.1 Sample names

g1a, **g1b** are two different samples containing one γ -alumina layer on top of AKP-30 α -alumina. Measurements on γ -alumina have the letter g; “g1” refers to standard γ -alumina, whereas “g2” is La-doped γ -alumina. Initially, both γ -alumina (g1) and La-doped γ -alumina (g2) were going to be used in the sorption measurements. Due to a lack of time, g2 was left out.

sil a, **sil b** were given a different name initially, but stand for the same sample. The sample contains one γ -alumina layer and one silica layer on top of an AKP-30 α -alumina support.

sil c is a different sample than the above mentioned silica sample but has been made according to the same procedure. It also contains one γ -alumina layer and one silica layer on top of an AKP-30 α -alumina support.

5.6.2 Data files

Raw data files that are generated by the ellipsometer control software, are text files (type *.txt). For each measurement series, a folder has been made with the date of that experiment. The data has been processed in Excel files referring to the raw data files therein.

Every Excel file contains processed measurement data as well as the log for the corresponding experiment in the first sheet. Also the Excel files have the date of the experiment in the file name. Then, all water sorption measurements have the abbreviation “ws_” and the long-term measurements have “lt_”, followed by the sample name (see the previous paragraph). The abbreviations “ads” and “des” indicate adsorption and desorption measurements, respectively. The following list gives the .xls file names (the last one is part of the explorative measurements and is an collection of several measurement series):

- 031205-08 lt_g1a
- 031211 ws_g1b
- 031212 ws_g1b des
- 031217-18 ws_sil a
- 031223 ws_sil b-ads
- 040120 ws_sil b-des
- 040226-27 ws_sil c
- 040227 ws_sil c dryHe
- 040317 ws_sil c-2
- ellipso sorption

Furthermore, Excel files were created for the determination of the Langmuir characteristics:

- Langmuir isotherm (isotherm at 55°C)
- Langmuir isotherm II (isotherm at 31°C)
- Arrhenius plot (determination of K_L)
- L kinetics (adsorption kinetics at 52–56°C)
- L kinetics II (adsorption kinetics at 31°C)
- L kinetics -des (desorption kinetics at different temperatures in dry He)

5.7 Measurement statistics

There are two types of errors involved in the experiments done: Accidental errors, due to changes in external conditions (such as temperature, carrier gas flow and pressure) and the systematic instrumentation errors.

The main accidental error is the helium flow. The (over)pressure of the helium is set with the pressure controller and changes in flow resistance through the system as well as temperature changes in the sample cell, result in a change in flow. Compared to the flow, changes in overpressure applied by the helium flow, and the internal temperature of the ellipsometry sample cell are negligible. However, the absolute value of temperature could not be determined accurately and the uncertainty was set to $T \pm 2$ °C.

Measurement deviations

In most cases, the number of measurements for the determination of a value is much greater than 10. In that case, the standard deviation in a series of measurements reads:

$$s^2 = \frac{\sum_{i=1}^n (y_i - \bar{y})^2}{n-1} \quad (5.15)$$

where: s standard deviation in one single measurement (value)
 y_i value of measurement i
 \bar{y} mean value of the complete measurement series
 n number of measurements

The standard deviation in the mean value \bar{y} is given by:

$$\bar{s} = \frac{1}{\sqrt{n}} s \quad (5.16)$$

After calculating θ_ψ , the standard deviation of this value is calculated in two steps. First, the standard deviation for numerator and denominator in eq. (5.5) are calculated similarly using:

$$s_i^2 = s_{i1}^2 + s_{i2}^2 \quad (5.17)$$

where:

s_i standard deviation of numerator (num) or denominator (den)
 s_{i1}, s_{i2} standard deviation of the two terms of the numerator or the denominator

Then, the total standard deviation s_{θ_ψ} is calculated from:

$$\left(\frac{s_{\theta_\psi}}{\theta_\psi} \right)^2 = \left(\frac{s_{num}}{num} \right)^2 + \left(\frac{s_{den}}{den} \right)^2 \quad (5.18)$$

The following formulas are used in the subsequent calculations:

$$\text{For } y = ab \text{ or } y = a/b: \quad \left(\frac{s_y}{y}\right)^2 = \left(\frac{s_a}{a}\right)^2 + \left(\frac{s_b}{b}\right)^2 \quad (5.19)$$

$$\text{and for } y = \ln a: \quad s_y = s_a/a \quad (5.20)$$

Least squares linear regression

The linear fit of produced plots has been calculated with a least squares linear regression method, accompanying the spreadsheet software¹ used for data processing. The confidence level was set to 95%. The output values R^2 and the slope of the curve were used subsequently. The R^2 value gives an indication of the accuracy of the regression and is calculated as follows:

$$R^2 = 1 - \frac{n \sum_{i=1}^n (y_i - \bar{y})^2}{n \left(\sum_{i=1}^n y_i^2 \right) - \left(\sum_{i=1}^n y_i \right)^2} \quad (5.21)$$

Also the error (standard deviation) is given in the regression output, enabling a determination of the standard deviation in the calculated value from the slope (e.g. the adsorption rate constant).

¹ Microsoft Excel 2000, Data Analysis add-in.

6 Results & discussion

6.1 Introduction

The results that are presented here are based on experiments that are explained in Chapter 1. Please refer to that Chapter for additional information.

Paragraphs 6.2 and 6.3 discuss the first explorative measurements. The most important conclusion of the explorative measurements is the fact that sorption processes can be traced using ellipsometry. Then, results for blank measurements (6.4), energy scans (6.5) and time scans (6.6) are discussed separately. The time scans have been used to obtain Langmuir kinetic data. The isotherms are presented in paragraph 6.7 and both adsorption and desorption kinetics in the last paragraphs, 6.8 and 6.9.

6.2 Set-up operation and debugging

The first measurements were done in order to familiarize with the set-up whereas debugging could be done since it was a new set-up. Leakage of the sample cell roof occurred several times due to bad sealing of the electrical wires through the roof. Moreover, problems with leaking piping and failing thermostatic baths were solved.

Samples that were used contained a γ -alumina layer, which had been prepared with a bad boehmite sol (referred to as “bb” in the data files). Although the γ -alumina may not have been suitable for membrane applications, the material is the same and therefore, very well usable in explorative measurements. Also, one silica sample was used containing one γ -alumina layer, one TC6⁽¹⁾ layer and one silica layer.

The data has been put together in one single Excel file, named “ellipso sorption”. The first worksheet gives an overview of the different measurements and this overview is presented in Appendix A.1. Furthermore, a calibration has been carried out of the heating rope control. The result is a plot of voltage vs. rope temperature and can be found in Appendix C.

6.3 Long-term measurements

Since γ -alumina is known to be unstable in water vapor environments at elevated temperature, long-term measurements were carried out in water vapor. Again, the measurements were explorative, i.e. they were used to determine if any change could be observed using ellipsometry. A major unwanted restriction was the fact that the oil bath of the sample cell was limited to temperatures up to ~ 115 °C, resulting in a maximum cell temperature of around 100 °C (depending on the flow rate). Turning on the lamp at the backside of the sample would have increased the temperature, but this could not solve the problem since the ellipsometry signal became too bad. The resulting plots of long-term water sorption measurements can be found in Appendix A.2.

¹ ‘TC6’ is an organic (C6) surfactant templated silica layer in between the silica top layer and γ -alumina intermediate.

6.4 Blank measurements

Measurements of the blanks were done to determine if the sample would have changed after the adsorption/desorption cycle. Figure 6.1 gives an example of two blanks indicating that the optical characteristics stayed the same.

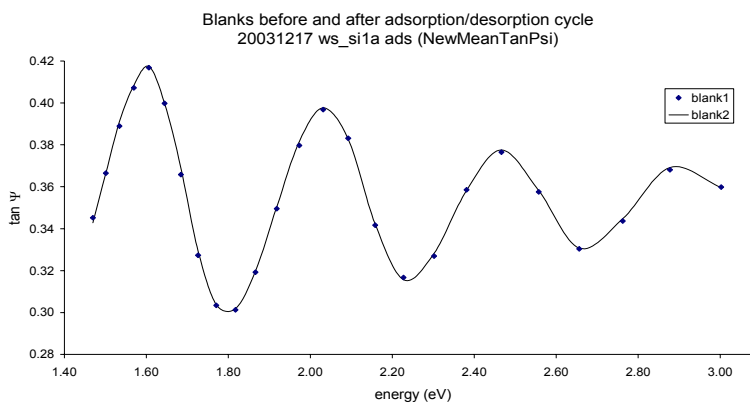


Figure 6.1. Example of comparing blanks before and after an adsorption/desorption cycle. Sample is silica/ γ -alumina. $T_{\text{cell}} \sim 54^\circ\text{C}$

6.5 Energy scans

The processing of measurement data was done using spreadsheets. In case of a significant difference in the values of the two zones ($+20^\circ$ and -20°), one of the two zones was marked as wrong and only the corresponding value of the other zone was used, if possible. Therefore, a new set of $\tan \Psi$ values ('NewMeanTanPsi') was assigned, in which the mean $\tan \Psi$ values were placed by default except for the points with only one zone value.

The first sorption energy scans were explorative. They were made in a sequence during the adsorption of water. Ten minutes after the new water vapor pressure had been reached, a scan was made. Figure 6.2 and Figure 6.3 show the result after adsorption on γ -alumina and silica/ γ -alumina samples, respectively.

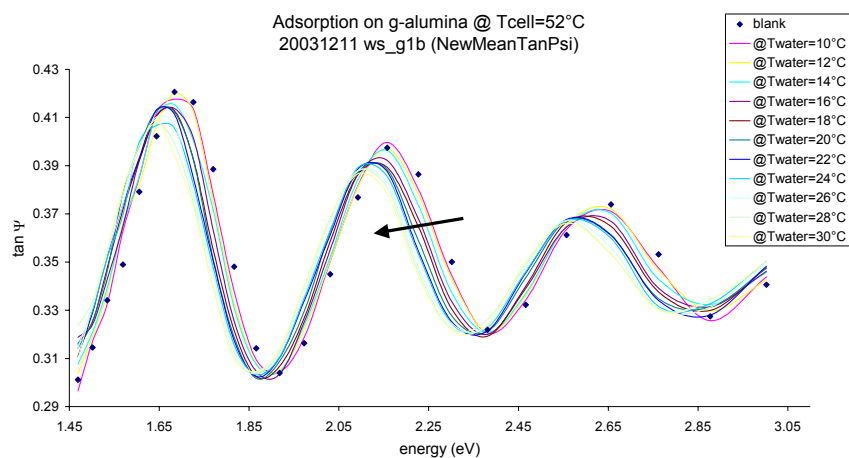


Figure 6.2. Adsorption sequence of energy scans. The arrow indicates the progress of adsorption. Sample is γ -alumina.

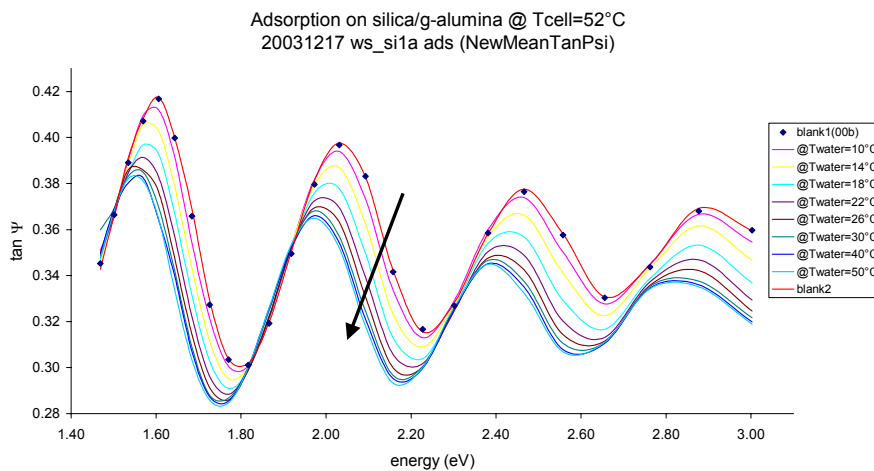


Figure 6.3. Adsorption sequence of energy scans. The arrow indicates the progress of adsorption. Blank1 (◆) and blank2 (—) are at the same position. Sample is silica/γ-alumina.

The measurement of desorption of the γ -alumina (g1b) failed. The idea was to obtain energy scans in a loop, which would be carried out automatically by the ellipsometry software. Unfortunately, the monochromator gave an error. Consequently, the next desorption measurement had been done in steps, manually.

The desorption of the silica/γ-alumina (si1a) gave a remarkable result: no desorption was observed at all. Figure 6.4 shows the series of energy scans which resulted in mainly two 'plots'. The upper plot is the blank after desorption and the lower 'plot' are all measurements at stepwise decreasing relative water vapor pressure. Both adsorption and desorption measurement were carried under similar conditions (i.e. He flow = 30-33 ml/min and $p_2 = 0.74$ bar). Later on, desorption from si1c had been measured as well, but again, no desorption was observed.

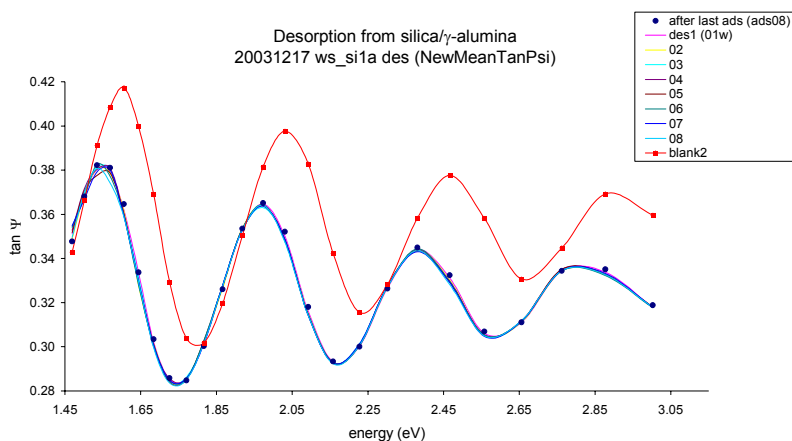


Figure 6.4. Desorption from silica/γ-alumina. No desorption occurred and all series of the sequence are at the same place: lower graph. The higher graph is blank2.

The first *time scans* showed that equilibrium was reached much later than the ten minutes that had been assumed. As a consequence, time scans were used for two reasons: 1) to determine the moment when equilibrium was reached and 2) to monitor the adsorption process. Also, the part of the scan at equilibrium has been used to determine the corresponding $\tan \Psi$ value.

Next, Figure 6.5 shows a ‘correct’ series of energy scans. Each scan has been obtained at equilibrium which was determined in a preceding time scan. In the following chapter, more is explained about the time scans.

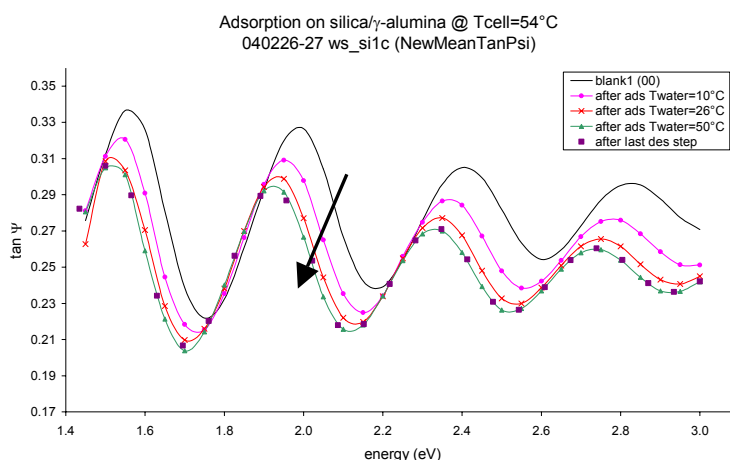


Figure 6.5. A ‘correct’ series of energy scans. Each scan has been made at equilibrium, the moment of equilibrium being determined by a preceding time scan. The arrow indicates the progress of the adsorption.

6.6 Time scans

The time scans are the measurements obtained from adsorption and desorption cycles using ellipsometry that resulted in Langmuir isotherms and kinetic data.

After the new temperature of the bubbler was set, flow, pressure and temperature values were recorded, at least in the beginning to determine the moment of reaching steady flow conditions. The values were recorded for measurement numbers (‘pt#’), since the time is given for each measurement (point) in the output file of the ellipsometer control software. The log of each measurement series is presented in the first sheet of the corresponding Excel file. Also, the logs are given in Appendix A. The plateau region (equilibrium) has been determined manually. An example of a time scan and the plateau region is given in Figure 6.6. The moment at which steady flow had been reached, is indicated in the graph at ~280 s.

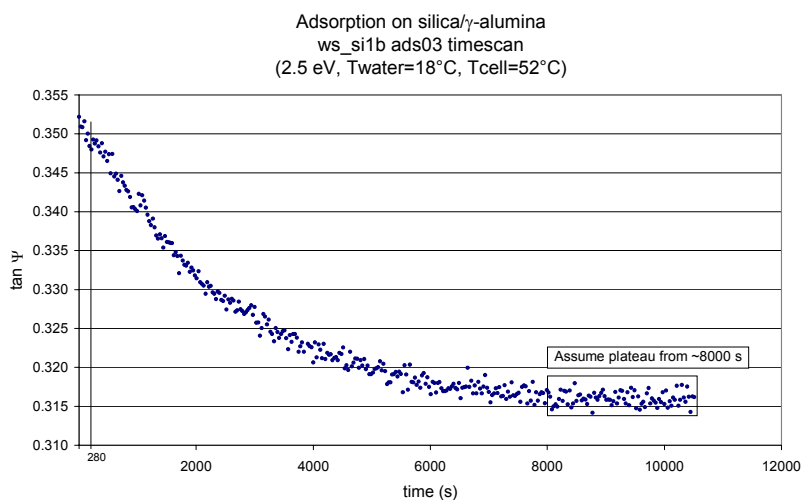


Figure 6.6. Example of a time scan. The start of a steady wet flow is marked on the left at ~280 s. The plateau is determined in the plot at sight.

Table 6.1, Table 6.2 and Table 6.3 provide an overview for adsorption and desorption processes, in combination with flow conditions and the total time that was needed to reach equilibrium.

**Table 6.1. Adsorption conditions for the given silica samples at $T_{\text{cell}} = 31 \pm 2$ °C.
The time scan at $p_r = 0.94$ failed, although equilibrium was reached.**

sample	T_{water} [°C]	relative pressure [-]	flow [ml/min]	p2 [bar]	T_{cell} [°C]	total time [h]
silc	4	0.18	43	0.70	31	5.9
silc	10	0.27	43	0.71	33	6.8
silc	19	0.49	46	0.71	31	3.8
silc	30	0.94	45	0.71	30	n/a

**Table 6.2. Adsorption conditions for the given silica samples at $T_{\text{cell}} = 52 - 56$ °C.
The time scan at $T_{\text{water}}=50$ °C was not recorded due to an ellipsometer error, but equilibrium was reached.**

sample	T_{water} [°C]	relative pressure [-]	flow [ml/min]	p2 [bar]	T_{cell} [°C]	total time [h]
silc	10	0.08	38	0.73	56	2.6
silb	18	0.14	34	0.74	52	2.1
silc	26	0.22	37	0.74	56	2.6
silb	40	0.49	34	0.73	52	1.9
silc	50	0.82	35	0.73	55	n/a

Table 6.3. Desorption conditions for the given silica samples in dry helium (no water vapor pressure present)

sample	T_{cell} [°C]	flow [ml/min]	p2 [bar]	total time [h]
silc	50	> 200	0.70	152
silb	85	46	0.74	110
silb	133	46	0.74	33
silb	161	46	0.74	10

6.7 Langmuir isotherms

The Langmuir isotherms have been obtained for two different temperatures, 31°C and 55°C. The isotherm at 31°C was created more recently, after the isotherm of 55°C. The temperature of ~30°C was chosen in order to have a temperature significantly different from 55°C. Also, the lowest T_{water} that could be reached with the thermostatic bath using demineralized water, is 4°C and a relative pressure for the first adsorption measurement should not have been higher than 0.20. With the minimum T_{water} of 4°C, the cell temperature should be 30°C, which resulted in a relative pressure of less than 0.20. Eventually, the cell temperature was established at 31 ± 2 °C.

The reason why the relative pressure of the first point should not be higher than 0.20, is the fact that a Langmuir type isotherm was expected. The Langmuir isotherm has a steep slope at low pressures and hence, the amount of measurements in this region should be relatively high. For the same reason, only one point had been acquired at a relative pressure higher than 0.5.

Both isotherms have been obtained using sample si1c. Adsorption measurements with sample si1b have been carried out at approximately the same temperature (52°C) as the first series of si1c (55°C) and the samples have been made according to the same procedure, but the ellipsometry sample cell broke and was replaced after the measurements with si1b and before the measurements (with si1c). The new cell was made according to the original design. However, the angle between the cell windows was different from the first cell and hence, the incident angle of the ellipsometer light beam had to be changed from 67.5° to 64.5°. The change seems small, but the $\tan(\Psi)$ values depend on the incident angle. Because of the different $\tan(\Psi)$ values, the measurements of si1b and si1c could not be combined.

6.7.1 Coverage from $\tan(\Psi)$: θ_Ψ

In order to normalize the $\tan(\Psi)$ values at equilibrium, the maximum values are required. The $(\tan \Psi)_0$ values have been obtained from the first time scan of an adsorption/desorption cycle. In the first part where a dry helium flow is still present and hence, the $\tan(\Psi)$ value for zero coverage can be obtained.

The water vapor pressure could not be related to a saturated water vapor pressure accurately. Theoretically, p_{sat} is the saturated water vapor pressure for known temperature and ambient pressure, at which water starts to condensate instead of being adsorbed onto the solid surface. Consequently, the cell temperature would be equal to the water temperature in the bubbler. However, the exact point (i.e. pressure) for saturation is not known. Moreover, the cell temperature could not be determined accurately which also makes it difficult to determine the exact value p_{sat} .

A direct consequence of the above procedure is that the $\tan(\Psi)$ values at the highest water vapor pressures (for $T_{\text{water}} = 30^\circ\text{C}$ and 50°C , respectively) are not exactly at saturated water vapor pressure. In order to estimate the $\tan(\Psi)$ value at saturated condition, a correction factor (cf) has been introduced which adjusts the $\tan(\Psi)$ values for $T_{\text{water}} = 30$ and 50°C , respectively. The cf values for both isotherms are very low, which indicates that the mentioned values for $\tan(\Psi)$ are in the flat region of the corresponding isotherm and that they are close to the saturated values.

However, two isotherms have been obtained and they were used to estimate the isosteric heat of adsorption E_{ads} . In order to combine both isotherms in an Arrhenius plot, the corresponding K_L values have to be based on the same pressure region. This means that the pressure values for both isotherms had to be related to their corresponding p_{sat} . So, although the exact p_{sat} values are unknown, the p_{sat} values were taken to be the saturated water vapor pressures at the corresponding (cell) temperature, i.e. 31°C and 55°C .

The results for the isotherms at 31 and 54 °C are summarized in Table 6.4 and Table 6.5, respectively. The isotherms are plotted in Figure 6.7, including the corresponding fits that are discussed in the next paragraph. Obviously, the isotherms are of type I, as expected. The standard errors of the points for the coverage are too small to show in the graphs.

Table 6.4. Results for adsorption isotherm at 31 °C sample temperature

sample	T _{water} [°C]	p [Pa]	p _r [-]	tan Ψ @2.5 eV	\bar{s}	θ_{Ψ}	\bar{s}	flow [ml/min]	p2 [bar]
silc-2	dry	0	0	0.282950	8.0E-05	0	-	45	0.74
silc-2	4	813.59	0.18	0.239419	5.6E-05	0.7218	1.2E-02	43	0.70
silc-2	10	1228.1	0.27	0.228800	2.8E-05	0.9835	1.5E-02	43	0.71
silc-2	19	2197.8	0.49	0.225304	2.2E-05	0.9559	1.6E-02	46	0.71
silc-2	30	4245.5	0.94	0.22425	2.7E-05	0.9733	1.6E-02	45	0.71

Source for the water vapor pressure (3rd column): Lide, 2002.

"p2" = pressure difference from standard pressure, measured at PM2

Table 6.5. Results for adsorption isotherm at 55 °C sample temperature

sample	T _{water} [°C]	p [Pa]	p _r [-]	tan Ψ @2.5 eV	\bar{s}	θ_{Ψ}	\bar{s}	flow [ml/min]	p2 [bar]
silc	dry	0	0	0.282775	9.1E-05	0	-	40	0.77
silc	10	1228.1	0.08	0.250431	6.2E-05	0.5632	1.0E-02	38	0.73
silc	26	3362.9	0.21	0.234685	4.7E-05	0.8374	1.8E-02	37	0.74
silc	50	12344	0.78	0.228323	7.1E-05	0.9482	1.8E-02	35	0.73

Source for the water vapor pressure (3rd column): Lide, 2002.

"p2" = pressure difference from standard pressure, measured at PM2

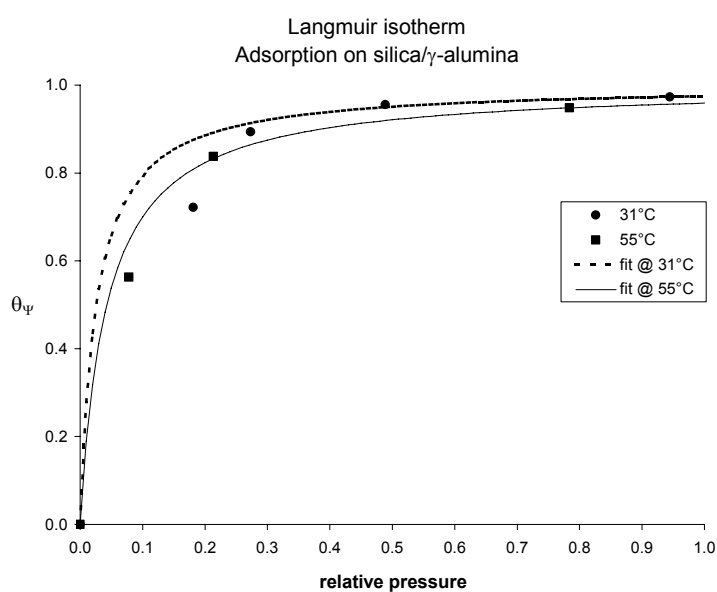


Figure 6.7. Isotherms obtained for two different temperatures.

It is remarkable that in both isotherms, the measurements at lower pressures are lower than the fit. A large deviation exists at 31°C, at relative pressure of 0.27. This might be explained by the following. During the corresponding time scan (measurement ws_si1c-2-03), a problem occurred with the oil bath of the sample cell. Several 'plateaux' could be determined in the graph of $\tan(\Psi)$ vs. time, which is shown in Figure 6.8. Due to the temperature drop to 19 °C, surface coverage increased.

The next measurement (04) was carried out in order to determine the correct equilibrium value and this measurement involved a desorption back to the plateau of $T_{\text{cell}} = 31^\circ\text{C}$. The most reliable value is assumed to be the plateau in measurement 04, but the position of the assumed plateau is inaccurate because of the missing trend of the preceding adsorption process.

Also, the fact that the $\tan \Psi$ value is a result of the reflection from both silica and γ -alumina, might have induced a difference in adsorption behavior as well. Although it is unknown to which extent adsorption has taken place in the γ -alumina layer, the contribution of the mesoporous γ -alumina to the isotherm should be taken under consideration.

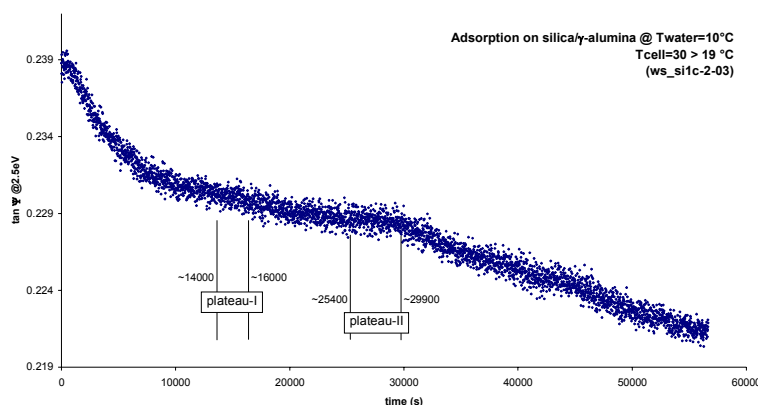


Figure 6.8. Adsorption on silica/ γ -alumina for $T_{\text{water}}=10^\circ\text{C}$. Due to a problem with the oil bath, T_{cell} dropped to 19°C .

6.7.2 Fitting the Langmuir isotherms

The fit of the Langmuir isotherms involved two parameters: the previously mentioned correction factor cf and the Langmuir constant K_L . The correction factor cf was connected to the K_L estimation. The cf was chosen at which the R^2 value of the K_L estimation is as high as possible. Consequently, the range of K_L values (error) and corresponding cf -s is an arbitrary value and a statistical error of K_L could not be assigned.

Nevertheless, the value of K_L has an error range, which is dependent on the $\tan(\Psi)$ values used for the isotherms. First of all, both fits were constructed under the assumption that the measured values were accurate and hence, the K_L estimation should be as good as possible. However, the variable $\tan(\Psi)_{\text{sat}}$ has been estimated manually by choosing a cf . Not only does this estimated $(\tan\Psi)_{\text{sat}}$ value influence the K_L estimation, it also adds an error to all θ_Ψ values since $\tan(\Psi)_{\text{sat}}$ is used for the corresponding calculation.

Moreover, the isotherm at 31°C has a significant error in the second point (at $p_r=0.18$). The measurement (040317 ws_si1c-2-01) took almost 7 hours and had to be stopped by the end of the day. It was assumed that the end had a plateau, but it is not completely convincing. Therefore, the θ_Ψ value at this point could be too low. A higher value at this point would enhance the quality of the fit (R^2).

The fit of the isotherm at 31°C without the point at $p_r=0.18$ has also been determined. The quality of the fit is higher but the fit is only slightly different. However, the estimated K_L values are significantly different.

Table 6.6. Results of the Langmuir constant estimation;
 cf = correction factor to determine $(\tan \Psi)_{\text{sat}}$

T_{cell} (°C)	cf	R^2 of K_L estimation	K_L estimated
31	-0.007185	0.965522	39
55	-0.013035	0.998528	23

6.7.3 Isothermic heat of adsorption

The determination of the isothermic heat of adsorption E_{ads} has been done according to paragraph 5.4.3, using the estimated values of K_L . The estimation is very rough since it is based on only two different temperatures. The result is an isothermic heat of adsorption of 17 kJ/mol. This value is an indication of physisorption which is supported by the fact that a first order fit could be used for the isotherms.

The value is also in good agreement with results for adsorption measurements by Bhandarkar *et al.*, 1992. They performed water adsorption measurements on bulk material of amorphous microporous silica hollow fiber membranes. Two Langmuir constants were obtained, 31.7 at 30°C and 15.4 at 70°C, resulting in an isothermic heat of adsorption of 16 kJ/mol.

Also, De Vos and Verweij (1998; and references herein) give an overview of isothermic heats of adsorption on microporous silica that has been produced in a similar way as the samples in the current study. Except for hydrogen (6 kJ/mol), the values of isothermic heat of adsorption for CH_4 , CO_2 , N_2 and O_2 are all in the range of 10 to 28 kJ/mol.

The values of K_L and E_{ads} are in the same order as of the mentioned references, but it should be emphasized that the results of the current study are based on measurements on both silica and γ -alumina. The influence of the latter material on the results is unknown and therefore, direct conclusions cannot be given.

6.8 Adsorption kinetics

The adsorption processes at different partial vapor pressures of water have been analyzed in order to obtain kinetic adsorption data. If a certain equation gives a reasonably good fit of the measured data it does not provide sufficient evidence for a particular mechanism of adsorption. Dissociation of water on the solid surface upon adsorption is highly unlikely due to the low temperatures, hence, the measurement data have been fitted with a first order estimation.

The data used for the fit have been limited to low coverages, since desorption starts playing a role at higher coverages. Also, the data measured in the first part of the experiment (in the order of 1000 s) are omitted. These data are likely to include time dependent behavior of the set-up, involving the establishment of a steady flow, especially at the start of the wet flow for the first adsorption step.

In Figure 6.9, the adsorption plots are given. The plots include the linear regression estimates. Due to the fact that an average equilibrium coverage (θ_e) was used, some measured values at higher coverages, became meaningless since the \ln -value returned an error. The error resulted in a value of zero in the graph.

All data obtained from the different sheets, were combined and the result can be found in Table 6.7a (at 31°C) and Table 6.7b (52–56°C). The adsorption rate constants are given including the R^2 values indicating the accuracy of the regression. The rate constants decrease with increasing relative pressure while the coverage difference decreases as well. However, the coverage difference for each step (denoted by $\Delta\theta$) is not related to the time needed to complete the step as the figures differ too much.

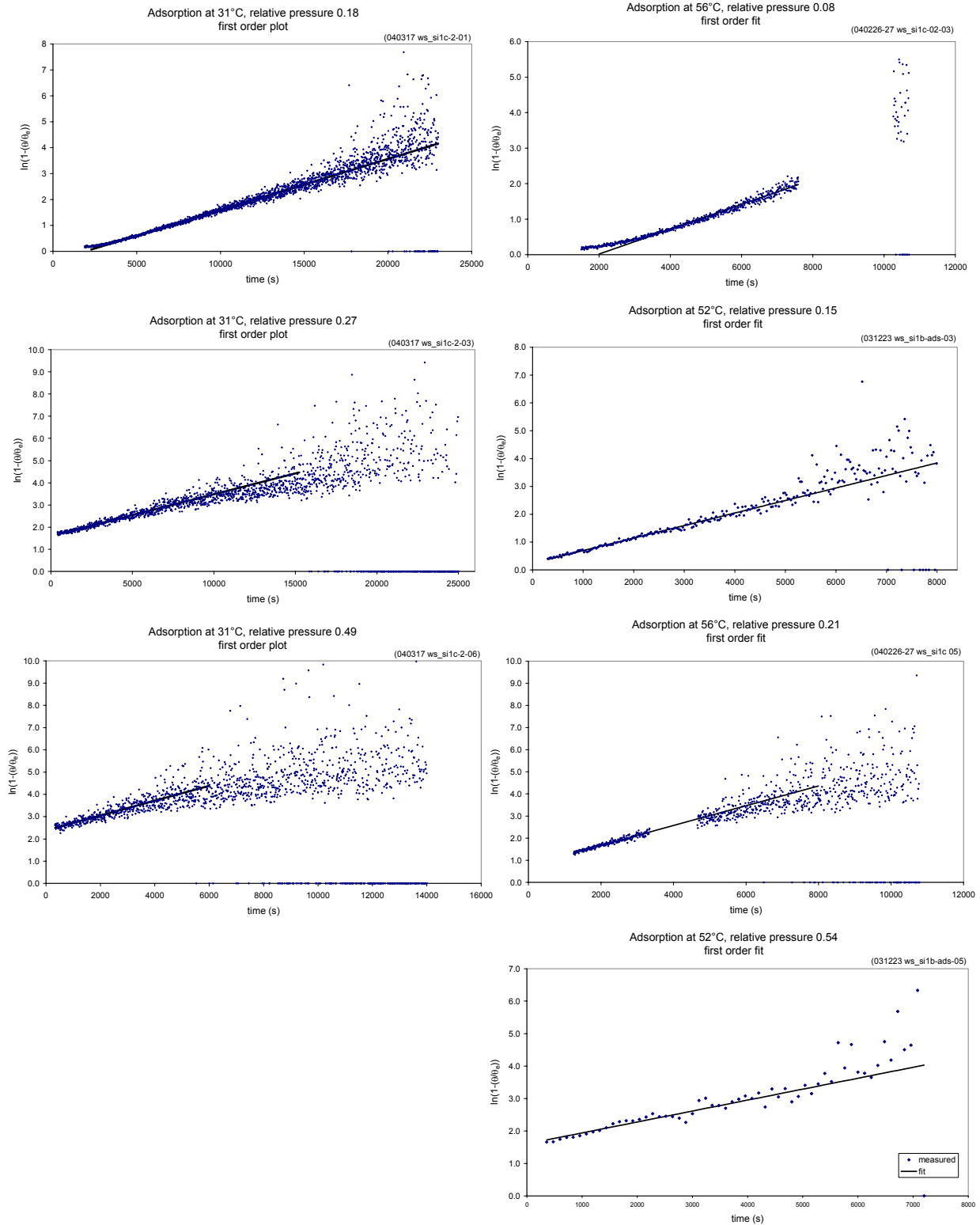
Table 6.7a. Adsorption constants determined at 31°C and different relative water vapor pressures. A first order fit has been used; R^2 indicates the accuracy of the regression and # indicates the number of measurements used for the fit. $\Delta\theta$ is the absolute coverage difference of the step. The last column gives the total time for the adsorption step.

sample	p_r [-]	$k_{ads,1}$ [s^{-1}]	\bar{s}	R^2	#	$\Delta\theta$	total time [h]
si1c-2	0.18	7.9E-04	1E-05	0.99	950	0.72	5.9
si1c-2	0.27	6.2E-04	1E-05	0.93	373	0.17	6.8
si1c-2	0.49	6.5E-04	3E-05	0.73	267	0.06	3.8

Table 6.7b. Adsorption constants determined at 52-56 °C and different relative water vapor pressures.

sample	T_{cell} [°C]	p_r [-]	$k_{ads,1}$ [s^{-1}]	\bar{s}	R^2	#	$\Delta\theta$	total time [h]
si1c	56	0.08	2.53E-03	5E-05	0.98	459	0.56	2.6
si1b	52	0.15	2.3E-03	3E-04	0.98	123	0.57	2.1
si1c	56	0.21	1.75E-03	5E-05	0.94	210	0.27	2.6
si1b	52	0.54	6.0E-04	8E-05	0.91	39	0.19	1.9

Figure 6.9. Adsorption plots at different relative pressures; in the left column, adsorption at 31°C and in the right column, adsorption at 52–56°C. The first and the third plot in the right column show a gap in the measurement series. That was because of a recording failure by the ellipsometer control software. Since the process of adsorption continued anyway, the recording was continued in a subsequent measurement taking into account the time elapsed during the error.



6.9 Desorption kinetics

Also, some desorption measurements have been analyzed in order to obtain kinetic information. It has been mentioned in previous results that desorption did not occur, even though the relative water vapor pressure was low. As a consequence, desorption measurements had to be carried out in dry helium.

6.9.1 Adsorptive pressure dependence

According to the Langmuir theory, desorption rate is independent of the partial vapor pressure of the adsorptive in the ambient of the sample. Hence, measurements in dry helium would give useful information. However, a complication occurred with the last desorption measurement. After the time scan had started, the flow was switched to dry helium and consequently, desorption should have occurred but hardly any change could be observed. Then, the helium flow rate was increased from ~ 40 to >200 ml/min which started desorption instantaneously. Figure 6.10 illustrates the entire process.

The effect of increasing the flow rate of helium is as if the pressure is decreased and hence also the pressure of water vapor which appears to influence the gradient of adsorption. Some desorption might have had taken place upon the switch to dry flow, but due to the low flow rate of helium, some sort of equilibrium was established soon after. Hence, desorption had been limited. In the first part, before the switch to high flow rate, the signal does not completely stay unchanged and it seems to increase. Still, this behavior is different from the start of the high flow rate and some influence of water vapor near the sample surface is concluded.

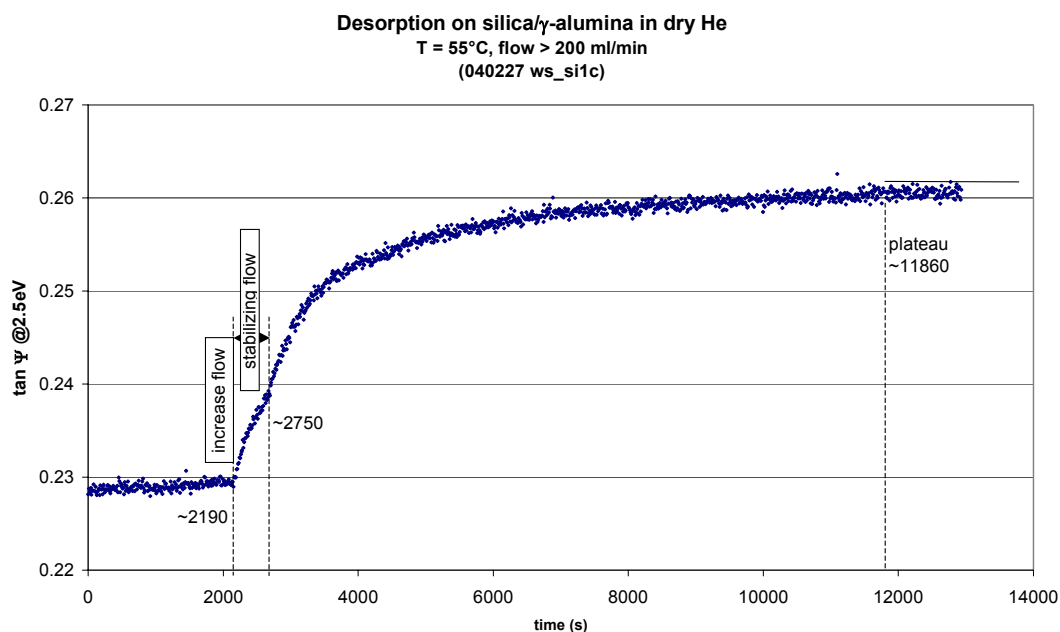


Figure 6.10. Desorption from silica/ γ -alumina at constant temperature in dry helium

6.9.2 Temperature dependence

Desorption is also induced by increasing the temperature. It depends on the temperature to which extent desorption takes place. So, at the end of an isothermal desorption step, a plateau is reached but complete desorption is not necessarily the case. In this way, several desorption steps were carried out in one run. Each subsequent desorption step occurred at a higher temperature and started at a lower adsorbate coverage. Figure 6.11 illustrates this measurement series.

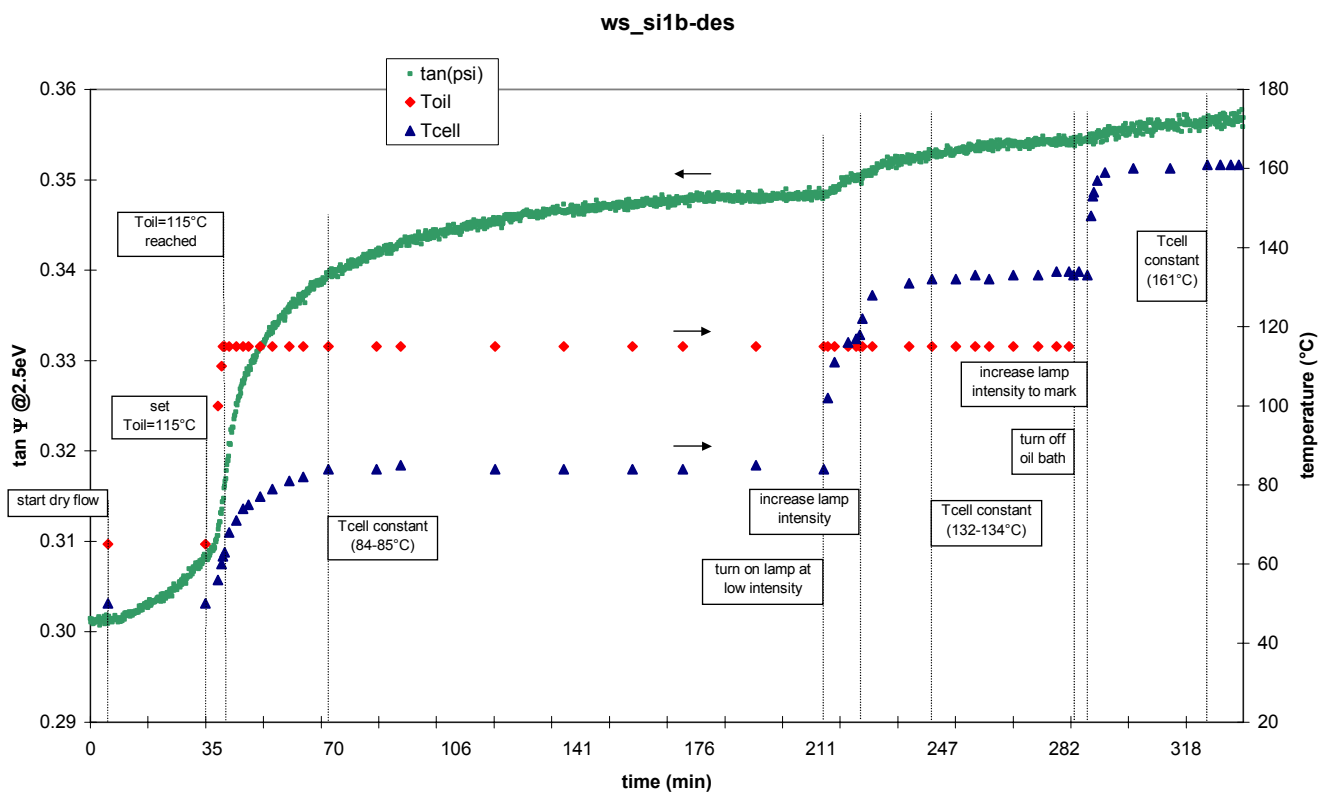


Figure 6.11. Desorption steps in one run. The sample is silica/ γ -alumina and helium flow is ~ 46 ml/min.

As can be seen in Figure 6.11, the oil bath for heating the sample cell was turned off at some point. This was done since the halogen lamp behind the cell had been turned on and consequently, the cell temperature increased. A major disadvantage of the halogen lamp was that the ellipsometer signal got worse whereas scattering of the measured points increased.

Table 6.8. Overview of desorption constants determined at constant temperature and in dry helium. A first order fit has been used; R^2 indicates the accuracy of the regression and # indicates the number of measurements used for the fit. The last column gives the total time for the adsorption step.

T_{cell} [°C]	$k_{\text{des},1}$ [s^{-1}]	st.dev.	R^2	#	total time [min]
55	2.7E-04	4E-06	0.93	301	152
85	3.0E-04	3E-06	0.97	386	110
133	8.0E-04	1.4E-04	0.32	196	33

Using the measurements presented in Figure 6.10 and Figure 6.11, desorption kinetics have been obtained. As in the adsorption steps, linear regressions were performed at the beginning. Also, the coverage at equilibrium has been determined separately. Table 6.8 gives the results.

The two desorption steps at the highest temperatures, i.e. 131 and 161°C, gave problems and for 161°C, a plateau could not be determined. The problems are mainly due to the mentioned increased scattering of the measurements as the halogen lamp was switched on. The high inaccuracy due to the halogen lamp is obvious at 133°C where the R^2 value is less than 0.4. Nevertheless, a clear increase of the desorption rate constants can be determined.

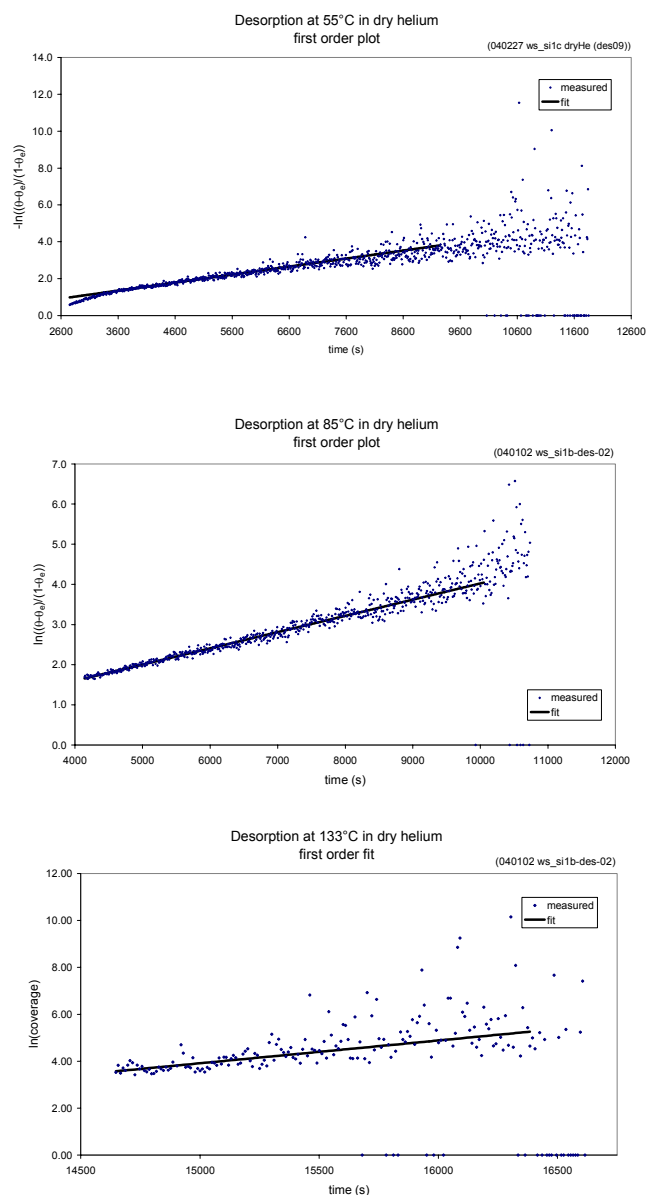


Figure 6.12. Desorption plots at different relative pressures and temperatures

7 Conclusions

The aim was to develop a gas-delivery set-up in combination with an ellipsometer in order to obtain water sorption characteristics of state-of-the-art hydrogen-selective silica membranes.

Experimental set-up

An experimental set-up has been developed for the controlled delivery of a gas and/or water vapor to the ellipsometry sample cell. The sample cell had already been designed and used by Benes *et al.* (2001) and modifications have been applied to the sample cell in order to fit the cell into the complete system. The possibility of mixing another gas instead of water vapor to the carrier gas is also possible, but has not been investigated.

The start of using the set-up involved several problems. Repairs as well as trial-&-error sessions were performed and measurements could be carried out eventually.

The current set-up has some advantages and limitations. The following table gives an overview. Note that virtually all limitations are related to the sample cell.

Table 7.1. Overview of main advantages and limitations of the used experimental set-up

Advantages	Limitations
Fast response of the thermostatic bath for the bubbler.	Measuring sample temperature indirectly via the thermocouple (-pit).
Simple control of flow by a valve at the end of the system (named V6).	An unknown difference of the measured T_{cell} from real T_{cell} .
Effective functionality of the heating rope.	Setting sample temperature indirectly – the real cell temperature might not be the same as that of the sample and cannot be set instantaneously.
Easy combination of any set-up with the ellipsometer.	Problems with aligning the ellipsometer light beam as the sample is not in the center of the cell.
Effective application of anti-fogging liquid onto the inside of the sample cell windows.	Pressure meter (PM2) near the sample cell. It would be better if the cell pressure was measured inside the cell.
	It is unknown if the carrier flow was fully saturated with the required water vapor pressure. So, the real water vapor pressure in the sample cell may have been lower than assumed.

Data collection

Adsorption isotherms were obtained using the Langmuir model. The results show that the model describes the measurements sufficiently with first-order kinetics. Also, kinetic adsorption and desorption data have been analyzed using a first order estimation and it is concluded that the adsorption of water is non-dissociative below 60°C.

From the isotherms, a value for isosteric heat of adsorption E_{ads} has been obtained being a rough estimation and it gives an indication of physisorption. This value for E_{ads} is in good agreement with literature. Values for other adsorbates on similar microporous silica indicate that the obtained E_{ads} in the current study is of the same order.

Based on the above mentioned results, it can be concluded that water sorption characteristics can be obtained well using the presented set-up.

The $\tan \Psi$ value has been related directly to the surface coverage. In order to obtain the coverage more accurately as well as other characteristics such as porosity, ellipsometry data has to be fitted to effective medium approximations (e.g. Bruggeman) that relate optical data of the solid matrix, the pores and the adsorbate to absolute values from the optical profile obtained by the ellipsometry.

8 Recommendations

The following recommendations should be taken into account for further research.

8.1 Adsorption and desorption characteristics of γ -alumina and silica separately

In order to distinguish between the characteristics of silica and of γ -alumina obtained simultaneously with ellipsometry, it is recommended to determine the optical properties of γ -alumina separately. Measurement data of *dry* γ -alumina samples are available, but *adsorption* (and desorption) measurement data presented in this research are not applicable. Adsorption measurements on γ -alumina have been done with one energy scan for each relative pressure, but should be done using time scans just like the silica samples were measured upon adsorption.

In order to obtain the characteristics of each layer separately, sorption studies could also be done on each porous layer itself. If it is a matter of determining *material* characteristics and not *membrane* characteristics, it should be considered to apply the porous layer on top of a dense substrate, for example a silicon wafer.

8.2 Fine-tuning gas-delivery

Relative water vapor pressure is independent of the applied (helium) pressure (see also paragraph 5.2.2), but that is a theory. In practice, there might be found a dependence of total pressure and the adsorption rate. Also, the used flow values were low (30-50 ml/min) and no change in adsorption rate is assumed since the relative water vapor pressure is independent of flow. Again, this might be different in practice.

An important remark should be made with respect to the possible use of hazardous gases or vapors. The gas vent system at the lab of the ellipsometer is not suitable for severe chemicals, such as ammonia gas. The use of hazardous gases would mean a serious alteration of the set-up. Not only because of the vent after the bubbler (at stream 10) to the ambient, but also because the whole system has to be perfectly gas-tight. Gas leakage has occurred regularly, although it has not been detected recently.

Another point of consideration is the set-up for the water bubbler. It is unknown if the carrier gas was completely saturated with water. Therefore, a preceding bubbler can be installed at a higher temperature than needed in the next bubbler. In this way, the incoming wet flow into the second bubbler will be saturated for sure. In Figure 8.1, the set-up is drawn schematically.

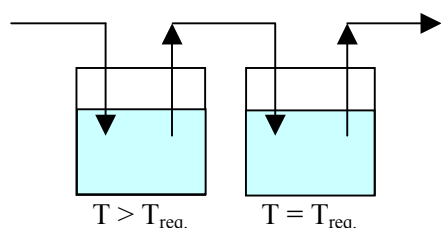


Figure 8.1. Two water bubblers in a sequence in order to assure the carrier gas of being saturated with water vapor at the required temperature (T_{req}).

8.3 New ellipsometry sample cell

During the last phase of the current research project, a new ellipsometry sample cell has been developed. A short description of the design is presented in the following.

Limitations of the current set-up have been mentioned in Chapter 7 (Conclusions) and problems were related to the temperature control of the cell and –more importantly– of the sample. This problem was the main focus in the design of the new cell. Further enhancements were made and are (in random order):

Multi-angle ellipsometry

The cell is closed by a quartz glass bulb, which is cylindrical in the region where the light beam enters the cell (and leaves after reflection). The top of the cylinder is again made of quartz and is half a sphere. The sample is placed exactly in the center of the cylinder and hence, the light beam will always enter the cell perpendicular to the cylinder surface.

Heating plate behind the sample and directly in contact with the sample

The heating plate will have been calibrated in order to set the exact temperature wanted. The sample temperature can be known with high accuracy at the center of the cell, which is the place where the light beam hits the sample.

Sample temperatures of 30 to 600 °C can be established

The possibility of high temperature measurements is very useful, especially with regard to the effect of water vapor.

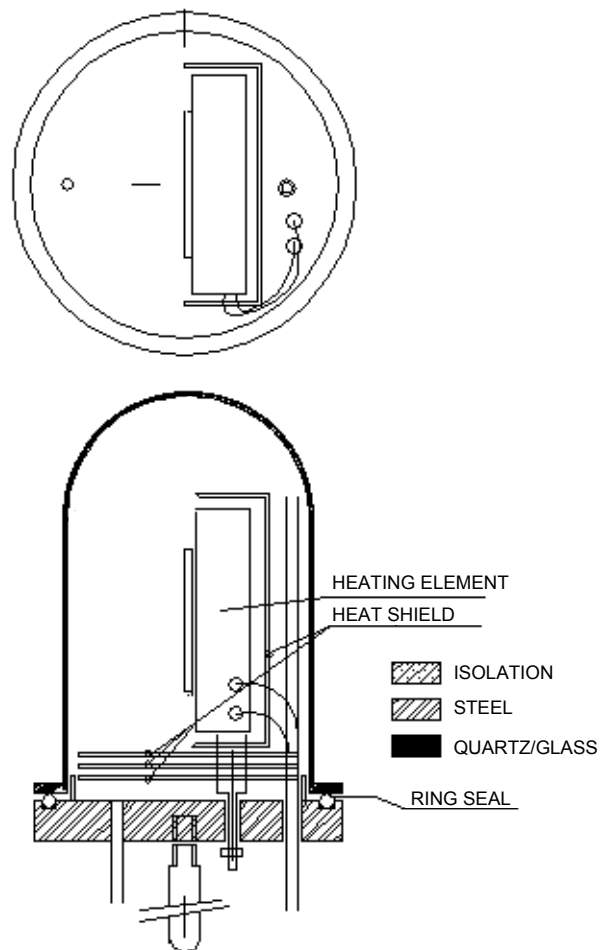


Figure 8.2. Design of new ellipsometry sample cell.

8.4 Further calculations

Calculation of surface area, pore size and PSD requires the value of the amount of adsorbed particles or volume. In the Langmuir isotherm, the height of the saturation plateau represents this value. Also, the Langmuir equation can be used to calculate the value. As mentioned in the Conclusions, no quantitative analysis can be performed based on only the isotherms.

As pointed out shortly in Chapter 1, quantitative characteristics of the samples can be obtained using a similar model based on the Bruggeman EMA, presented by Benes *et al.*, 2001. Consequently, thickness, porosity and PSD can be obtained.

8.5 Use of the current cell

Although as new cell will be used in future research, the current cell may still be useful. Probably not in the current field of research, but it may be used for measurementents in less demanding environments, for example surfactant adsorption studies (Denoyel, 2002). These measurements are normally done at room temperature and the sample is placed in a solvent. Still, temperature control has to be assured and is assumed to improve already due to the higher rate of heat transfer in liquid than in gas. Hence, the sample temperature will be most probably be the same as the cell temperature and temperature changes can be established relatively fast.

References

- Alvarez-Herrero A., Guerrero H., Bernabeu E. and Levy D., 'Analysis of nanostructured porous films by measurement of adsorption isotherms with optical fiber and ellipsometry', *Appl. Opt.* 41(31) (2002) 6692–6701.
- Alvarez-Herrero A., Heredero R.L., Bernabeu E. and Levy D., 'Adsorption of water on porous Vycor glass studied by ellipsometry', *Appl. Opt.* 40(4) (2001) 527–532.
- Atkins P.W., *Physical chemistry*, Oxford University Press, Oxford etc., 5th ed., 1994.
- Azzam R.A.M., and Bashara N.M., *Ellipsometry and polarized light*, Elsevier, Amsterdam, 1986.
- Baklanov M.R. and Mogilnikov K.P., 'Non-destructive characterisation of porous low-k dielectric films', *Microelec. Eng.* 64 (2002) 335–349.
- Baklanov M.R., Mogilnikov K.P., Polovinkin V.G. and Dultsev F.N., 'Determination of pore size distribution in thin films by ellipsometric porosimetry', *J. Vac. Sci. Technol. B* 18(3) (2000) 1385–1391.
- Benes N.E., Nijmeijer A., Verweij H., 'Microporous silica membranes', in: Kanellopoulos N. (ed.), *Separations with Microporous membranes*, Elsevier, Amsterdam, 2000.
- Benes N.E., Spijksma G., Verweij H., Wormeester H. and Poelsema B., 'CO₂ sorption of a thin silica layer determined by spectroscopic ellipsometry', *AIChE J.*, 47(5) (2001) 1212–1218.
- Bhandarkar M., Shelekhin A.B., Dixon A.G. and Ma Y.H., 'Adsorption, permeation, and diffusion of gases in microporous membranes. I. Adsorption of gases on microporous glass membranes', *J. Membr. Sci.* 75 (1992) 221–231.
- Born M. and Wolf E., *Principles of optics*, 6th ed., Pergamon Press, Oxford, 1986.
- Chaplin M., website *Water structure and behavior*, <http://www.lsbu.ac.uk/water/>, martin.chaplin@lsbu.ac.uk, March 19, 2004.
- Denoyel R., 'Microcalorimetry and ellipsometry in surfactant adsorption studies', *Colloids and Surfaces A* 205 (2002) 61–71.
- De Vos R.M. and Verweij H., 'Improved performance of silica membranes for gas separation', *J. Membr. Sci.* 143 (1998) 37–51.
- Dobkin D.M., website *Fundamentals of Chemical Vapor Deposition, Special topic: Vapor delivery*, http://www.batnet.com/enigmatics/semiconductor_processing/CVD_Fundamentals/reactors/reactorTOC.html Oct, 2003.
- Dultsev F.N. and Baklanov M.R., 'Nondestructive determination of pore size distribution in thin films deposited on solid surfaces', *Electrochem. Solid-State Lett.* 2(4) (1999) 192–194.
- Fardad M.A., Yeatman E.M., Dawnay E.J.C, Green M. and Horowitz F., 'Effects of H₂O on structure of acid-catalysed SiO₂ sol-gel films', *J. Non-Crystall. Solids* 183 (1995) 260–267.
- Grillet Y. and Llewellyn P., 'Adsorption properties of the silica surface', p.23–81, in: Legrand A.P. (ed.), *The surface properties of silicas*, John Wiley & Sons, Chichester, 1998.
- Imai H., Morimoto H., Tominaga A. and Hirashima H., 'Structural changes in sol-gel derived SiO₂ and TiO₂ films by exposure to water vapor', *J. Sol-Gel Sci. Technol.* 10 (1997) 45–54.
- Legrand A.P. (ed.), *The surface properties of silicas*, John Wiley & Sons, Chichester, 1998.
- Lide, D.R. (ed.), *CRC Handbook of Chemistry and Physics*, CRC Press LLC, Boca Raton etc., 83rd ed., 2002.
- Muranova G.A. and Perveev A.F., 'Microporosity of thin films', *Sov. J. Opt. Technol.* 60(2) (1993) 91–100.
- Oura K., Lifshits V.G., Saranin A.A., Zotov A.V., and Katayama M., *Surface Science, An introduction*, Springer-Verlag, Berlin etc., 2003.
- Ranke W., *Modern methods in heterogeneous catalysis research: theory and experiment. Adsorption I*, <http://w3.rz-berlin.mpg.de/~jentoft/lehre>, Nov. 2002.
- Shaw D.J., *Introduction to colloid & surface chemistry*, Butterworth-Heinemann, Oxford etc., 4th ed., 1992.
- Shriver D.F., Atkins P.W., Langford C.H., *Inorganic chemistry*, Oxford University Press, Oxford etc., 2nd ed., 1994.

-
- Sing K.S.W., Everett D.H., Hall R.A.W., Moscou L., Pierotti R.A., Rouquérol J., and Siemienińska T., 'Reporting physisorption data for gas/solid systems', *Pure & Appl. Chem.*, 57(4) (1985) 603–619.
- Tolmachev V.A., 'Adsorption-ellipsometry method of studying the optical profile, thickness, and porosity of thin films', *J. Opt. Technol.* 66(7) (1999) 596–607.
- Tolmachev V.A., 'Estimating the pore size in thin films by ellipsometry', *J. Opt. Technol.* 68(5) (2001) 328–332.
- Tolmachev V.A., Okatov M.A. and Matsoyan E.F., 'Determining the porosity and true index of refraction of thin films by ellipsometry', *Sov. J. Opt. Technol.* 60(5) (1993) 327–329.

List of symbols

Latin symbols

Symbol	Unit	Description
a_m	m^2	effectively occupied area by an adsorbed molecule
A_s	m^2	surface area
cf	-	correction factor
d_p	m	pore diameter (usually in nm)
E_0	$J.mol^{-1}$	characteristic heat of adsorption (Dubinin-Radushkevich eq. 2.4)
E_{act}	$J.mol^{-1}$	activation energy (of sorption)
E_{ads}	$J.mol^{-1}$	isosteric heat of adsorption
E_p	-	light wave parallel to the plane of incident
E_s	-	light wave perpendicular to the plane of incident
f	-	volume fraction
I	$m^{-2}.s^{-1}$	flux
K_L	-	Langmuir sorption equilibrium constant
K_L^0	-	K_L at constant temperature for an ideal mono-atomic gas
k	-	extinction coefficient
$k_{ads,n}, k_{des,n}$	s^{-1}	adsorption/desorption rate constant for kinetic order n; an additional superscript 'p' indicates the rate from a precursor state
k_B	$J.K^{-1}$	Boltzmann constant
m	kg	adsorbate particle (molecule or atom) mass
n	-	kinetic order
\tilde{n}	-	complex refractive index
n_a	-	amount of adsorption sites occupied
N_{AV}	mol^{-1}	Avogadro number
n_{sat}	-	total amount of adsorption sites, or monolayer capacity
p	Pa	partial vapor pressure of the adsorptive
p_2	bar	pressure difference from standard pressure (1 bar)
p_{cal}	$^\circ$	polarization angle at which the amplitude is zero
p_r	-	relative vapor pressure (eq. 2.2)
p_{sat}	Pa	adsorptive vapor pressure at which the adsorbent is saturated
R^2	-	indication of statistical regression quality ($R^2=1$ is ideal)
r_{ads}, r_{des}	s^{-1}	rate of adsorption and desorption, respectively, an additional superscript 'p' indicates the rate from a precursor state
R_p, R_s	-	complex Fresnel reflection coefficients
s	-	sticking coefficient
s_0	-	(initial) sticking coefficient at zero coverage
\bar{s}		standard deviation
T	K	temperature
V_m	$m^3.mol^{-1}$	molar volume of a gas
w_0	m	average pore width (Dubinin-Radushkevich eq. 2.4)

Greek symbols

Symbol	Unit	Description
β	-	affinity coefficient (Dubinin-Radushkevich eq. 2.4)
Δ	rad or °	angle which indicates phase shift upon reflection of linearly polarized light
$\varepsilon_{\text{ads}}, \varepsilon_{\text{des}}$	J	precursor energy barriers for adsorption and desorption, respectively
$\tilde{\varepsilon}$	-	complex dielectric function
θ	-	surface coverage; an additional subscript 'p' indicates precursor surface coverage; subscript 'e' indicates equilibrium
θ_{Ψ}	-	coverage expressed in terms of Ψ
λ	m	wavelength (usually in nm)
φ	rad or °	angle of incidence
ρ	-	complex ratio of reflection coefficients
σ	-	condensation coefficient (eq. 2.9)
τ	s	mean stay time or mean surface lifetime (eq. 2.22)
Ψ	rad or °	angle which indicates change in amplitude after reflection of linearly polarized light
$(\tan \Psi)_{\text{sat}}$	-	value of $\tan \Psi$ at maximum coverage
$(\tan \Psi)_0$	-	value of $\tan \Psi$ at zero coverage (blank)

Appendices

Table of contents

A	Measurement logs/overview sheets (*.xls).....	2
A.1	ellipso sorption.....	2
A.2	031205-08 lt_g1a.....	3
A.3	031211 ws_g1b.....	4
A.4	031212 ws_g1b des.....	4
A.5	031217-18 ws_sila.....	5
A.6	031223 ws_silb-ads.....	6
A.7	040120 ws_silb-des.....	7
A.8	040226-27 ws_silc.....	8
A.9	040317 ws_silc-2.....	9
B	Plots.....	10
B.1	Adsorption.....	10
B.1.1	031223 ws_silb-ads.....	10
B.1.2	040226-27 ws_silc.....	11
B.1.3	040317 ws_silc-2-.....	12
B.2	Desorption.....	15
B.2.1	040226-27 ws_silc.....	15
B.2.2	040120 ws_silb-des.....	15
B.2.3	040227 ws_silc dryHe.....	16
C	Heating rope calibration plot.....	17

A Measurement logs/overview sheets (*.xls)

A.1 ellipso sorption

Measurement file description					
measurement files are named "energyscan" in addition to the "base" name ("first", "second", etc.); e.g. "firstenergyscan.txt")					
bb=bad boehmite					
date	sample	additional sheet name	description	remarks	# runs in file
1112	1 γ (bb) no.1	first	blank, 1.5-3.0 eV, 20steps, shutter 10/10, gain=0, 1zone, calibration@2.5eV, Tcell=100		2
1113	1 γ (bb) no.1	first	blank, 1.5-4.0 eV, rest same as 1112, p2=0.77, flow >200		1
		second	blank, same as first but 1.5-3.0 eV	leaking bolt	1
1114	1 γ (bb) no.1	first	blank, 1.5-3.0 eV, 61 steps(size 0.025), shutter 10/10, gain=0, 2zone, calibration@2.5eV and gain=3, flow ~10, Tcell=100	cell still leaking	1
		second	wet flow, stabilizing during 1st run, 3 full runs, 4th run unfinished(error), water@80°C, p2=0.94, flow ~8	error during 4th run	3(+)
		third	continuing "second" after ~10 min.		5
		diff.	calculation of (absolute) difference wet scans from blank		
1117	1 γ (bb) no.2	first	blank, 1.7-2.9 eV, 48 steps(size 0.025), 1zone, gain=0, calibration@2.3eV and gain=3, flow ~10, Tcell=100	leak >200 (hole in bolt), repaired with Si-kit	1
1118	1 γ (bb) no.1	first	blank, 1.7-2.9 eV , 48 steps(size 0.025), 2zone, gain=0, calibration@2.3eV and gain=3, flow ~14, Tcell=100, but energy range might not be enough after all -> "second"	lamp: (+)side 100°C, (-)side 285°C	1
		second	blank, 1.5-3.0 eV , 61 steps(size 0.025), 2zone, gain=0, calibration@2.25eV and gain=3, flow ~14, Tcell=100		2
		third	wet flow, stabilizing during 1st run, 3 full runs, 4th run unfinished(error), water@80°C, p2=0.91-0.92, flow=10-13, start 13:27, end 16:32	first point of run not always measured at 1.5eV, but before return of monochromator	32
		diff.	calculation of (absolute) difference wet scans from blank		
		diff. (2)	calculation of difference wet scans from blank		
1119	1 γ (bb) no.1	sixth	blank, 1.5-3.0eV, 2zone, gain=0, using fifthcalibration (@2.25eV and gain=3)	degassing overnight	3
		seventh	wet flow, 1.5-3.0, 2zone, start gain=3, water@95°C, using fifthcalibration, flow stabilizing during first run, flow ~15, p2=0.95	tried with lamp on -> unsuccessful	
		diff.	calculation of difference wet scans from blank		
		diff. (2)	calculation of (absolute) difference wet scans from blank		
1121	1 γ /1tc6/1SiO2 piece of XPS sample	first-blank	blank, 1.5-3.0 eV, 61 steps(size 0.025), 2zone, startgain=3, calibration@2.25eV and gain=3, Tcell=96	degassing overnight	2
		first-wet	wet flow, 1.5-3.0, stepsize x2: 0.050 , 2zone, water@40°C, flow stabilizing during first run, flow ~15, p2=0.95, Tcell=96, startgain 3	after measurement: yellow (more than other pieces)	15
		diff.	calculation of (absolute) difference wet scans from blank		

A.2 031205-08 lt_g1a

date	20031205-08				
long term on gamma1 @ 100°C (T-thermoc. = 98-100 °C)					
Problems were detected with monochromator; error of ~9 nm when run from low energy to high. Therefore, it is recommended to run spectroscopic ellipsometry measurements from low wavelength to high.					
==>	begin	413.0 nm	(=3.002 eV)		
	end	826.0 nm	(=1.501 eV)		
Two zone 59 steps, stepsize 7.0 nm Alignment: 130° best, 170° good Calibration @ 2.25 eV					
Measurements					
longt_g00	blank	afterwards alignment check: bad			
longt_g01	blank2				
longt_g02	blank3 (duplo)				
Wet flow : longt_g03 (Twaterbath set @30°C)					
start	15:00	flow stabilizing during 1st run halfway (600nm) : p2=0.88 flow=16 Twater=33.5			
		<u>p2</u>	<u>flow</u>	<u>Twaterbath</u>	<u>time (hr)</u>
-	start 2nd run	0.88	16.0	33.5	0.23
-	end 2nd run	0.88	16.6	34.0	0.46
-	after 4th run	0.88	17.6	34.6	0.92
-	16:08	0.88	18.0	35.1	1.13
-	17:00	0.87	18.8	35.9	2
end	8/12, 9:00	0.88	20	38.8	66
-					
==> increasing water-temp and increasing flow stabilized after a relatively short time					
031208					
lt_g1_00	blank				
lt_g1_01	blank2 (duplo)				
Data processing					
g03-20 and later appear to have problems: zone1 and 2 differ much Therefore, the NewMeanTanPsi has been used for "Chart1", especially for these measurements. The wrong point has been eliminated in the mean value, thus using only the corresponding value of the other zone.					

A.3 031211 ws_g1b

20031211					time			energy scans 413.0 - 826.0 nm	calibration@2.25eV	
Twater	filename	flow	p2	Tcell	start	finish	next T reached	23 steps, stepsize 18.0nm	shutter open/closed 10/10	Cell: Toil = 65°C
	ws_g1-				+ 10min!					
--	00	36	0.80	52	0:00	0:00	--		startgain 3	
10	01	32	0.77	52	0:10	0:16	0:20			
12	01w	31.8	0.77	52	0:23	0:29	--			time estimation
	02	32	0.77	52	0:31	0:37	0:41			96 1.6
14	02w	31.4	0.77	52	0:41	0:47	--	2 pnts 2nd run - delete!		150 2.5
	03	32	0.77	52	0:51	0:57	1:01			246 4.1
16	04w	32	0.77	52	1:01	1:07	--			
	04	32	0.77	52	1:11	1:17	1:21			
18	05w	32	0.77	52	1:21	1:27	--			
	05	32.5	0.77	52	1:31	1:37	1:41			
20	06w	31.6	0.77	52	1:41	1:47	--			
	06	32.5	0.77	52	1:51	1:57	2:01			
22	07w	32	0.77	52	2:03	2:09	--			
	07	33	0.77	52	2:13	2:19	2:23			
24	08w	31.4	0.75	52	2:23	2:29	--			
	08	32.9	0.77	52	2:33	2:39	2:44			
26	09w	32	0.77	52	2:44	2:50	--			
	09	33.6	0.77	52	3:00	3:06	3:10			
28	10w	33	0.77	52	3:10	3:16	--			
	10	34	0.77	52	3:20	3:26	3:30			
30	11w	31.5	0.77	52	3:30	3:36	--			
	11	33.5	0.77	52	3:40	3:46				
desorption	des	34.5	0.80	52	3:48					

A.4 031212 ws_g1b des

20031212					time			energy scans 413.0 - 826.0 nm	calibration@2.25eV
desorption	filename	start	finish					23 steps, stepsize 18.0nm	shutter open/closed 10/10
run #	ws_g1-des-	daytime						startgain 3	
1	00	15:19							
10	01								
20	02								
30	03								
40	04								
50	05								
60	06								
70	07								
80	08								
90	09								
100	10								
110	11								
120	12								
130	13								
140	14								
150	15								
160	16								
170	17								
180	18								
191	19								

Result 20031211 ws_g1b
NewMeanTanPsi

	time	flow	p2	Tcell
11-Dec	15:19	34.5	0.80	52
12-Dec	9:00	36	0.78	53
	10:00	37	0.79	53
	12:10	36	0.78	53
	13:44	36	0.78	53
monochromator error ==> stop				

A.5 031217-18 ws_si1a

20031217								
Twater	filename	flow	p2	Tcell	time			
					start	finish	next T reached	
	ws_si1a-ads-				+ 10min!			
--	00	34	0.78	57	--	--	--	
	00b	34	0.78	55	--	--	--	
	00c	34	0.78	51	--	--	--	
10	01w	>200	0.30	51	0:00	0:06	--	
	01	30.5	0.74	51	0:10	0:16	0:21	
14	02w	27	0.74	51	0:21	0:27	--	
	02	30	0.74	51	0:33	0:39	0:44	
18	03w	28	0.74	51	0:44	0:50	--	
	03	30	0.74	51	0:54	1:00	1:05	
22	04w	28.3	0.74	51	1:05	1:11	--	
	04	30.5	0.74	51	1:15	1:21	1:25	
26	05w	29	0.74	51	1:25	1:32	--	
	05	30.6	0.74	51	1:35	1:41	1:45	
30	06w	27	0.74	51	1:45	1:51	--	
	06	31	0.74	51	1:55	2:01	2:06	
40	07w	22	0.74	51	2:05	2:11	--	
	07	31	0.74	51	2:16	2:22	2:27	
50	08w	21	0.74	51	2:27	2:33	--	
	08	30.9	0.74	51	2:37	2:43	2:54	
	ws_si1a-des-							
40	01w	37.2	0.74	51	2:54	3:00	--	
	01	33.5	0.74	51	3:05	3:10	3:22	
30	02w	36.8	0.74	51	3:22	3:28	--	
	02	33.6	0.74	52	3:32	3:38	3:44	
26	03w	34.9	0.74	52	3:44	3:50	--	
	03	33	0.74	52	3:54	4:00	4:05	
22	04w	34.5	0.74	52	4:05	4:11	--	
	04	33	0.74	52	4:16	4:22	4:28	
18	05w	34.5	0.74	52	4:28	4:34	--	
	05	33.1	0.74	52	4:38	4:44	4:49	
14	06w	34.6	0.74	52	4:49	4:55	--	
	06	33	0.74	52	5:00	5:06	5:11	
12	07w	34.4	0.74	52	5:11	5:17	--	
	07	33	0.74	52	5:21	5:27	5:31	
10	08w	33.5	0.74	52	5:31	5:37	--	
	08	32.8	0.74	52	5:41	5:47	--	
	blank2-00	measured 031218, same conditions as blank1						

energy scans 413.0 - 826.0 nm	alignment: 170° and 130°: best
23 steps, stepsize 18.0nm	calibration@2.25eV , phase, fast, step 0.50°
shutter open/closed 10/10	startgain 3, endgain 0
startgain 3, 2zone	

Measurement loop	
1 a	at t=(next T reached) + 10 min, start actual run
b	record start time, flow, p2, Tcell
2 a	directly after run, set next temp
b	and set monochromator back to 413nm
c	and set next file name (w-file)
3 a	at t=(next T reached), start w-run
b	record start time, flow, p2, Tcell
4 a	after w-run set monochromator back to 413.0nm
b	and set next file name
5 a	see 1a

A.6 031223 ws_si1b-ads

20031223							start each scan at t=0 time
Twater	filename	flow	p2	Tcell	T set	T reached	
ws_si1b-ads-							
--	00	36.5	0.78	53	--	--	energy scan (413-826nm, step 18nm (23x), shutter 10/10, startgain 3)
10	01	>200	0.18	52	0:00:40		signal stable after 10 min; time T set is actually time start wet flow
		32.5	0.73	52			
14	02	28	0.74	51	0:00:15	0:04:20	14min20: signal seems to decrease 16min 50: still decreasing 19min 50: signal seems stable stop after 23 min
		32	0.74	51			
18	03	31	0.74	51	0:00:20	0:04:40	15min: still decreasing 19min 50: signal seems stable 22min: enlargement scale ==> still decreasing 24min40: still decreasing 27min10: seems stable
		33.5	0.74	51		0:30:00	
		33	0.74	51		0:33:00	
		33	0.74	51		0:41:00	still decreasing
		33	0.74	51		1:06:00	change seems to be slowing down pt 159 has been made at ~ 1:19:40
		34	0.74	51-52		2:04:00	seems stable
		35	0.74	52		2:34:00	
		34	0.74	52		2:45:00	seems stable ==> continue for another 10 min.
		35	0.74	52		2:55:00	stop after 2h55min

Previous measurement took longer than expected.
Therefore, energy scan is made before next step.
Also, next scans at **0.5pt/min** and a large Twater-step is applied (18 ==>40).

18	04	35	0.74	52	--	--	energy scan (413-826nm, step 18nm (23x), shutter 10/10, startgain 3)
40	05	24	0.74	52	0:00:20	0:05:51	
		34	0.73	52			1:02:00
		34	0.74	52			1:24:00
		34	0.73	52			1:53:00
							2:34:00 stop after 2h34min

20040107

-- blank2 30 0.78 53 has been measured on 040107
blank2b has been measured on 040107
In the last sheet, it has been determined which blank2 will be used as good measurement.

time scans, 2 pnt/min alignment:170° good-best, 130° good
one zone (~170°) calibration@2.5eV, phase, fast, step 1°
shutter open/closed 20/20 startgain 3, endgain 3
startgain 3 Tcell ~ 50°C (Toil=65°C)

Measurement steps
1 start scan (t=0)
2 set new T & record time
3 record time new T reached
4 run scan for at least 10 min after T reached

A.7 040120 ws_si1b-des

energy scans 3.0 - 1.5 eV
 30 steps, stepsize -0.050
 shutter open/closed 50/20
 startgain 5 (endgain automatically 5)
 two zone

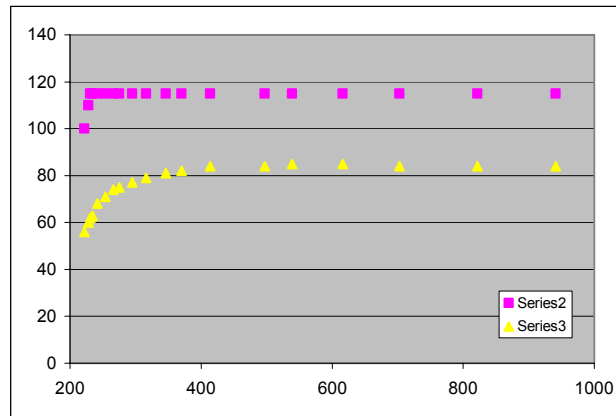
alignment:170° and 130°: good
 calibration@2.25eV , phase, fast, step 0.50°
 startgain 3, endgain 0

20040120

Chart1 gives overview

timescans @2.5 eV
 onezone 170°
 6 pt/min
 shutter 80/20
 run as long as signal is changing

filename	flow	p2	pt#	time	Toil	Tcell	time (s)
ws_si1-des2- si1-b-des-blank1							
n.a.	40	0.71			65	50	on 040112
00							saturation overnight 6pm-9.30am
01							energy scan
02			0	0:00:00			time scan; stopped, wrong p angle
			31				time scan
	46	0.74	200		65	50	start dry He flow
			222		100	56	flow&p2 stable / set Toil at 115°C
			228		110	60	
			231		115	62	
			234		115	63	
			242		115	68	
			254		115	71	
			266		115	74	
			275		115	75	
			295		115	77	
			316		115	79	
			346		115	81	
			370		115	82	
			414		115	84	
			497		115	84	
			539		115	85	
			616		115	85	
			703		115	84	
			822		115	84	
			941		115	84	



1273	115	84
1280	115	102
1291	115	111
1315	115	116
1329	115	117
1335	115	118
1340	115	122
1357	115	128
1421	115	131
1460	115	132
1535	115	133
1559	115	132
1601	115	133
1644	115	133
1676	115	134
1698	115	134
1706	--	133
1715		134
1730		133
1736		148
1739		153
1741		154
1747		157
1760		159
1809		160
1873		160
1938		161
1960		161
1978		161
1992		161

turn on lamp, low intensity

increase lamp intensity

turn off oil bath

increase lamp intensity to mark

blank2

measured on 040121

A.8 040226-27 ws_si1c

filename	flow	p2	pt#	time (real)	Tcell	time (s)	Twater	
20040226-27								energy scans 3.0 - 1.5 eV 30 steps, stepsize -0.050 shutter open/closed 50/20 startgain 5 (endgain automatically 5) two zone
20040305 (blank2)								timescans @2.5 eV; 6 pt/min onezone ~170° shutter 80/20 start + end gain 5 run as long as signal is changing
ws_si1c-								alignment: 170° and 130°: 1,2,3 amplitude < -30 calibration@2.25eV , phase, fast, step 0.50° startgain 3, endgain 0, shutter 50/20
n.a.	~90	0.74			216 (end)			degassing overnight 7.30pm-8.30am
00					57			blank - energy scan
01								time scan; stopped, wrong p angle
02	40	0.77	1	10:18:00	56	0		Toil (65 +/- 0.3) °C
			54			540	10	start wet flow Twater=10°C
	38	0.73	200		56	1991		steady flow&p2 from ~2000
						7592		measurement error - adc pacer overrun
								restart ell. software
03-time	38	0.73	1	13:09:00	56	10260	10	start = 13:09 new measurement - determining if signal is constant
	38	0.73			56	11660		stop = ~13.30
03-energy	38	0.73		13:35:00	56		10	
04	38	0.73	1	13:49:00	56	0	10	
	~15	0.74	57		56	~560		set Twater=26°C
	24	0.74	85		56		26	
	28	0.73	88		56			
	34	0.73	107		56			steady flow&p2 appearing
	36	0.73	126		56			steady flow&p2
	37	0.73	144		56			
	37	0.74	170		56			
	37.5	0.73	189		56	~1880		
	38	0.74	238		56			
	38	0.74	338	14:45:00	56	3342		stop: adc pacer overrun
								restart ell. software
05	38	0.74	1	15:07:00	56	4662	26	continue measurement
	37.8	0.74	573		56			
06	37	0.74			56		26	energy scan
								stop during run; again "adc pacer overrun"
								restart ell. software
07	37	0.74			56		26	rerun energy scan 06
08			1				26	time scan - saturation overnight
2pt/min!	37	0.74	5		56			set Twater=50°C
								error in controllermodule!
09				17:55:00				rerun time scan (saturation overnight)
	34.5	0.73	1821	9:03:00	55		50	end:wrong data! Polarizer at 0° !!!!!
des00							50	energy scan - adc pacer overrun!!
des01							50	rerun energy scan des00
des02	34	0.73	1		55	0	50	time scan
6pt/min !	34	0.73	31		55			set Twater=26°C
	37	0.74	38		55			
	37.9	0.74	44		55		48.0	
	39.3	0.74	58		55		45.8	
	40.2	0.74	67		55		44.4	
	41.8	0.74	79		55		42.5	
	41.4	0.74	104		55		38.7	
	41.7	0.73	137		55		33.4	
	40.1	0.74	188		55		26.1	
			190			1891		Twater=26°C reached
	39.0	0.74	193		55		26.0	
	36.6	0.73	232		55		26.0	
			237	10:15:00		2362		stop: adc pacer overrun
								restart ell. software
des03	36.0	0.73	1	10:17:00	55	2482	26.0	continue time scan des02
	35.7	0.73	35		55		26.0	
	35.0	0.73	41		55		26.0	
	34.6	0.73	118		55		26.0	
	34.0	0.74	234		55		26.0	set Twater=10°C
	36.3	0.74	243		55		24.5	

A.9 040317 ws_si1c-2

energy scans 3.0 - 1.5 eV
 30 steps, stepsize -0.050
 shutter open/closed 50/20
 startgain 5 (endgain automatically 5)
 two zone

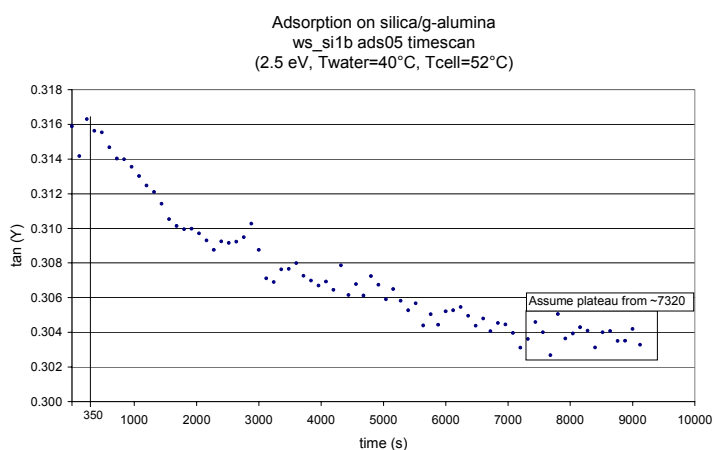
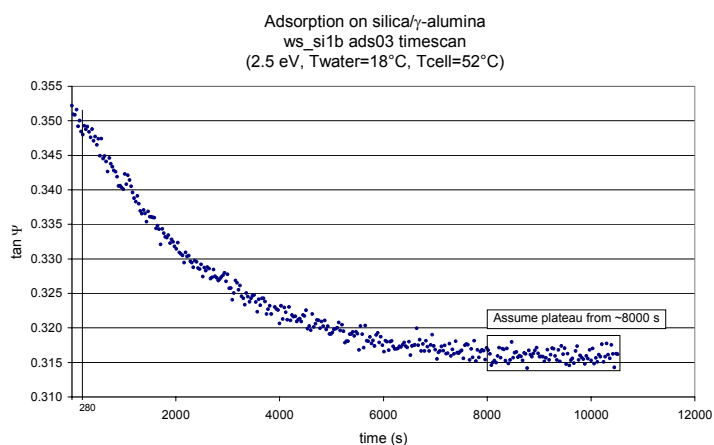
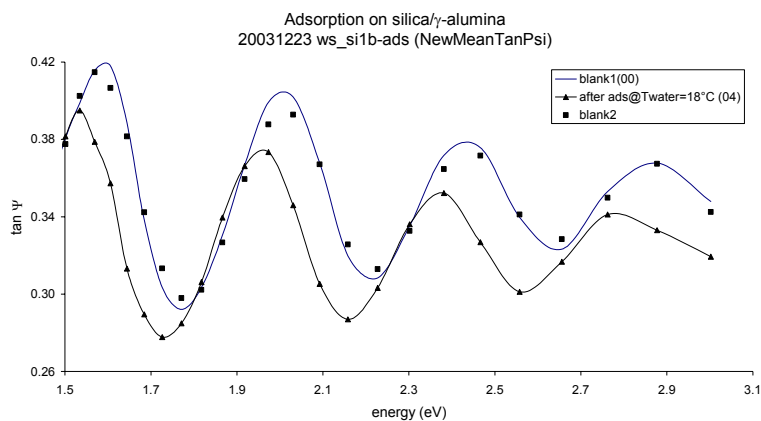
timescans @2.5 eV; 6 pt/min
onezone ~130°
 shutter 80/20
 start and end gain 5
 run as long as signal is changing

20040317	filename	flow	p2	pt#	time (real)	Tcell (°C)	time (s)	Twater	
	ws_si1c-2-					Toil=44.1 +/- 0.2 °C			alignment:170° good and 130° best
	00 energyscan	44.5	0.74			32			calibration@2.25eV , phase, fast, step 0.50° startgain 3, endgain 0, shutter 50/20
	01 timescan	44.5	0.74			32	0		
	zone=-20° !!! (~130°)			72		32	710	4.0	start wet flow
		39.5	0.70	125		31	1240	4.0	
		39.5	0.70	243		31	2421	4.0	flow stable from ca. 1900s
		40	0.70	540		32	5392	4.0	
		40.5	0.70	714		32	7133	4.0	
		40.5	0.70	859		32	8583	4.0	
		42.5	0.70	998		31	9974	4.0	
		43.5	0.70	1122		31	11215	4.0	
		43	0.70	1217		31	12165	4.0	
		42.5	0.70	1235		31	12345	4.0	
		43.5	0.70	1383		31	13826	4.0	
		43	0.70	1517		31	15166	4.0	
		42.5	0.70	1628		31	16294	4.0	
		43	0.70	2220		31	22216	4.0	
		43.5	0.70	2498	17:23:00	31	24997	4.0	
	02 energyscan	43	0.70			31		4.0	
	03 timescan	44	0.70	1	17:41:00	31	0	4.0	
	4pt/min			8		31	105		set Twater=10°C
	scan overnight	39	0.71	14		31	195	6.7	
		36	0.71	16			225	7.8	
		37.5	0.71	19			270	9.0	
		37	0.70	22			315	9.6	
		38.8	0.70	25			360	9.9	
		39	0.70	27			390	10.0	~400s: stable pressure
		39.5	0.70	29			420	10.1	
		40	0.70	34			495	10.1	
		42	0.71	43			630	10.0	
		44.5	0.70	3760	9:20:00	19	56397	10.0	
	<p>Apparently, the oil bath of cell failed! Actions:</p> <ul style="list-style-type: none"> - stop measurement - stop oil bath and turn on again - this seems to help because oil flows through cell again - extra heating by turning on lamp and turning off when 30°C was reached - after a few minutes, Tcell stays at 28°C; therefore, Toil in increased to 50°C for a short time 								
	04 timescan	44	0.70	1	9:40:00	32	0	10.0	4pt/min to determine equilibrium at Twater=10°C
		44.7	0.70	22		32	315	10.0	
		45	0.70	42		32	615	10.0	
		45	0.70	75		32	1110	10.0	
		45	0.70	158		33	2356	10.0	
		45	0.70	238		33	3556	10.0	
		45	0.70	278		33	4156	10.0	
		45	0.71	357		33	5342	10.0	
	05 energyscan	45	0.71			33		10.0	
	06 timescan	45	0.70	1	11:40:00	33	0	10.0	
				7			60		set Twater=19°C
		38.5	0.71	15		33	140	14.2	
		33.5	0.71	20		33	190	16.6	
		33	0.71	25		33	240	18.2	
		35	0.71	28		33	270	18.7	
		36.6	0.71	31		33	300	18.9	
		37.8	0.71	33		33	320	19.0	~320: pressure stable

B Plots

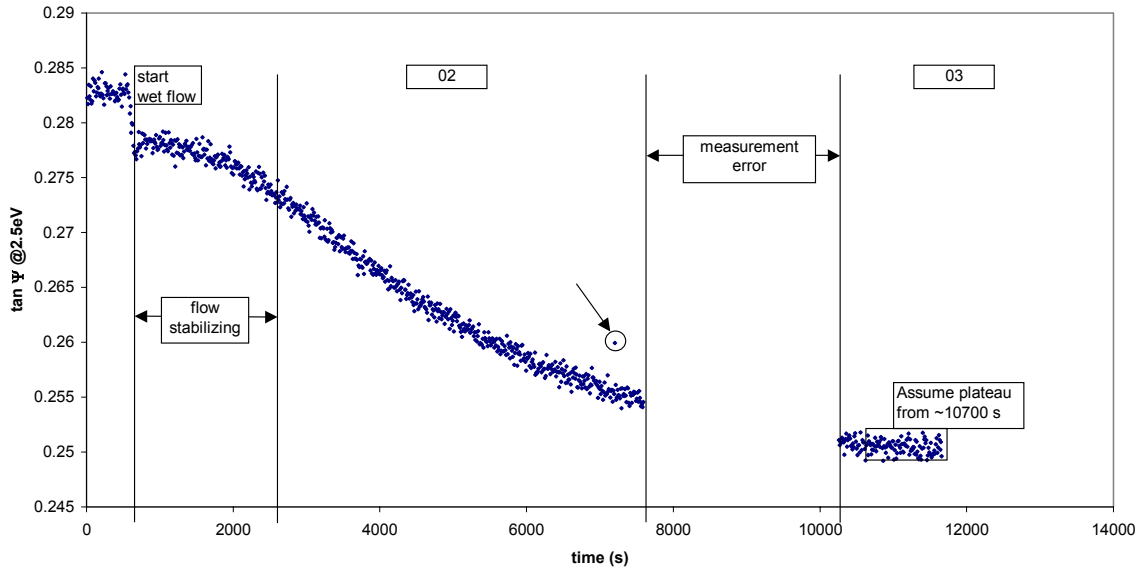
B.1 Adsorption

B.1.1 031223 ws_si1b-ads

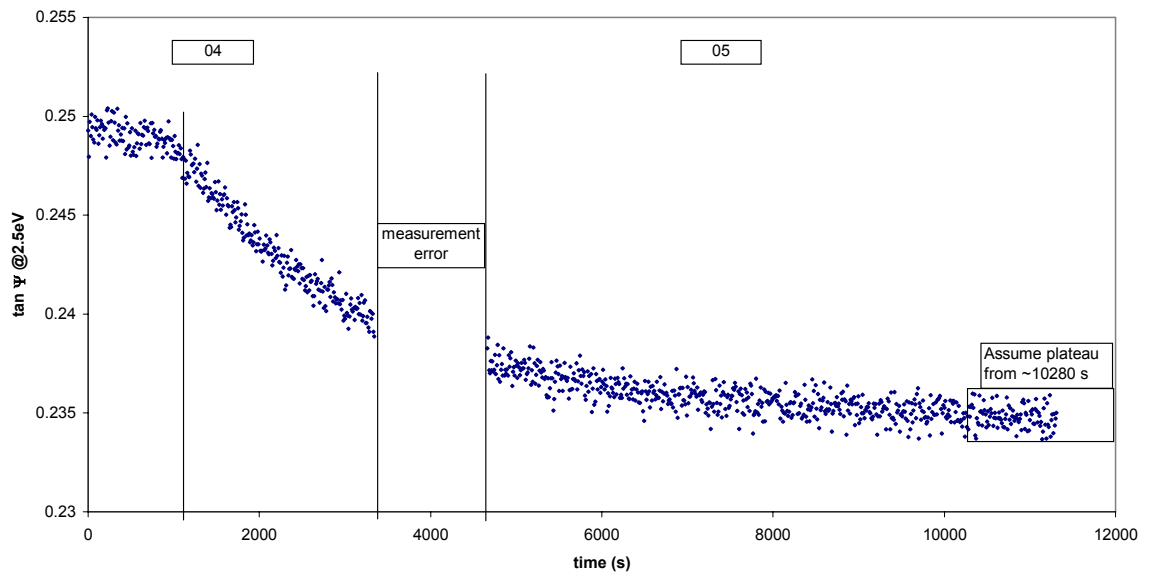


B.1.2 040226-27 ws_si1c

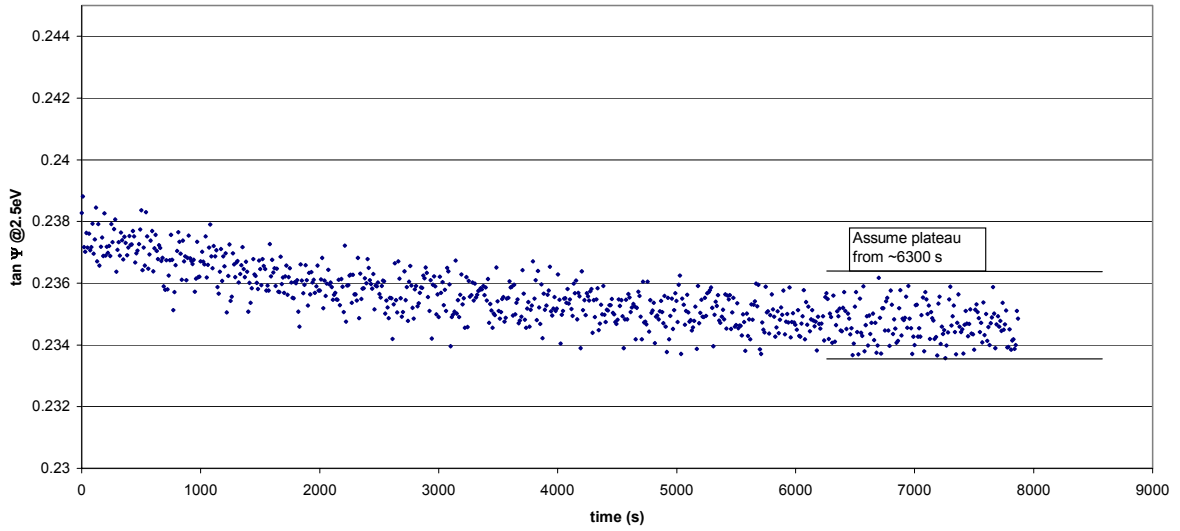
Adsorption on silica γ -alumina
 T_{water}=10°C, T_{cell} = 56°C
 ws_si1c 02 and 03



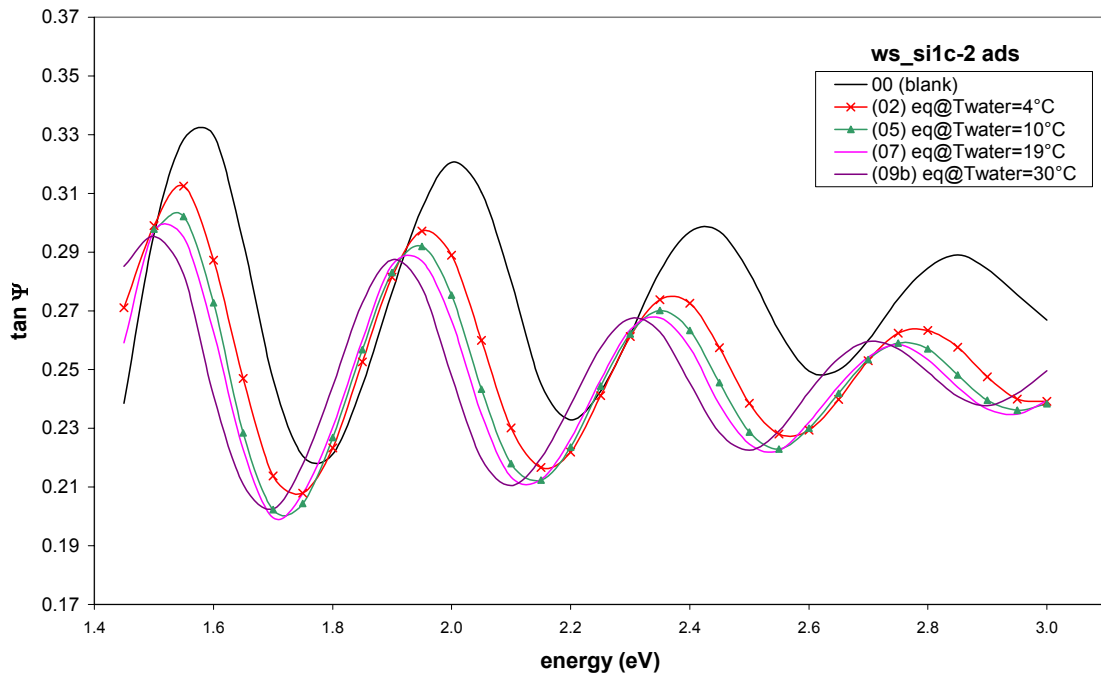
Adsorption on silica
 T_{water}=26°C
 ws_si1c 04 and 05



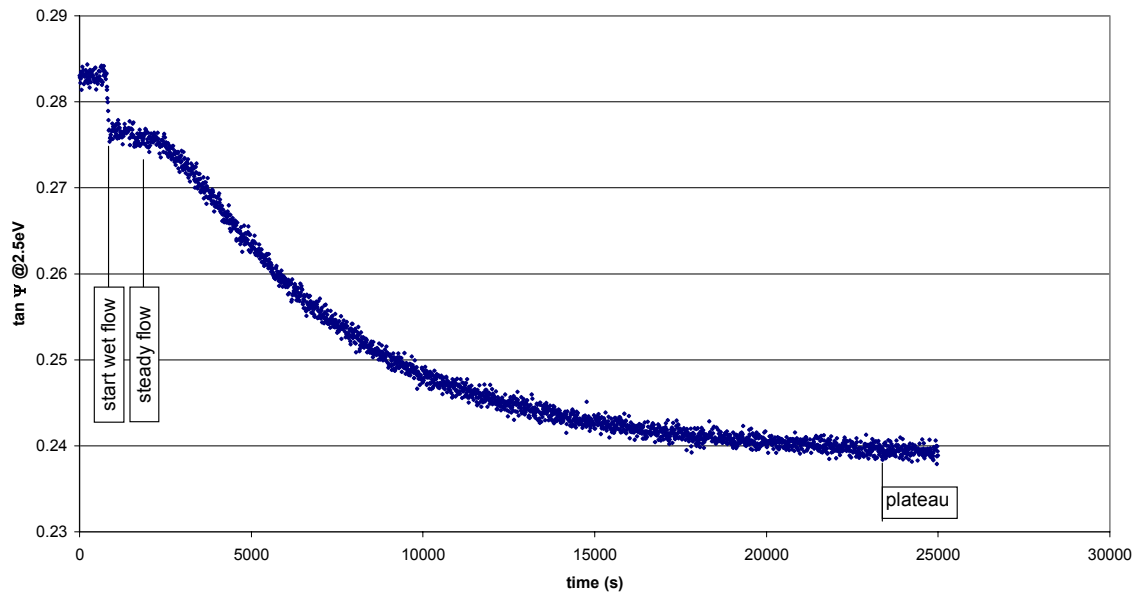
Adsorption on silica
 T_{water}=26°C
 ws_si1c 05



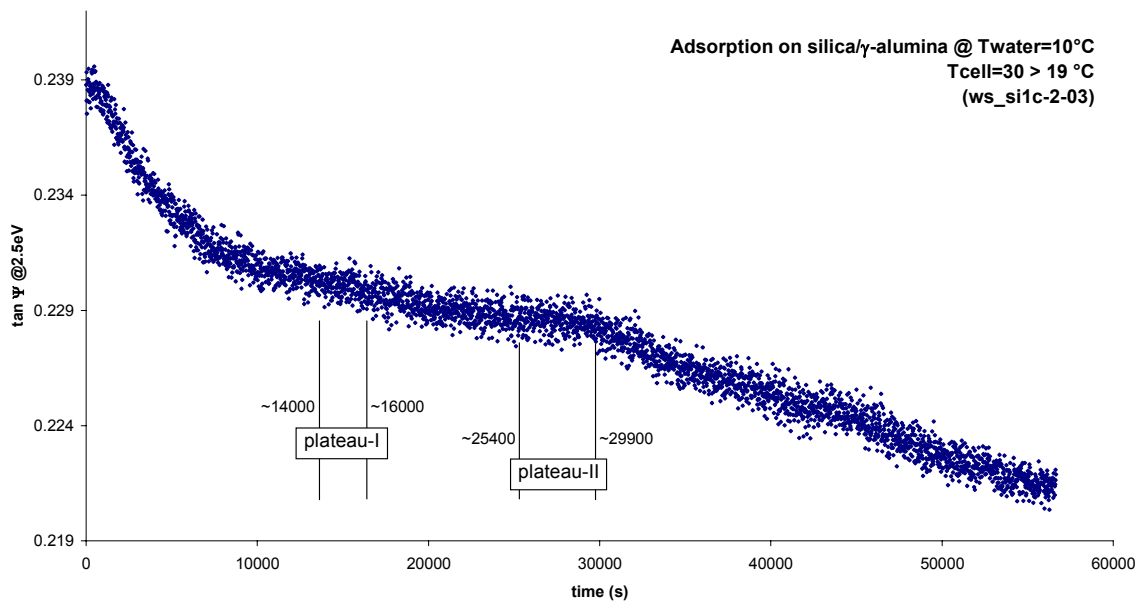
B.1.3 040317 ws_si1c-2-



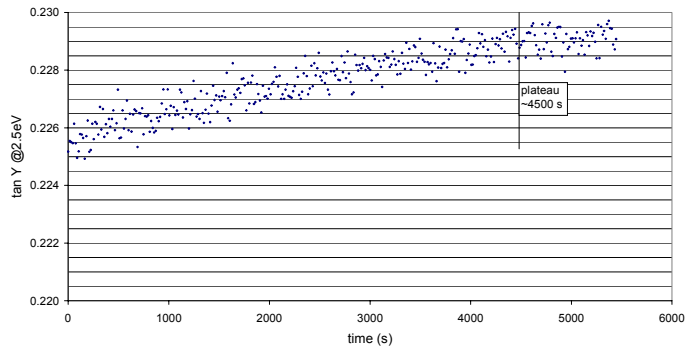
Adsorption on silica/ γ -alumina @ Tcell=30°C, Twater=4°C
(ws_si1c-2-01)



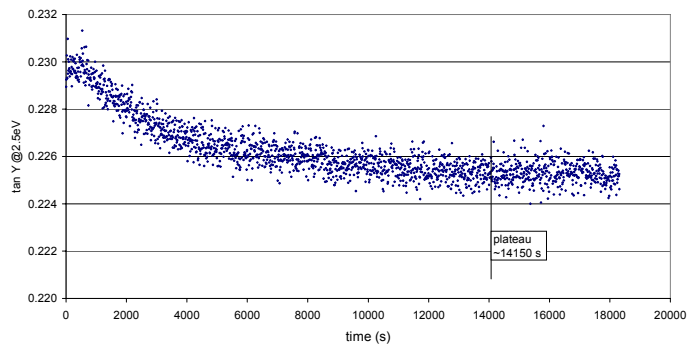
Adsorption on silica/ γ -alumina @ Twater=10°C
Tcell=30 > 19 °C
(ws_si1c-2-03)



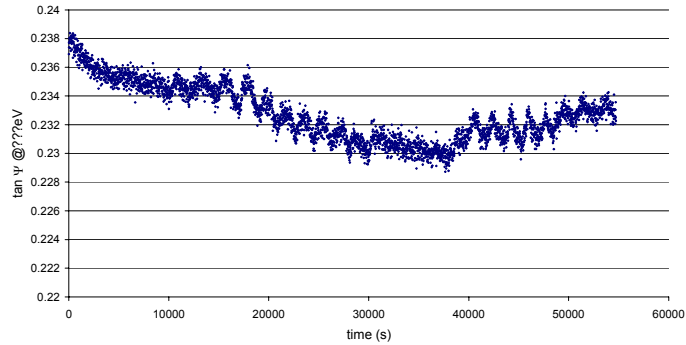
Determining equilibrium @ Tcell=30°C, Twater=10°C
(ws_si1c-2-04)



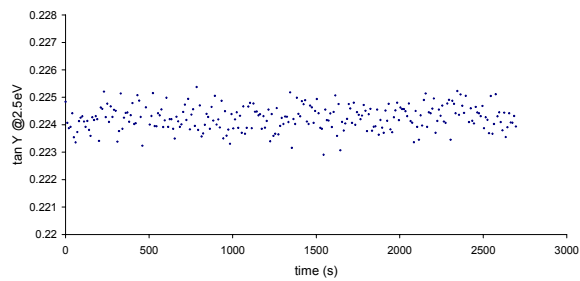
Adsorption on silica/γ-alumina @ Tcell=31°C, Twater=19°C
(ws_si1c-2-06)



Adsorption on silica/γ-alumina @ Tcell=30°C, Twater=30°C
(ws_si1c-2-08)

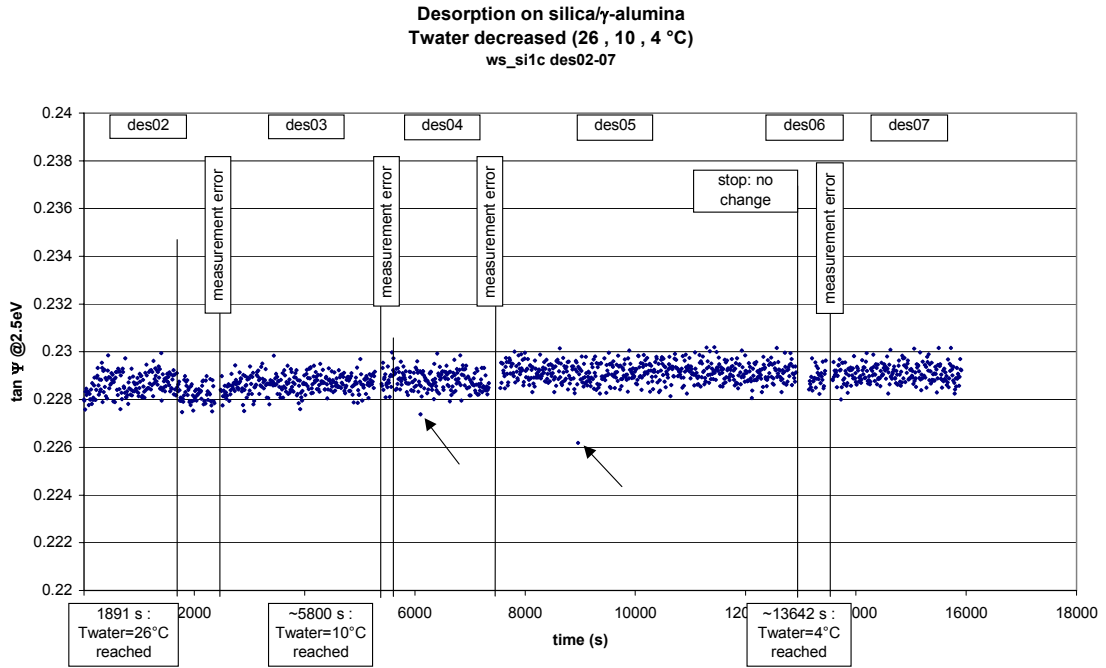


Adsorption on silica/γ-alumina @ Tcell=30°C, Twater=30°C
determining equilibrium
(ws_si1c-2-10)

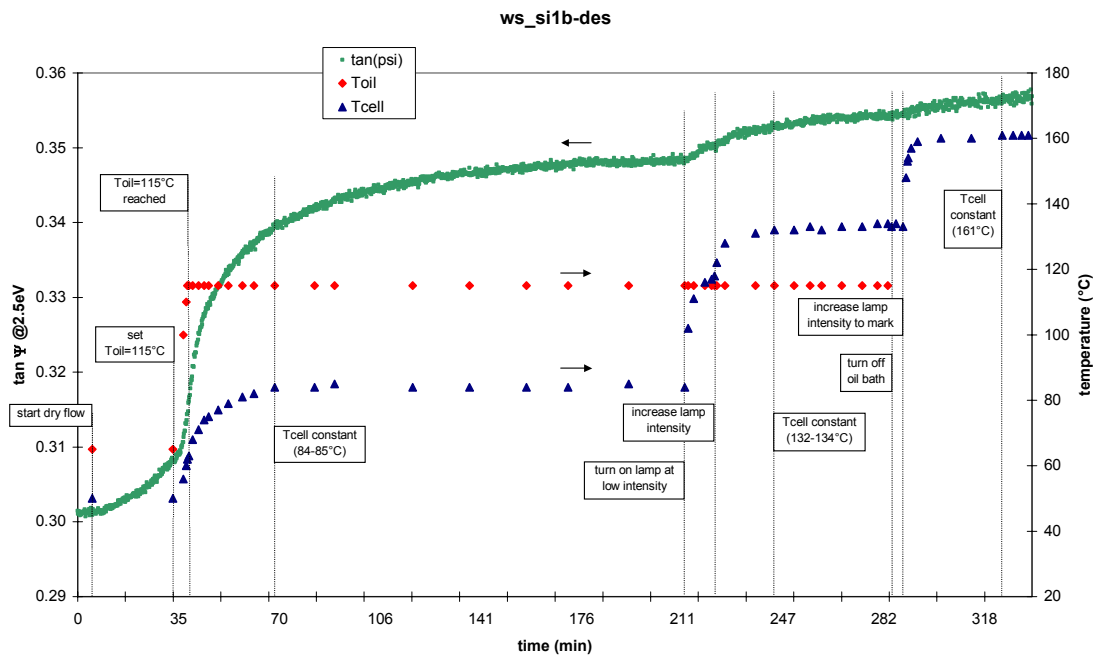


B.2 Desorption

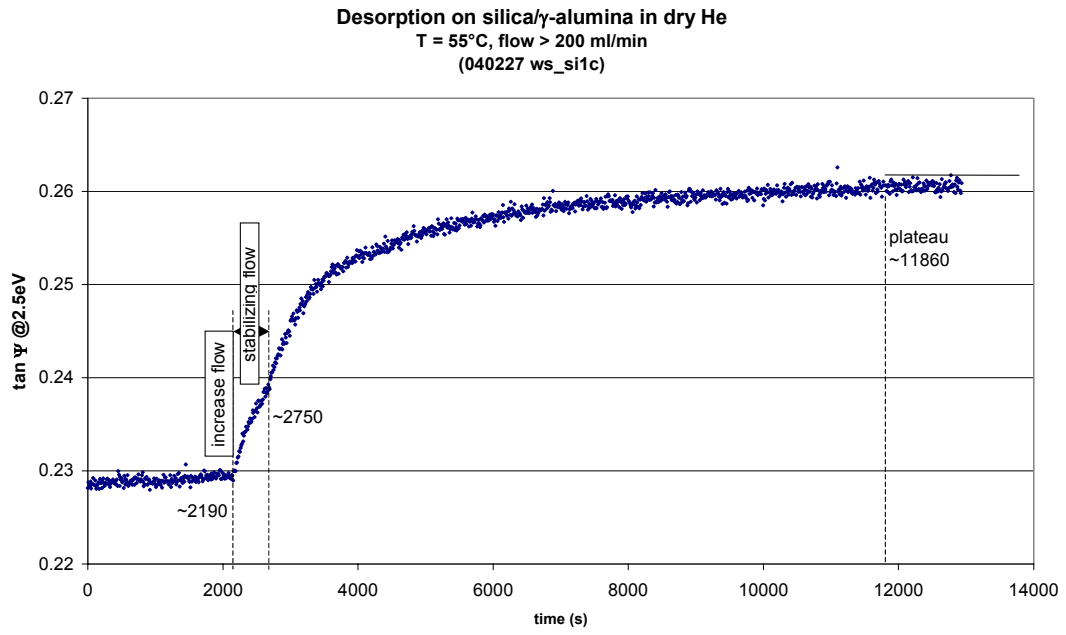
B.2.1 040226-27 ws_si1c



B.2.2 040120 ws_si1b-des

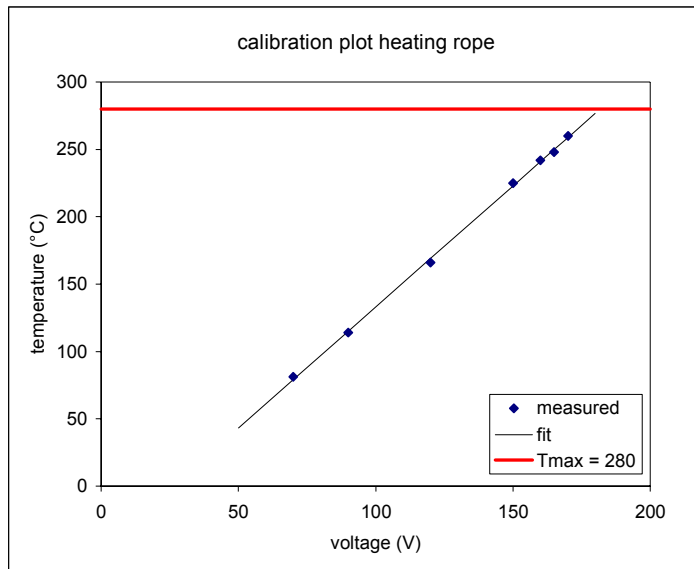


B.2.3 040227 ws_si1c dryHe



C Heating rope calibration plot

voltage (V)	temperature (°C)	fit (°C)	Tmax	= max temp for Teflon tubings
0	-		280	
50	-	43	280	
70	81	79	280	
90	114	115	280	
120	166	169	280	
150	225	223	280	
160	242	241	280	
165	248	250	280	
170	260	259	280	
180	-	277	280	
200	-		280	



SUMMARY OUTPUT

Regression Statistics	
Multiple R	0.999605631
R Square	0.999211418
Adjusted R Square	0.999053701
Standard Error	2.190404237
Observations	7

ANOVA					
	df	SS	MS	F	Significance F
Regression	1	30396.86779	30396.86779	6335.49121	5.93088E-09
Residual	5	23.98935361	4.797870722		
Total	6	30420.85714			

	Coefficients	Standard Error	t Stat	P-value	Lower 95%	Upper 95%	Lower 95.0%	Upper 95.0%
Intercept	-46.85931559	3.09917132	-15.11995006	2.29303E-05	-54.82597607	-38.89265511	-54.82597607	-38.89265511
X Variable 1	1.798935361	0.022600883	79.59579895	5.93088E-09	1.740838036	1.857032686	1.740838036	1.857032686